



GAS-COOLED REACTOR

ADVANCED REACTOR TECHNOLOGIES PROGRAM

July 18, 2024

Thermal Hydraulics Investigation of Horizontally Orientated Layout Micro HTGRs Under Normal Operation and PCC Conditions Using Integrated Advanced Measurement Techniques

Muthanna H. Al-Dahhan

*Curators' Distinguished Professor of Chemical & Biochemical Engineering and of Nuclear Engineering,
AIChE Fellow*



DOE ART GCR Review Meeting

Hybrid Meeting at INL

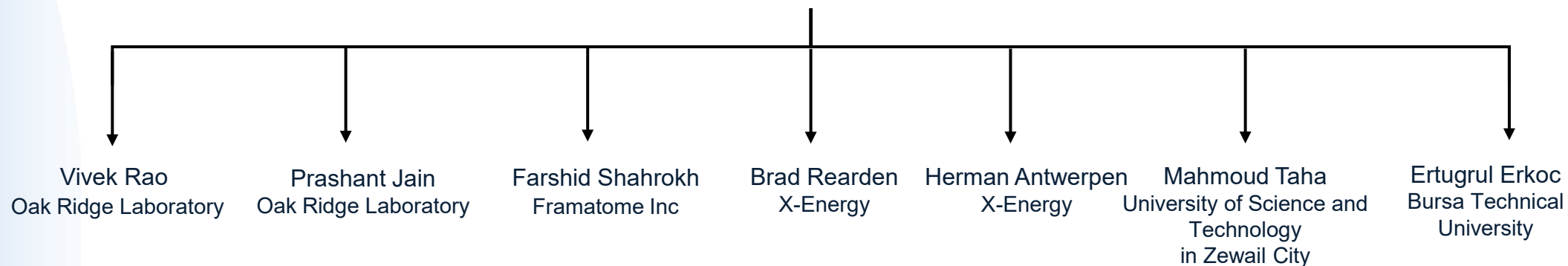
July 16–18, 2024

Principal Investigator (PI)

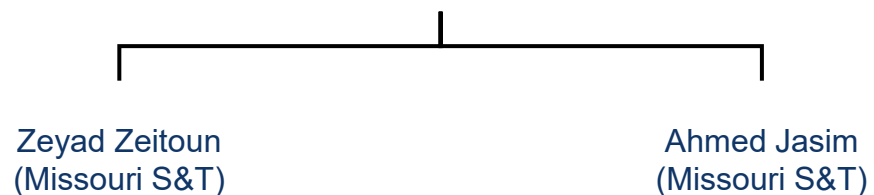
Muthanna H. Al-Dahhan
(Missouri S&T)

Students and Collaborators

Collaborators

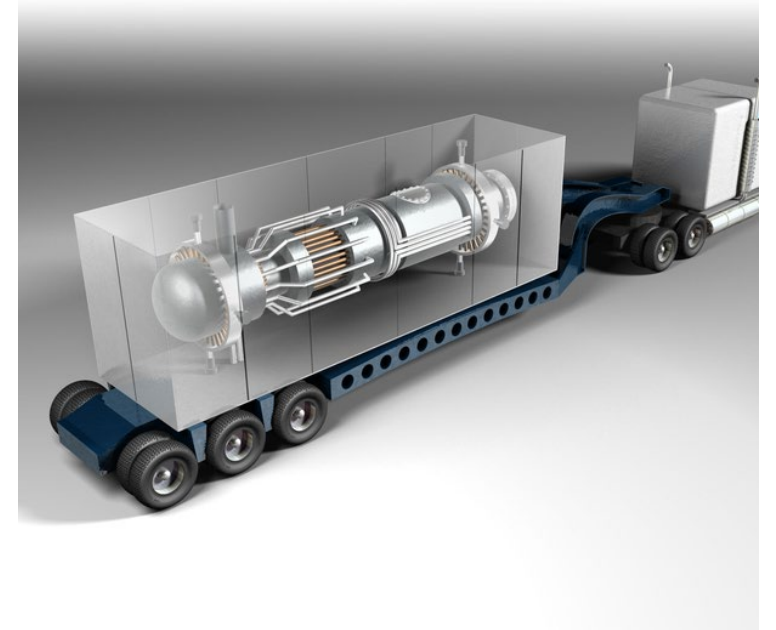


PhD Students



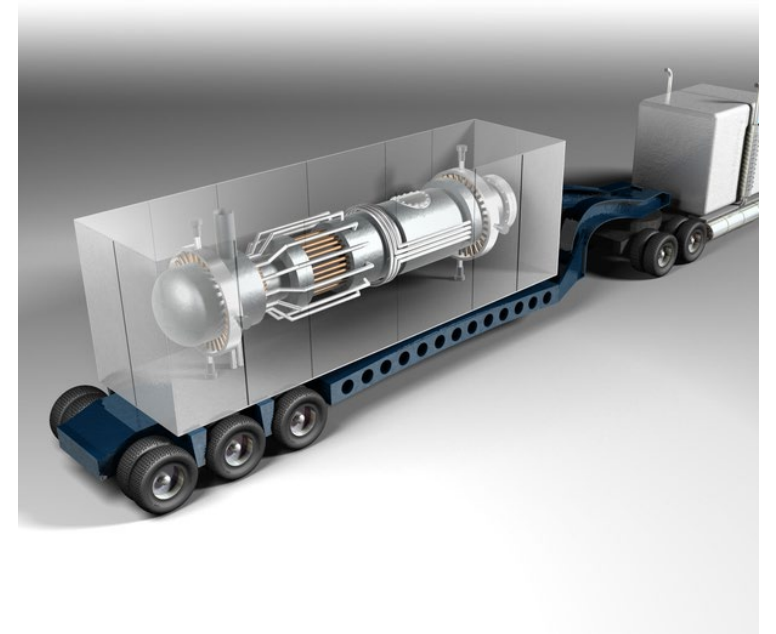
Introduction and Motivation

- Increasing interest in micro-high-temperature gas-cooled Reactors (HTGRs) (< 10 MWt) as reliable power sources for remote locations.
- Consideration of horizontal reactor layout for micro-HTGRs instead of the standard vertical prismatic HTGR design.
- Main challenge: helium coolant flows perpendicular to gravity in horizontal orientation, affecting buoyancy-driven natural convection during accidents like pressurized conduction cooldown (PCC) transients.



Introduction and Motivation

- Impact of horizontal layout:
 - Heat transfer rates and coefficients.
 - Peak fuel temperature location.
 - Helium flow direction in channels and gaps.
 - Timescales for the onset of natural convection.
 - Importance of low-velocity flow regime and core/vessel orientation on these parameters.
- There is an existing thermal-hydraulics knowledge gap in the literature regarding heat transfer and flow in horizontally oriented micro-HTGRs during normal operation and PCC conditions.



Objectives

- Proposed work aims to address this knowledge through:
 - Experimental and computation investigation of thermal-hydraulics in horizontally oriented high-temperature gas-cooled prismatic microreactors under normal operation and pressurized conduction cooldown (PCC) conditions at pressures up to 5 MPa and temperatures up to 1,500°C
 - Obtain benchmark data to validate predictions from computational fluid dynamics (CFD) codes



Parameters of interest

- Convective heat transfer coefficients along the channel and gaps, comparative rates of convective and radiative heat transfer.
- Temperature profiles over channel diameter and gap thickness, location of peak temperature, and its temporal variation.
- Local gas velocity profiles across the diameter of the channels and thickness of the gaps, and timescales for the onset of natural convection.
- Gas dispersion inside channels and gaps, crossflow through gaps between blocks.



Milestones and deliverables

- Modify and test the horizontal dual-channel P2PF and investigate the gas dispersion. (Task 1.1, Task 1.3)
- Investigate the effect of natural circulation intensity on convective heat transfer, and temperature and gas velocity profiles in the horizontal dual channel. (Task 1.2)
- Compare between horizontally and vertically oriented dual-channel natural circulation. (Task 1.4, Task 1.5, Task 1.6)
- Literature review and Design, develop, test, and utilize a horizontally oriented scaled down micro-HTGR. (Task 2.1, Task 2.2)
- Design, develop, test, and utilize a block integrated with advanced measurement techniques. (Task 2.3)

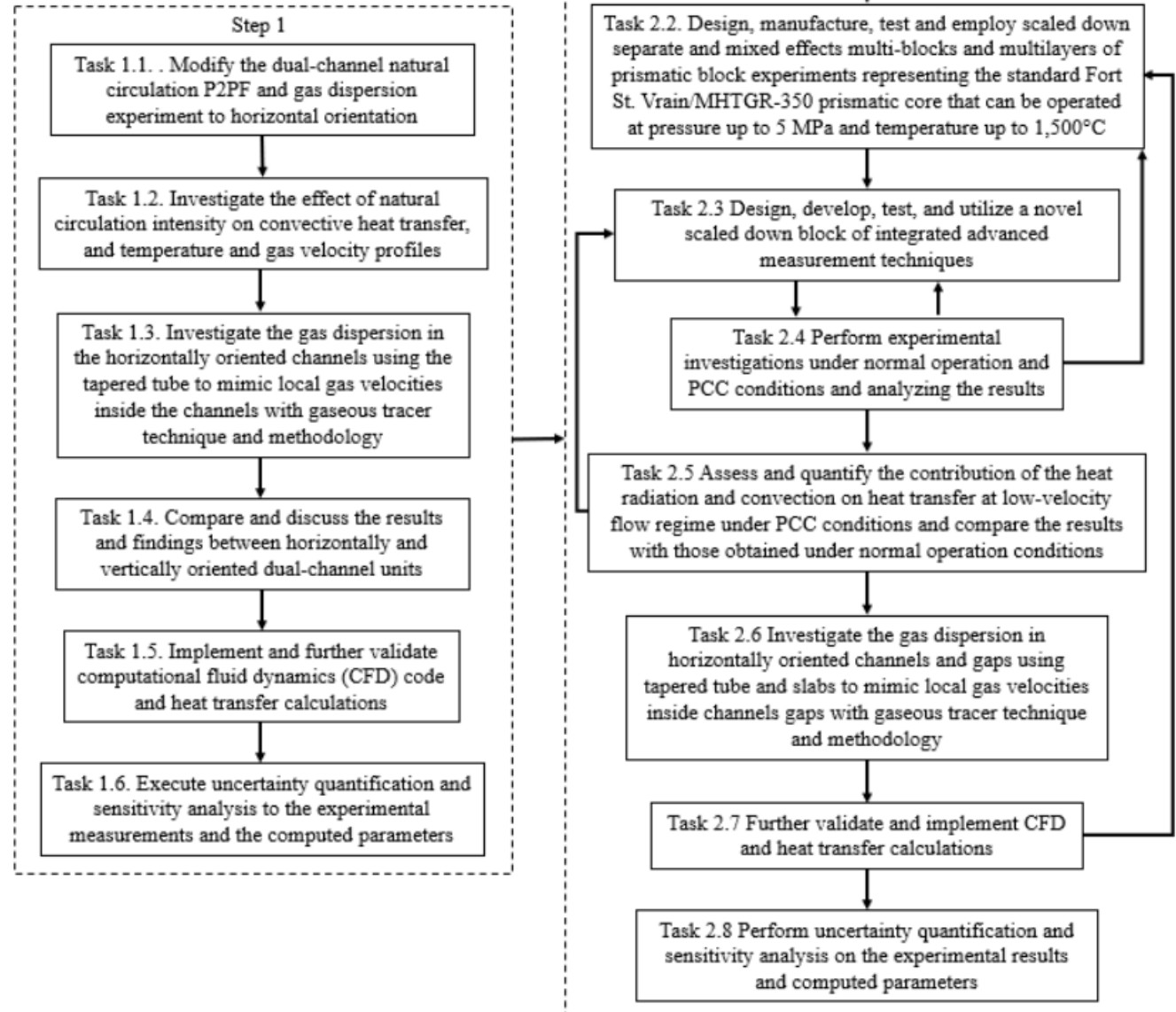


Milestones and deliverables

- Design, develop, test, and utilize a block integrated with advanced measurement techniques. (Task 2.3)
- Provide New knowledge and Perform Investigation under normal operation and PCC conditions. (Task 2.4, Task 2.6)
- Assess and quantify the contribution of radiative and convective heat rates under PCC conditions. (Task 2.5)
- Develop new benchmarking data and CFD validation with heat transfer calculations. (Task 2.7)
- Perform uncertainty quantification. (Task 2.8)



These are accomplished in two primary steps



Step 1

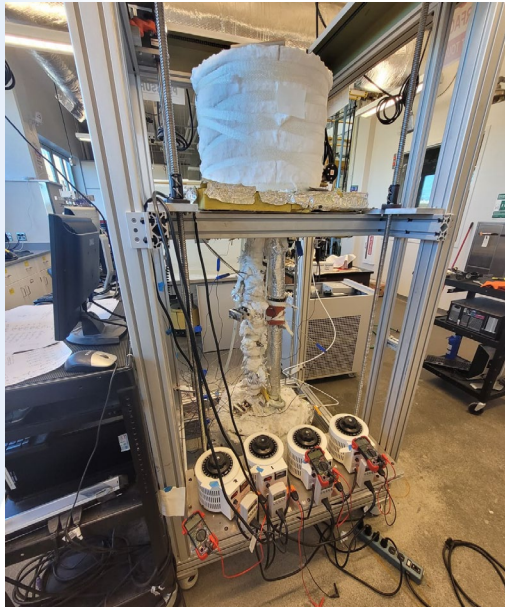


Task 1.1. Modify the dual-channel natural circulation P2PF and gas dispersion experiment to horizontal orientation.

Up-to-date accomplishments

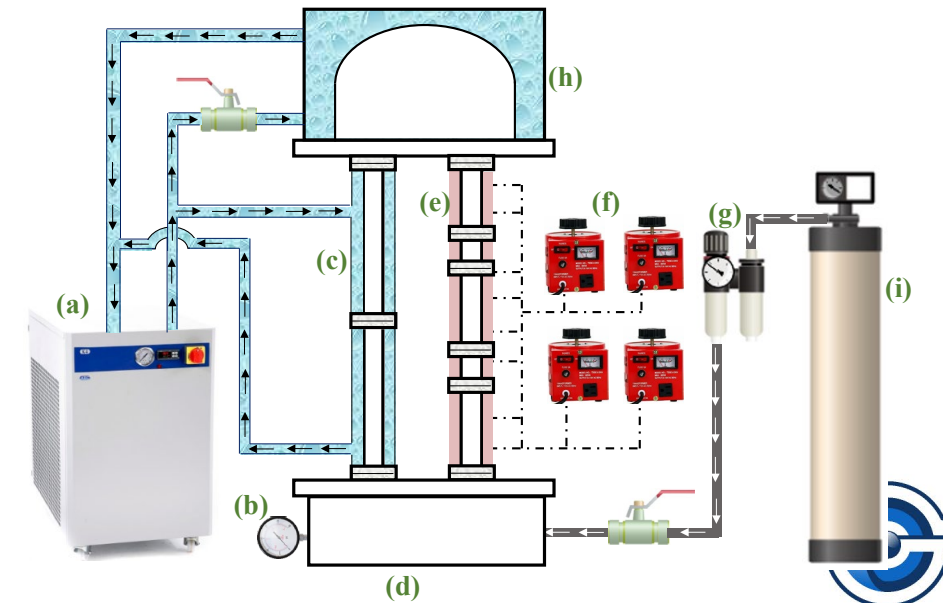
- Calibrated all measurement techniques.
- Renewed the insulation and tested the setup for gas leaks.
- Selected experiments were performed on the vertical setup to master measurement techniques.

The vertical dual-channel plenum-to-plenum facility



| | |
|---|------------------|
| a | Chiller |
| b | Pressure gauge |
| c | Cold channel |
| d | insulated plenum |
| e | Hot channel |
| f | Electric heaters |
| g | Air filter |
| h | Cold plenum |
| i | Air supply |

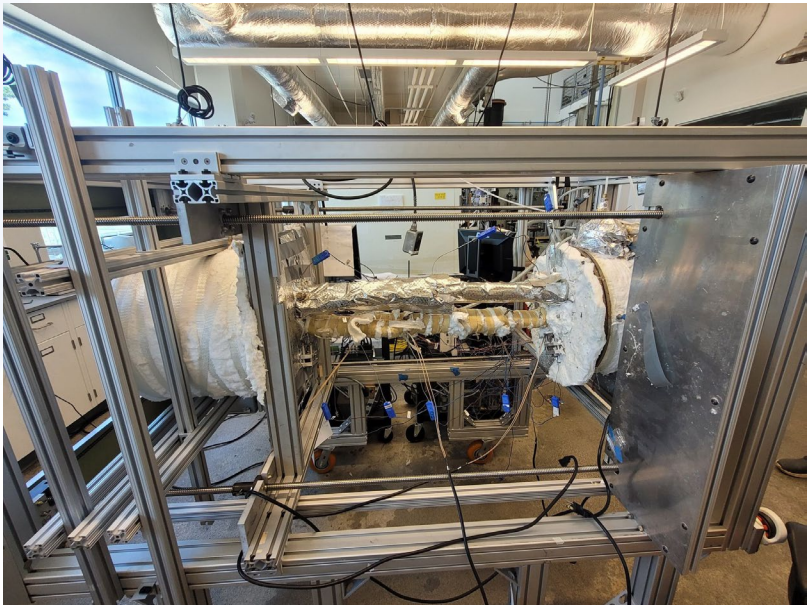
| Channel Dimensions | |
|--------------------|-------|
| Inner diameter | 16 mm |
| Outer diameter | 22 mm |
| Wall thickness | 3 mm |
| Channel length | 1 m |



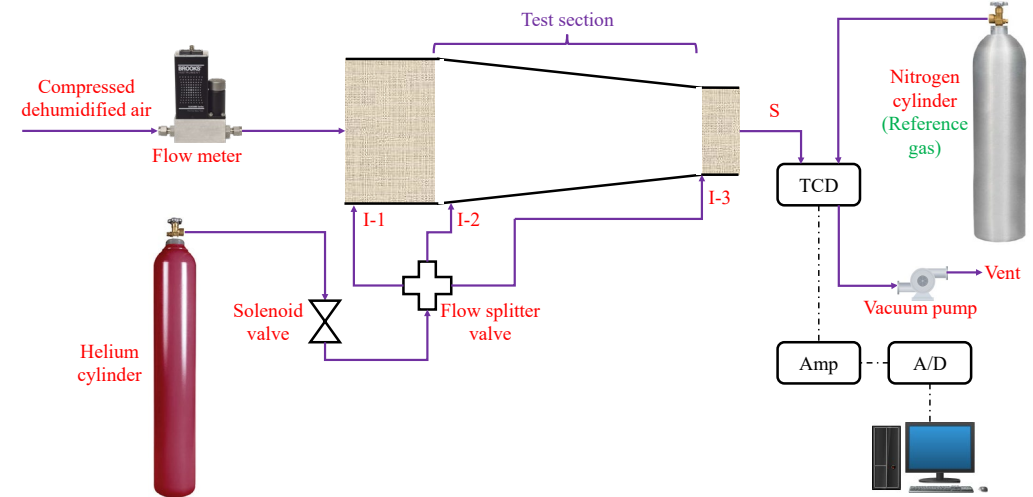
Task 1.1. Modify the dual-channel natural circulation P2PF and gas dispersion experiment to horizontal orientation.

Up-to-date accomplishments

- Added necessary supports and structures to adapt the setup to horizontal orientation.
- The convergent channel of the gas dispersion technique was adjusted to the horizontal configuration



Horizontal dual channel plenum-to-plenum facility



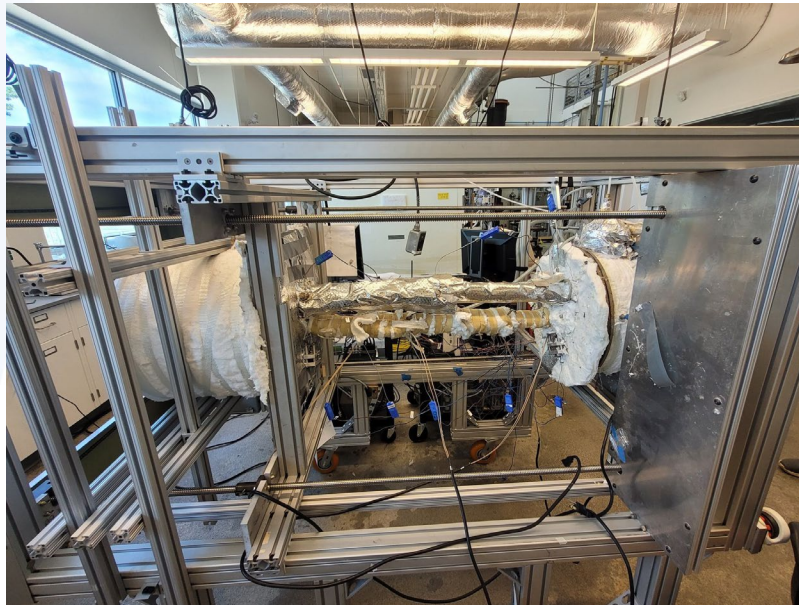
Gas dispersion measurement technique



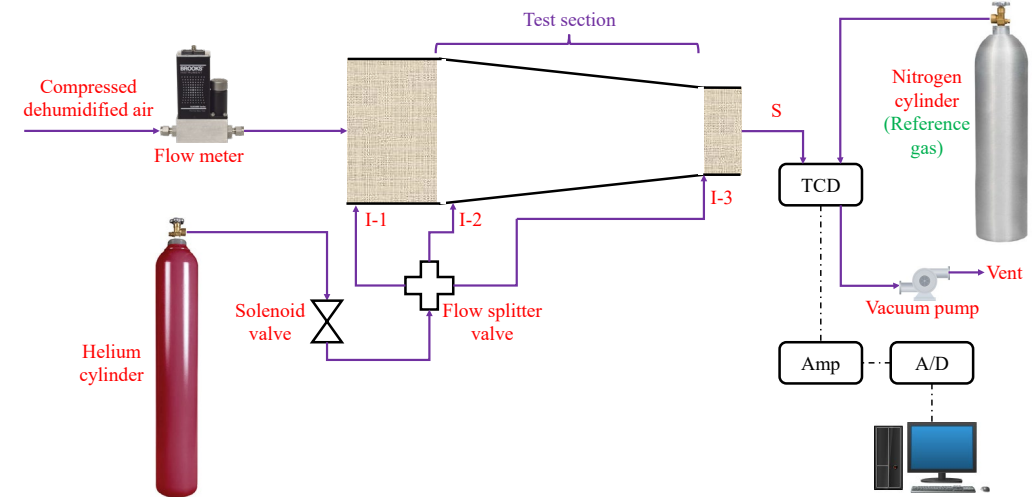
Task 1.1. Modify the dual-channel natural circulation P2PF and gas dispersion experiment to horizontal orientation.

Up-to-date accomplishments

- Added necessary supports and structures to adapt the setup to horizontal orientation.
- The convergent channel of the gas dispersion technique was adjusted to the horizontal configuration



Horizontal dual channel plenum-to-plenum facility



Gas dispersion measurement technique



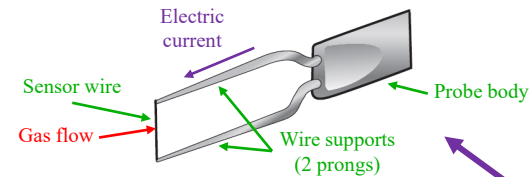
Task 1.1. Modify the dual-channel natural circulation P2PF and gas dispersion experiment to horizontal orientation.

- The integrated measurement techniques used for this study

- Thermocouple probe
- Micro-foil heat flux sensor
- Hot wire anemometer

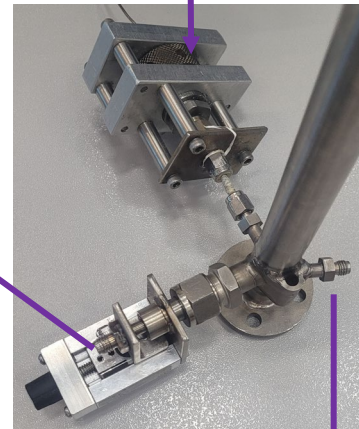
Heating intensities

| Distribution of the electrical heater tapes along the hot channel | | Heating profiles (W/m ²) | | | | |
|---|------------|--------------------------------------|-------|-------|-------|------|
| | | Set 1 | Set 2 | Set 3 | Set 4 | |
| 25 cm | Heater # 4 | Heater # 4 | 1720 | 860 | 1146 | 1433 |
| 25 cm | Heater # 3 | Heater # 3 | 1720 | 1720 | 1720 | 1720 |
| 25 cm | Heater # 2 | Heater # 2 | 1720 | 860 | 1146 | 1433 |
| 25 cm | Heater # 1 | Heater # 1 | 1720 | 860 | 1146 | 1433 |

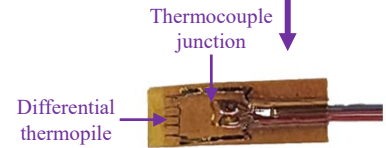


Hot wire anemometer radial adjustor
To measure gas **velocity** radially at each axial location

Thermocouple radial adjustor
To measure gas **temperature** radially at each axial location



Flush-mounted micro-foil sensor
To measure surface **temperature**

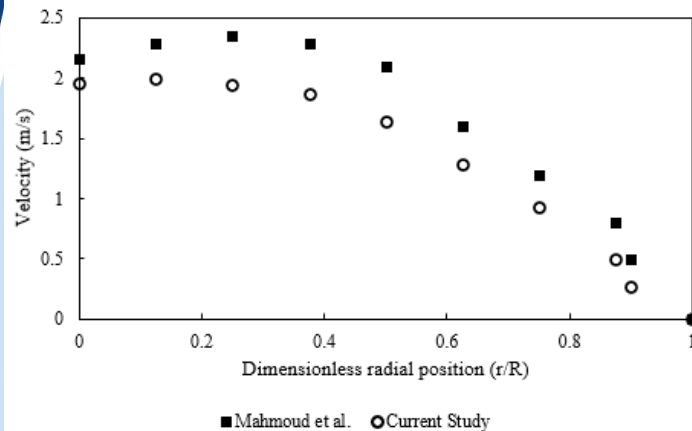


Task 1.1. Modify the dual-channel natural circulation P2PF and gas dispersion experiment to horizontal orientation.

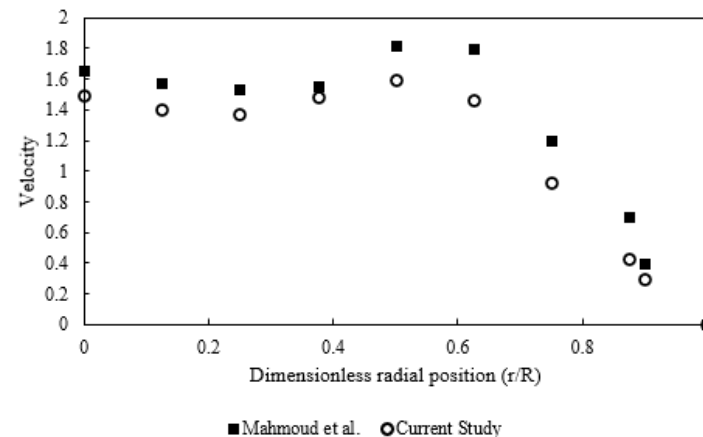
Up-to-date accomplishments

- Selected experiments were conducted on the vertical channel to master measurement techniques and build a data bank.
- This data bank will serve as a comparison reference for data obtained from horizontal orientation experiments.

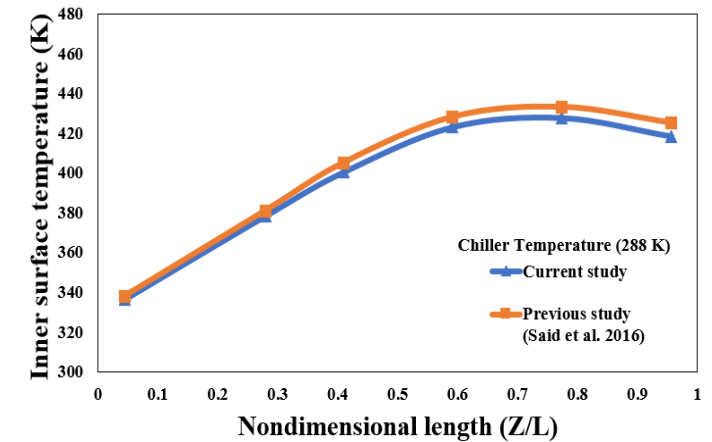
Comparison between previous and current hot wire anemometry results at $z/L = 0.591$



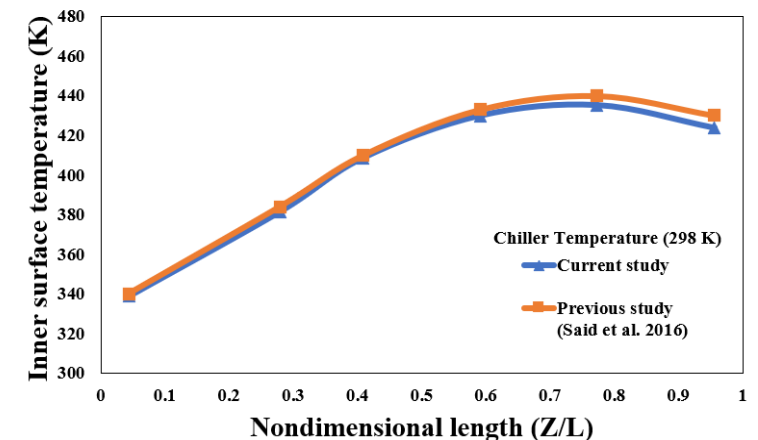
Comparison between previous and current hot wire anemometry results at $z/L = 0.044$



Comparison between current and previous studies according to the hot channel surface temperature



Comparison between current and previous studies according to the hot channel surface temperature

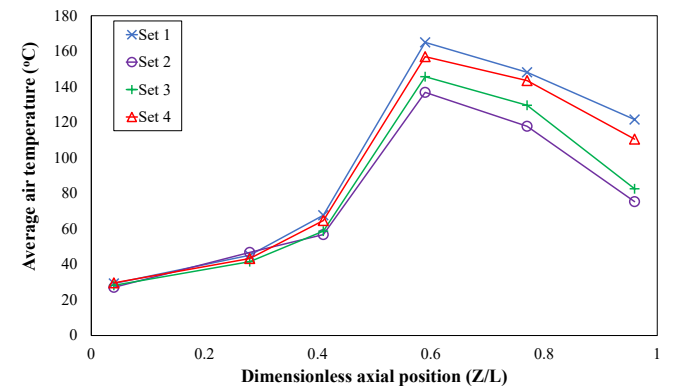
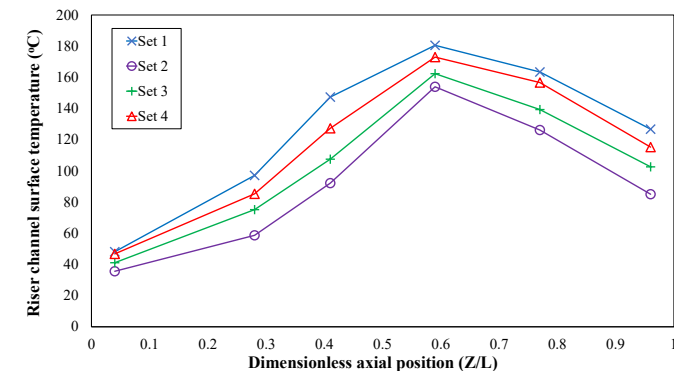


Task 1.1. Modify the dual-channel natural circulation P2PF and gas dispersion experiment to horizontal orientation.

Selected Experiments on the vertical dual-channel

- ***Effect of non-uniform heating*** on air thermal hydraulics in vertical dual channel P2PF

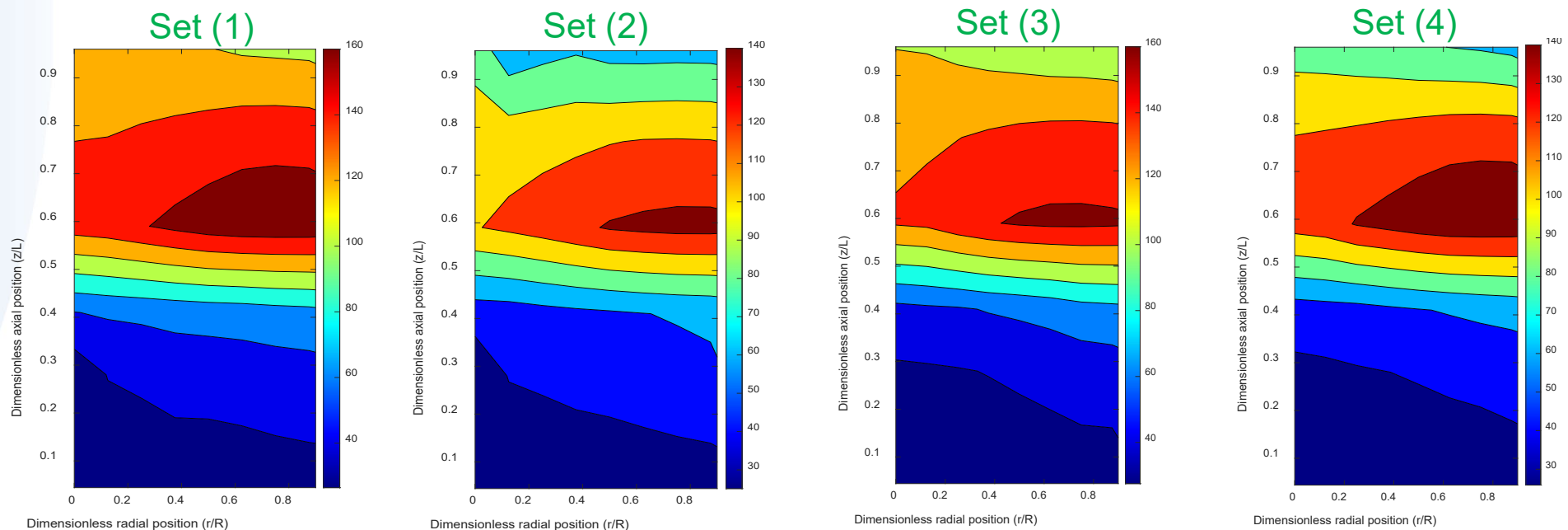
- *Riser/Hot channel temperature distribution*
- Surface temperature increases along the channel until an axial position $Z/L = 0.59$ beyond which temperature starts to decrease.
- This inflection is due to the axial heat losses by conduction through the flange connecting the riser channel by the cooled upper plenum.
- *Hot gas temperature distribution*
- Temperature increases due to heat transfer from the heated channel wall to the flowing air.
- Beyond the axial position of $Z/L=0.59$, the temperature begins to decrease, similar to the surface temperature.



Selected Experiments on the vertical dual-channel

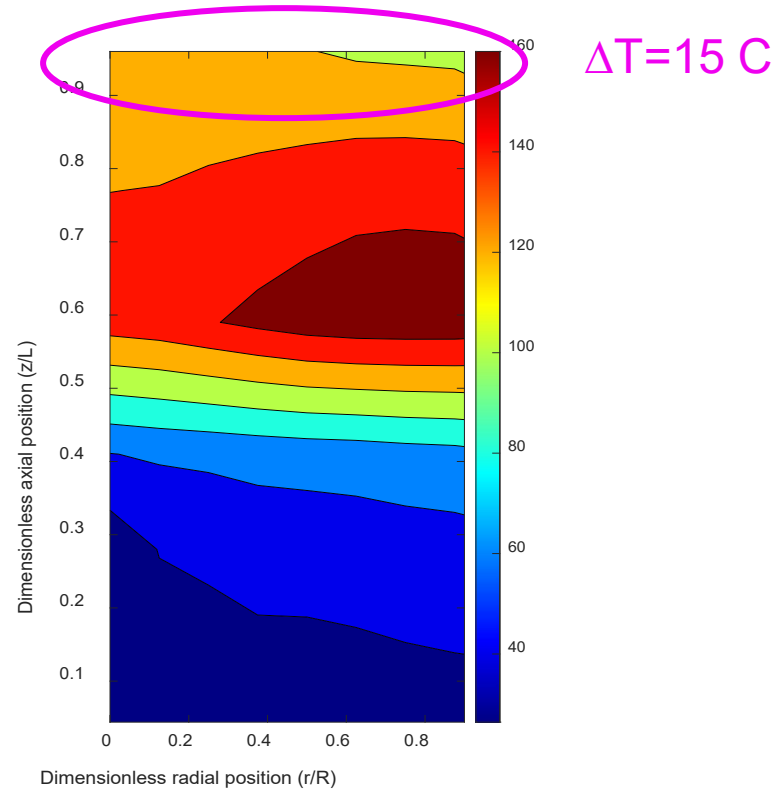
▪ Effect of non-uniform heating on air thermal hydraulics in vertical dual channel P2PF

- *Radial hot gas temperature distribution*
- From the channel entrance to $Z/L=0.59$, temperatures decrease as the thermocouples move from the wall toward the centerline of the channel.
- Beyond the axial position $Z/L=0.59$, the temperature distribution reverses, with temperatures increasing towards the centerline of the channel.
- This variation in radial temperature profiles was attributed to flow reversal.

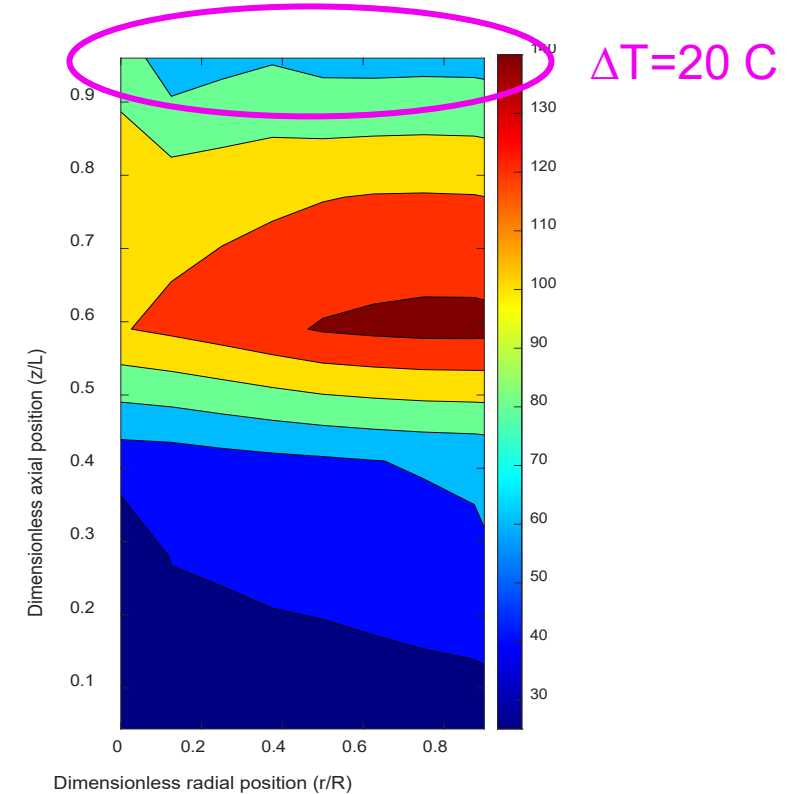


- Radial hot gas temperature distribution

Set (1) "Highest heating intensity profile"



Set (2) "Lowest heating intensity profile"



✓ Buoyancy parameter ($Gr/R e$) is calculated to describe the flow reversal and penetration depth

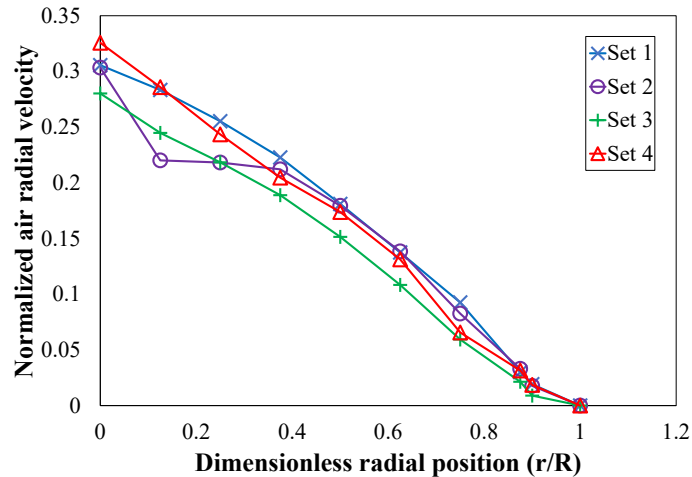
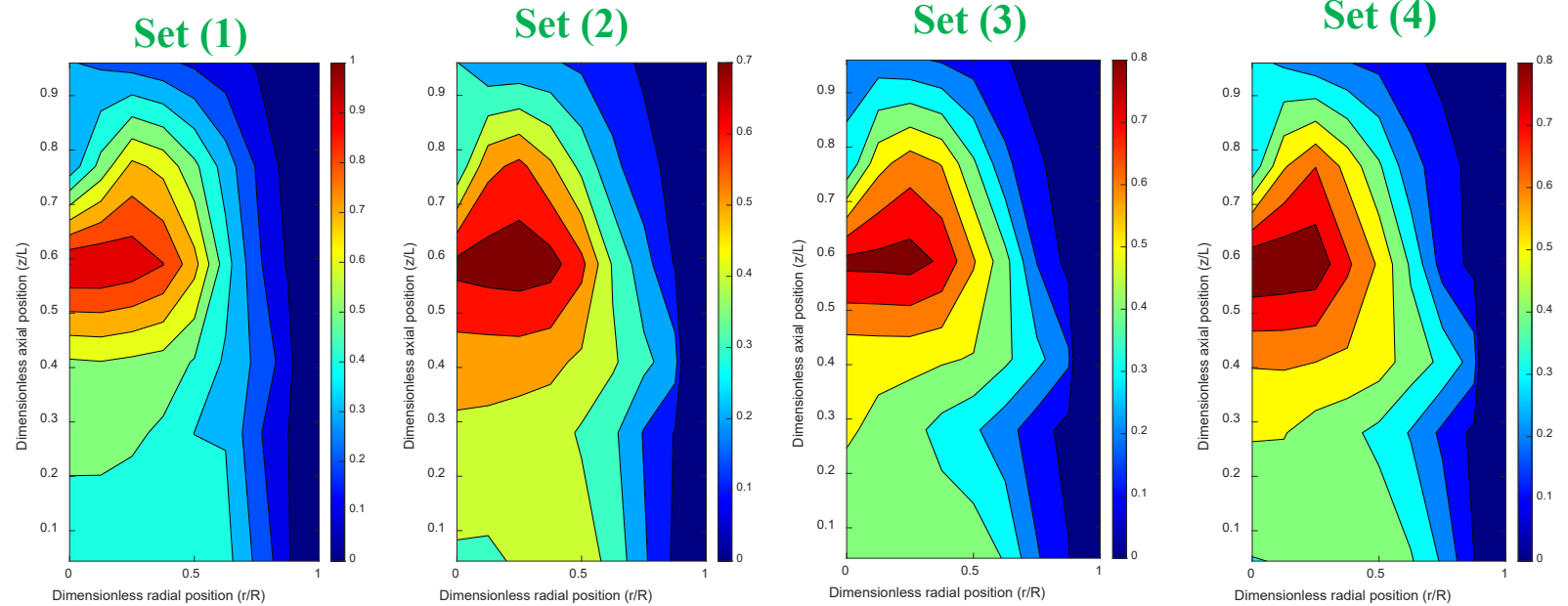
$$Gr_z = \frac{g \beta \Delta T_i l^3}{\nu^2}$$

➤ ($Gr/R e$) for set 1 = 2.02

➤ ($Gr/R e$) for set 2 = 7.09



- Hot gas radial and axial velocity distribution



Normalized gas velocity at the channel exit (Z/L=0.96)

$$Fr = \frac{U_{b,i}}{\sqrt{g \frac{T_{b,i} - T_{plenum}}{T_{b,i}} l}}$$

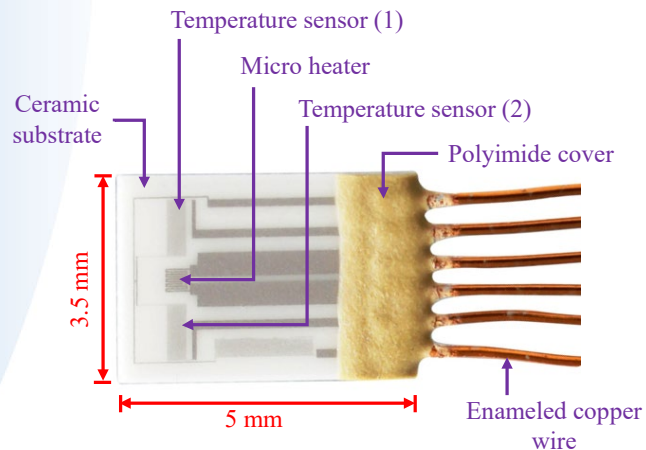
- ✓ Froude number for Set (1) is 0.68 < Froude number for Set (2) is 0.75
- ✓ This reveals the presence of intense jet flow.



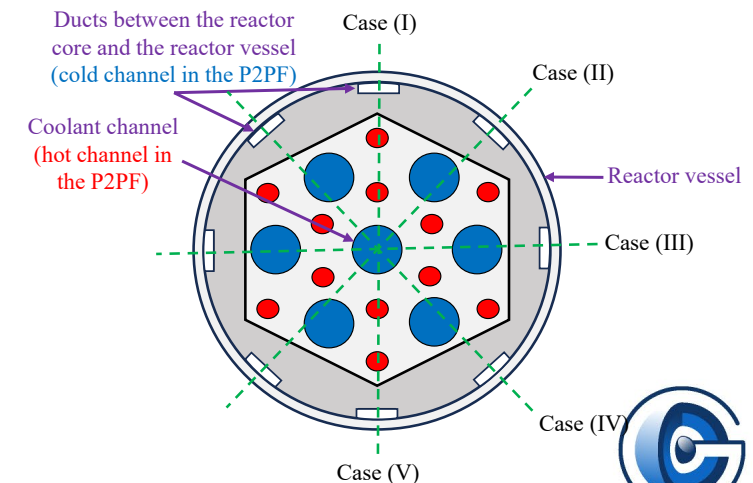
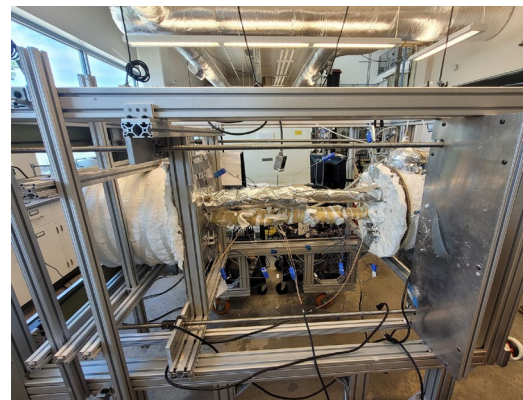
Task 1.2. Investigate the effect of natural circulation intensity on convective heat transfer, and temperature and gas velocity profiles.

Up-to-date progress

- Developed a thermal mass flow sensor to detect gas flow direction
- Investigated temperature profile, convective heat transfer coefficient, local gas velocities, gas flow direction, and natural circulation in different configurations of the dual channel.
- Conducted experiments at various temperature and pressure conditions to analyze these parameters comprehensively.



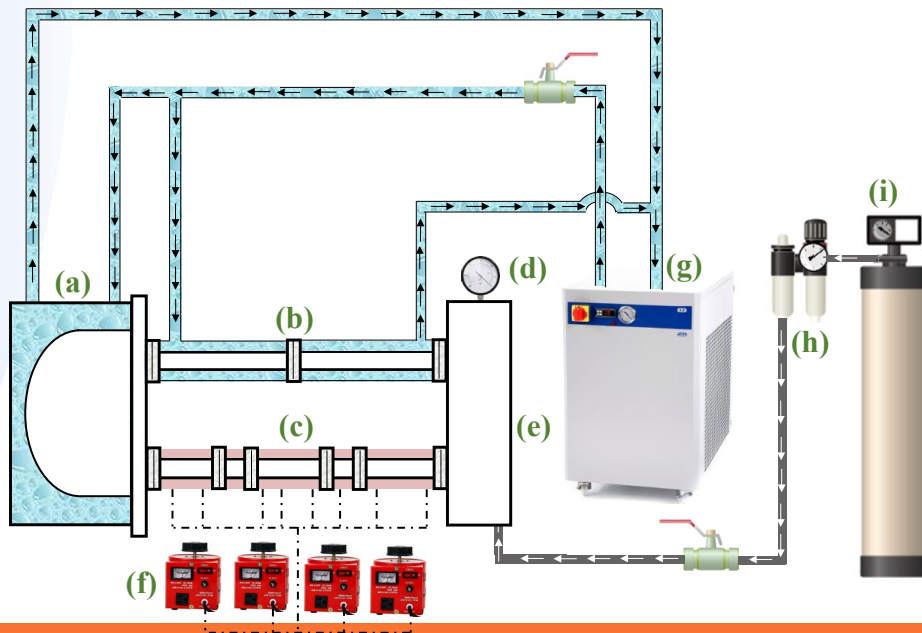
Thermal gas flow sensor



Task 1.2. Investigate the effect of natural circulation intensity on convective heat transfer, and temperature and gas velocity profiles.

Up-to-date progress

- **Selected experimental condition for the horizontal dual-channel**
 - Gas pressure (14.5 psig, 25 psig, 40 psig, 60 psig)
 - Heating intensities (125.39 W/m², 282.14 W/m², 501.56 W/m², 783.7 W/m²)
 - Cooling water temperature (5 °C, 10 °C, 15 °C, 20 °C)



| | |
|----------|------------------|
| a | Chiller |
| b | Pressure gauge |
| c | Cold channel |
| d | insulated plenum |
| e | Hot channel |
| f | Electric heaters |
| g | Air filter |
| h | Cold plenum |
| i | Air supply |

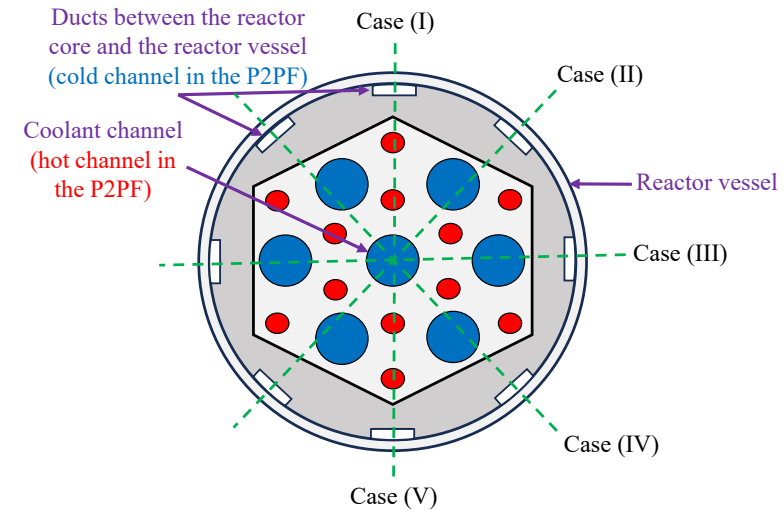


Task 1.2. Investigate the effect of natural circulation intensity on convective heat transfer, and temperature and gas velocity profiles.

- **Up-to-date progress**

- **Configuration of the channels**

- Five configurations of the dual channel were investigated
 - Case (I): The coolant channel lies below the duct at 90° to the horizontal axis.
 - Case (II): Both the coolant channel and duct are inclined at a 45° angle to the horizontal axis.
 - Case (III): The coolant channel and duct are aligned parallel to the horizontal axis.
 - Case (IV): Similar to case (III), but with the coolant channel positioned at a higher level than the duct.
 - Case (V): Analogous to case (I), but with the coolant channel situated above the duct.



Task 1.2. Investigate the effect of natural circulation intensity on convective heat transfer, and temperature and gas velocity profiles.

Major Challenges

Fragility of HWA Probes

- The HWA probe is very fragile and defects easily. It can only be repaired by the manufacturer, which usually takes several months.

Inability of HWA Probes to Detect Gas Flow Direction

- HWA probes cannot detect gas flow direction, which limits their effectiveness in certain applications.
- A thermal gas flow sensor was developed, tested, and calibrated to measure gas velocity and detect gas direction.



Task 1.2. Investigate the effect of natural circulation intensity on convective heat transfer, and temperature and gas velocity profiles.

Selected Experiments

1. Effect of cooling temperature on gas thermal hydraulics in the horizontal dual channel plenum P2PF
2. Model development to predict the experimental axial average Nusselt number
3. Effect of uniform heating and pressure on gas thermal hydraulics in the horizontal dual channel plenum P2PF
4. Effect of different horizontal orientations on gas thermal hydraulics in the horizontal dual channel plenum P2PF

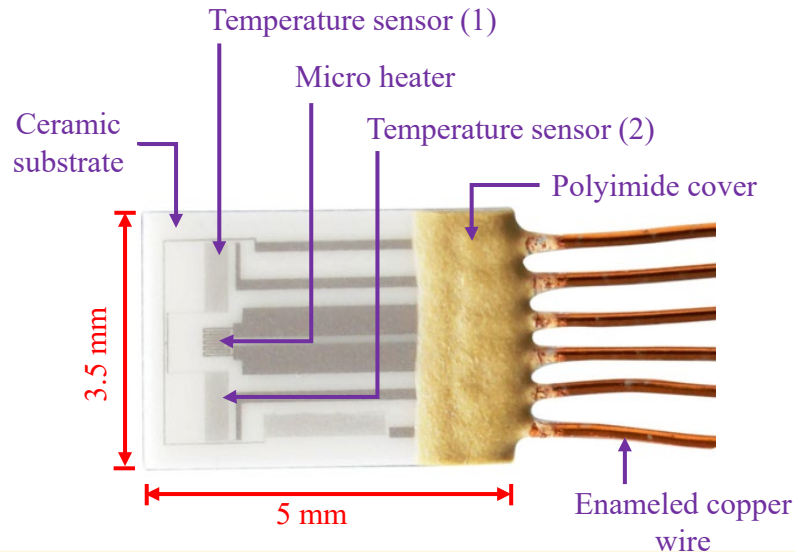


Newly developed thermal gas flow sensor

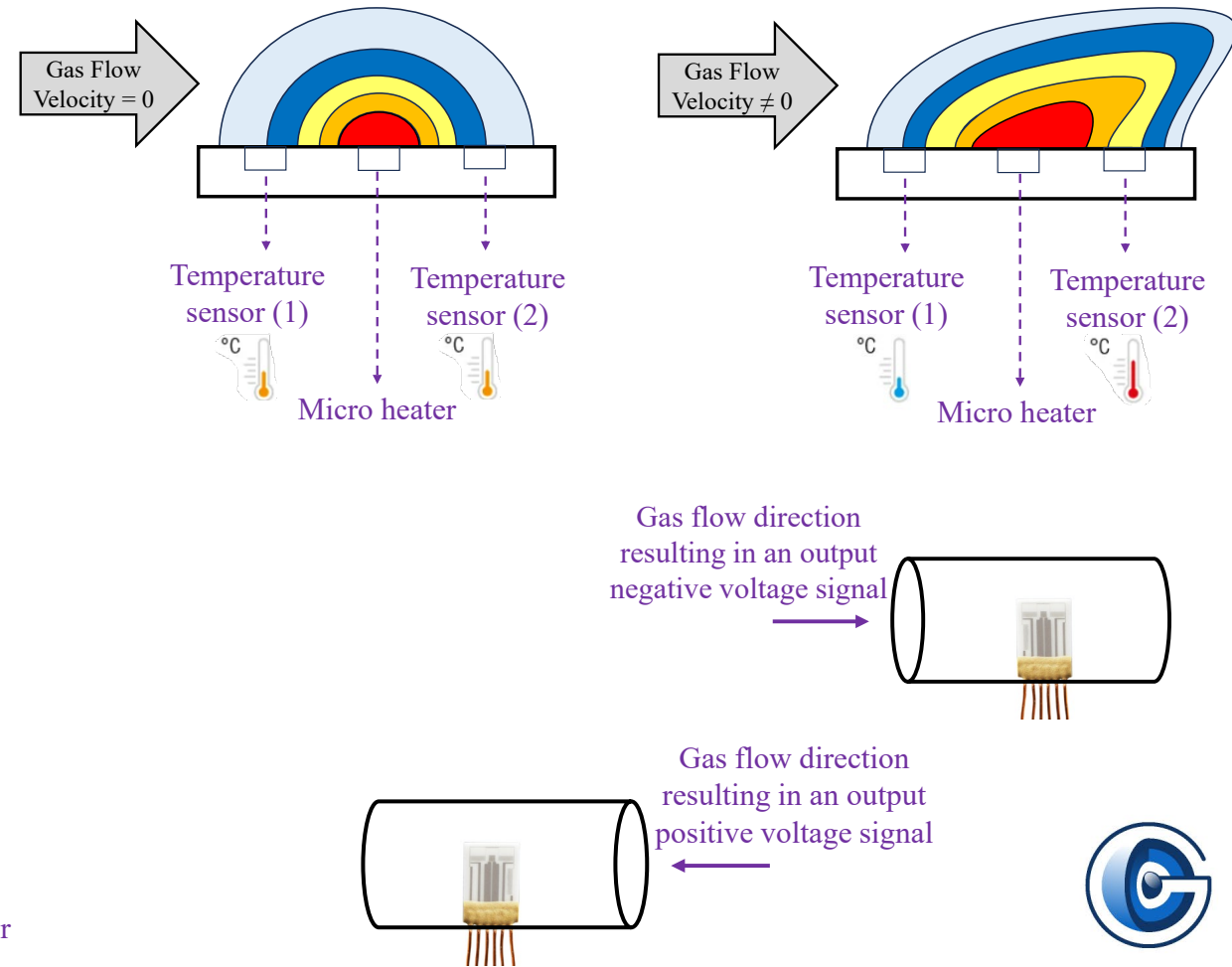
✓ Features:

- High sensitivity
- Long-term stability
- Easy calibration
- Absence of moving parts
- Small in size

✓ Structure

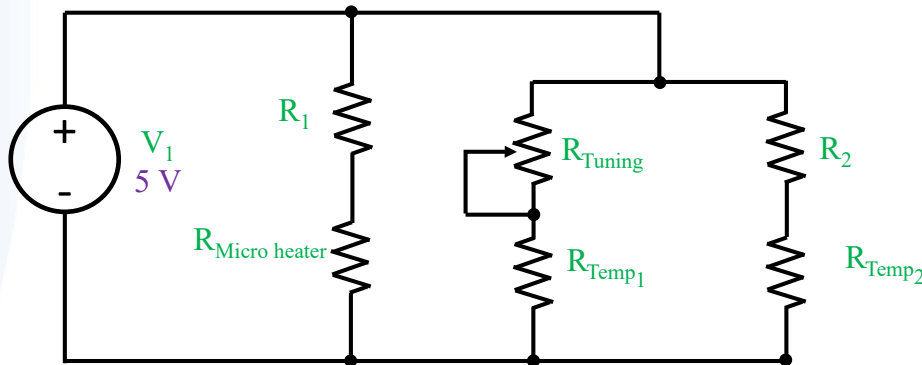


✓ Measuring principle

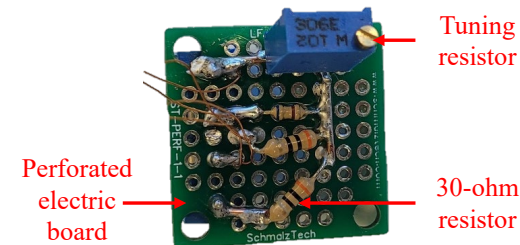


• Newly developed thermal gas flow sensor

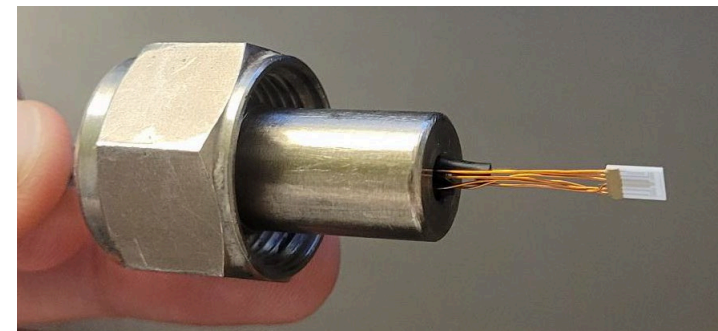
- Electric circuit design
 - Based on Wheatstone Bridge.
 - Tuning resistor: to ensure that the output voltage reading is zero when the sensor is inserted inside a horizontal channel and no gas is flowing.
 - 30-ohm resistors: to reconcile the voltage difference between the laptop charger (5 VDC) and the thermal gas flow sensor's maximum voltage tolerance (3 VDC).



Schematic representation for the thermal gas flow sensor circuit



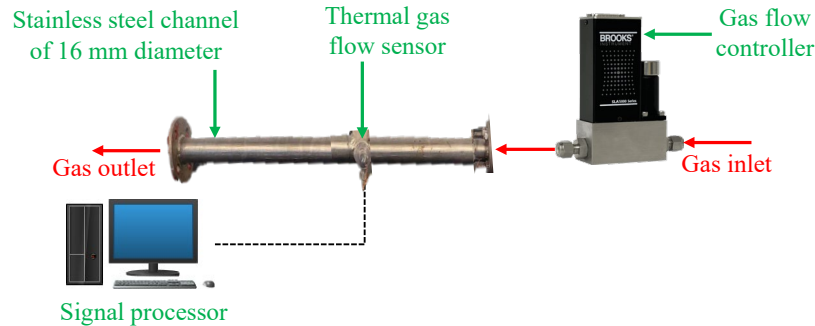
Pictorial for the thermal gas flow sensor circuit



Thermal gas flow sensor attached to a probe

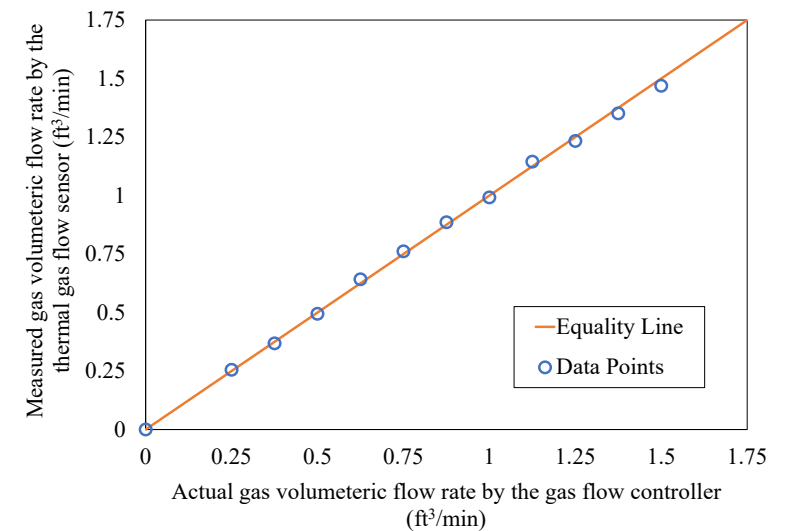
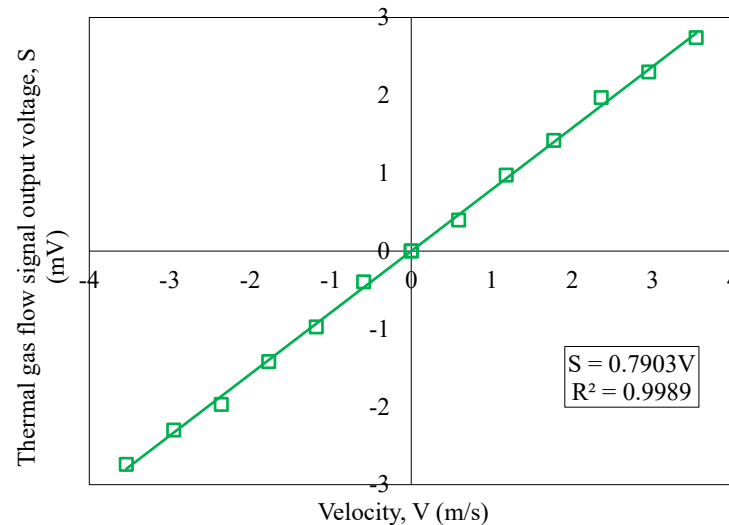
- Newly developed thermal gas flow sensor

✓ Calibration “0 to 1.5 ft³/min”



✓ Validation

- Rigorous testing is conducted within the calibrated range of 0 to 1.5 ft³/min.
- The difference between the predicted value and the actual value is minimal - less than 2%.
- This exceptional result underscores the remarkable performance of the newly developed thermal gas flow sensor.



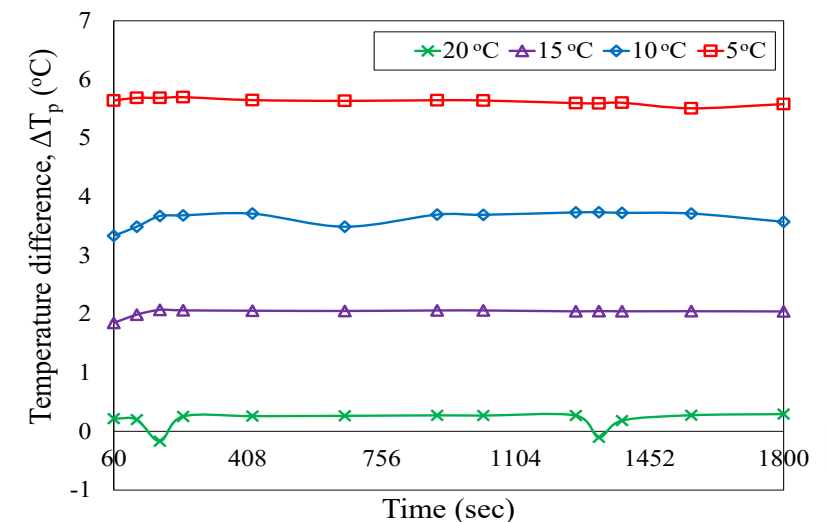
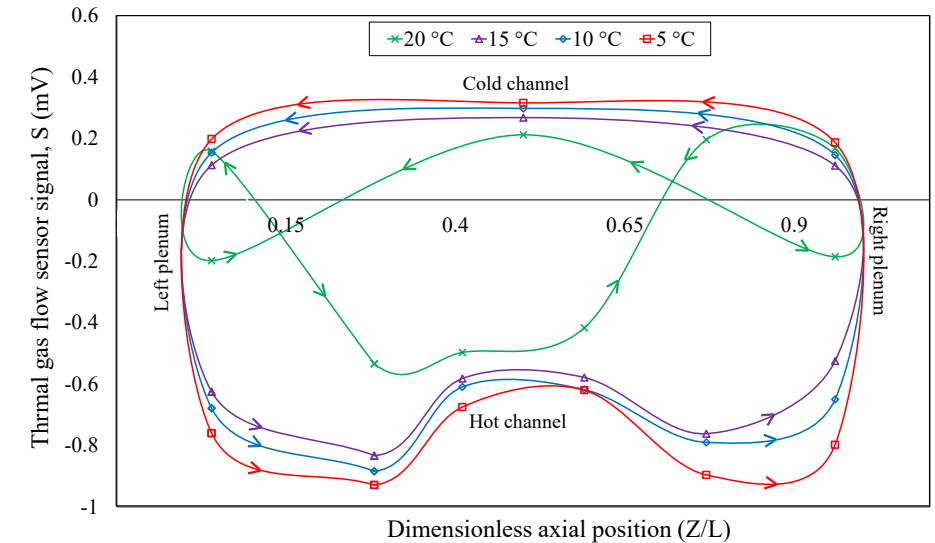
1. Effect of cooling temperature on gas thermal hydraulics in the horizontal dual channel plenum P2PF.

- Experimental conditions:

- Air pressure (60 psi)
- Heating intensity (783.7 W/m²)
- Cooling water temperatures (5 °C, 10 °C, 15 °C, 20 °C)

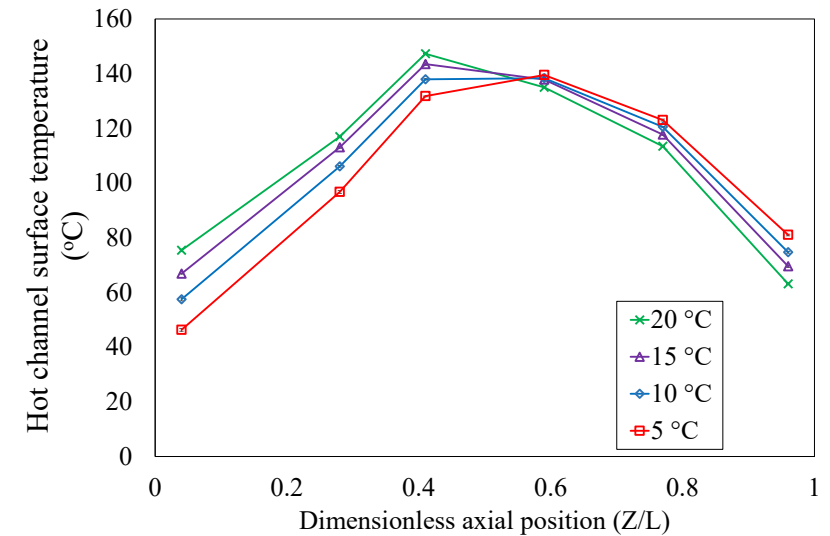
- Gas flow direction

- For cooling water temperatures (5 °C, 10 °C, and 15 °C), there is a unidirectional natural circulation as the sensors' signals on the hot and cold channels are negative and positive, respectively.
- For cooling water temperature (20 °C), there is no unidirectional natural circulation.

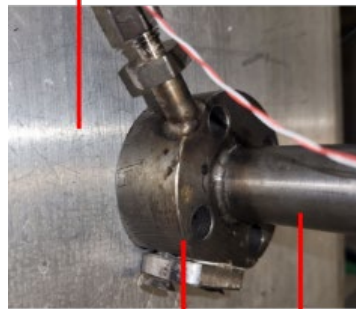


1. Effect of cooling temperature on gas thermal hydraulics in the horizontal dual channel plenum P2PF.

- Hot channel inner surface temperature
- The location of peak surface temperature is shifted from the axial position ($Z/L=0.409$) to ($Z/L=0.59$) as the cooling water temperature decrease.
- Surface temperature decreases at the channel exit due to heat losses by conduction heat transfer.

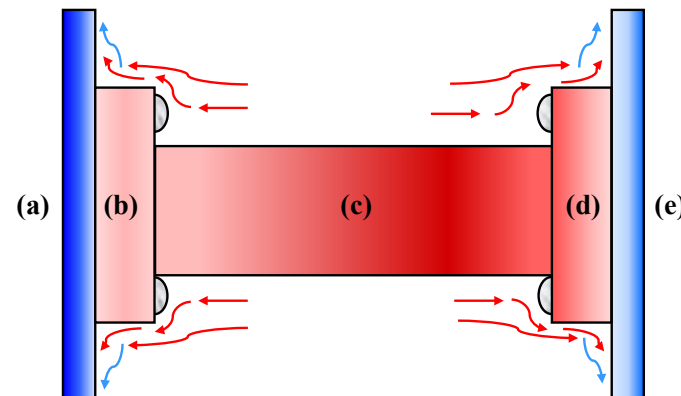


Lower surface of the plenum



Flange connecting the plenum to the hot channel

Hot channel

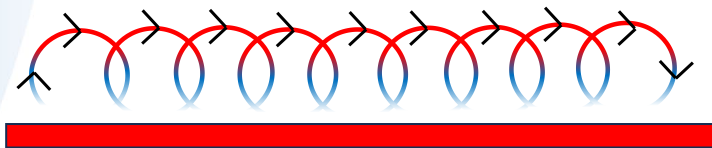
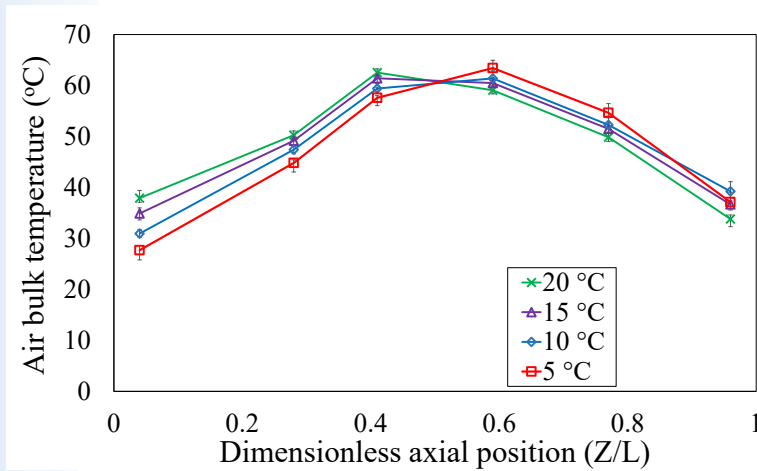


| | |
|---|---|
| a | Lower surface of the left plenum |
| b | Flange connecting the left plenum by the hot channel |
| c | Hot channel |
| d | Flange connecting the right plenum by the hot channel |
| e | Lower surface of the right plenum |

1. Effect of cooling temperature on gas thermal hydraulics in the horizontal dual channel plenum P2PF.

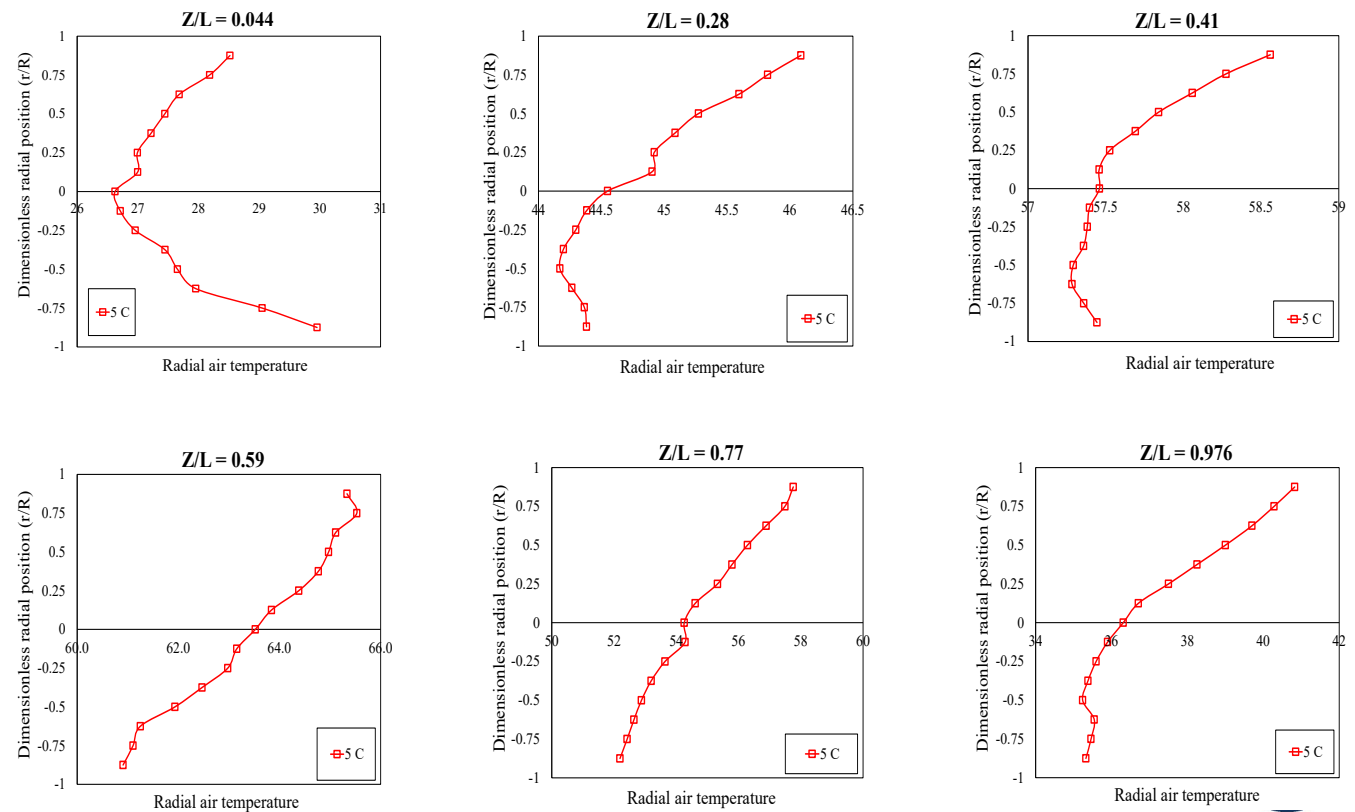
- Gas temperature distribution

Axial Gas temperature distribution



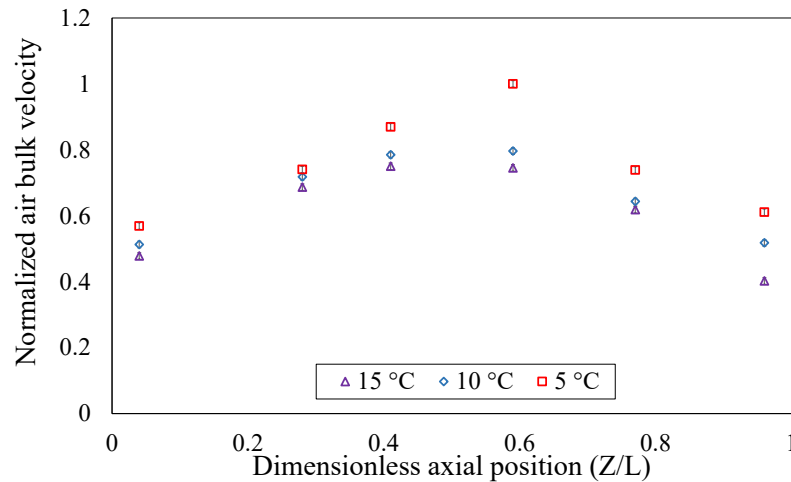
Schematic representation for the flow motion inside the hot channel (screw motion)

Radial gas temperature distribution for cooling water temperature (5 °C)



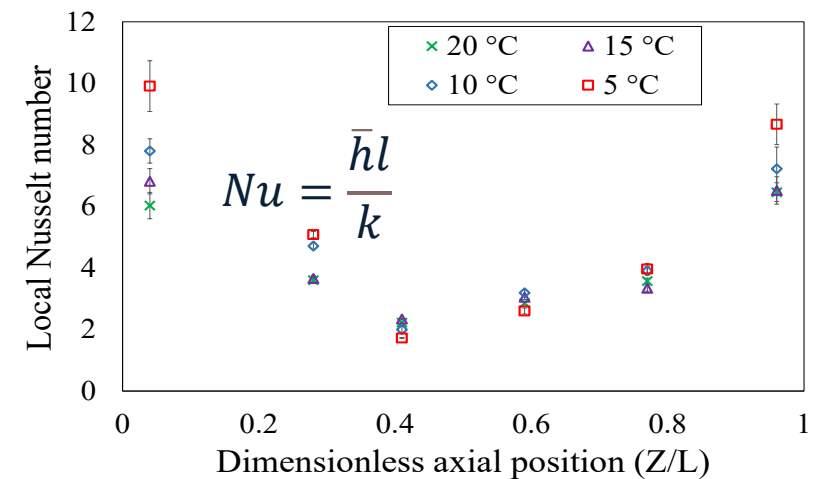
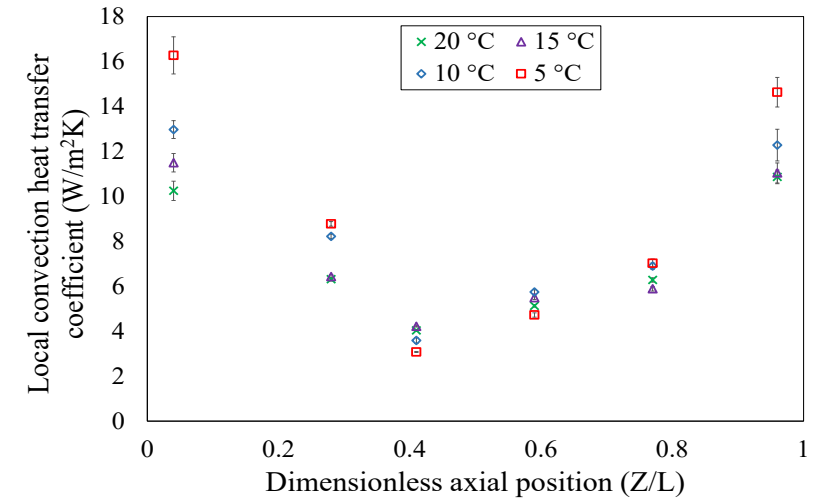
1. Effect of cooling temperature on gas thermal hydraulics in the horizontal dual channel plenum P2PF.

- Gas velocity



- Local convection heat transfer coefficient and Nusselt number

- The initial decrease in the convection heat transfer coefficient is due to the development of thermal boundary layers while the increase in the convection heat transfer coefficient is due to the flow reversal turbulence existing at the channel outlet.



2. Model development to predict the experimental axial average Nusselt number

The experimental axial average Nusselt number ($\overline{Nu}_{L,exp}$) is calculated by averaging of the 6 local Nusselt number (Nu) for each experimental condition

$$\overline{Nu}_{L,exp} = \frac{1}{n} \sum_{n=1}^{n=6} Nu$$

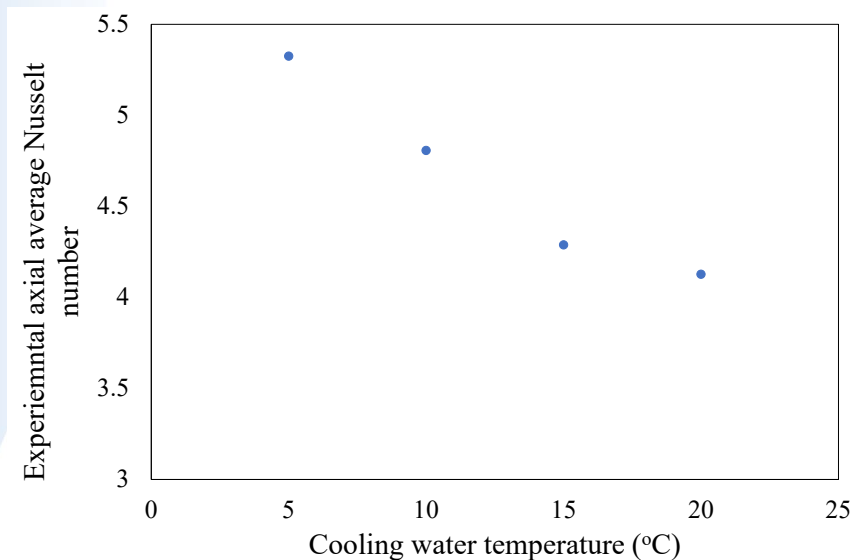
- The general correlation for natural convection in horizontal channels is expressed as Nusselt number function of Rayleigh number and the ratio between the channel diameter and channel length

$$\overline{Nu}_{L,predict} = f\left(\overline{Ra}_{L,exp}, \frac{D}{L}\right)$$

$$\overline{Ra}_{L,exp} = \frac{g\beta(T_{sL} - T_{b,iL})l^3}{\alpha\nu}$$

The Python package stats models, which implement the Ordinary Least Square (OLS) regression technique, has been used to predict the model

$$\ln(\overline{Nu}_{L,predict}) = 3.1761 \times \frac{D}{L} \times \ln(\overline{Ra}_{L,exp})$$




2. Model development to predict the experimental axial average Nusselt number

$$\ln(\overline{Nu}_{L,predict}) = 3.1761 \times \frac{D}{L} \times \ln(\overline{Ra}_{L,exp})$$

R^2 value, p-value, and AARE for the developed model.

| Experiment | $\ln(\overline{Nu}_{L,exp})$ | $\ln(\overline{Nu}_{L,predict})$ | R^2 | p-value | Overall AARE (%) |
|------------|------------------------------|----------------------------------|-------|---------|------------------|
| 5 °C | 0.7267 | 0.6627 | 0.995 | 0.00 | 6.16 |
| 10 °C | 0.6825 | 0.6641 | | | |
| 15 °C | 0.6329 | 0.6652 | | | |
| 20 °C | 0.6161 | 0.6657 | | | |

- The R^2 value is found to be 0.995, indicating that 99.5 % of the variation of the experimental axial average hot channel Nusselt number can be predicted by the developed model.
- The p-value is too low, showing that the model is statistically significant.
- The overall average absolute relative error (AARE) was found to be 6.16 %, indicating that the model provides excellent forecasting of the experimental axial average hot channel Nusselt number.

$$AARE = \frac{1}{n} \sum_{n=1}^{n=4} \frac{|\ln(\overline{Nu}_{L,predict}) - \ln(\overline{Nu}_{L,exp})|}{\ln(\overline{Nu}_{L,exp})}$$


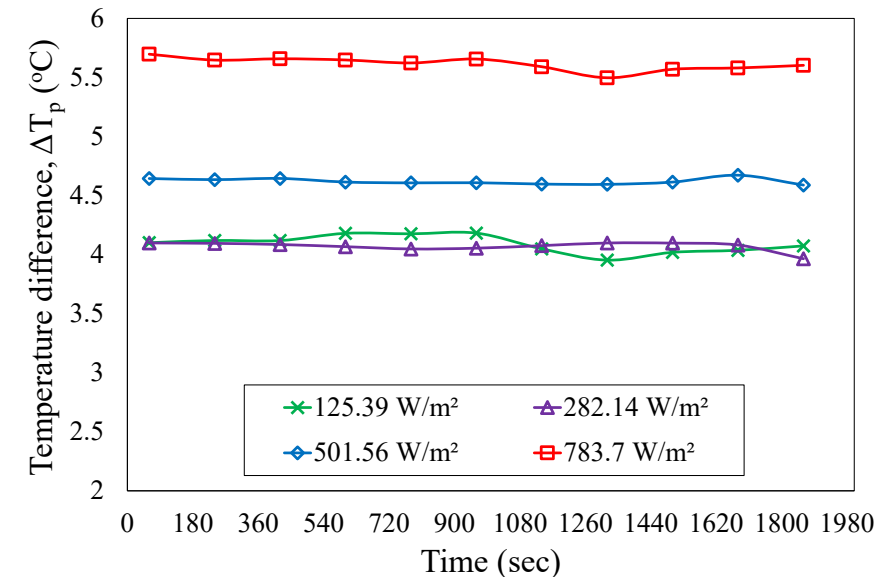
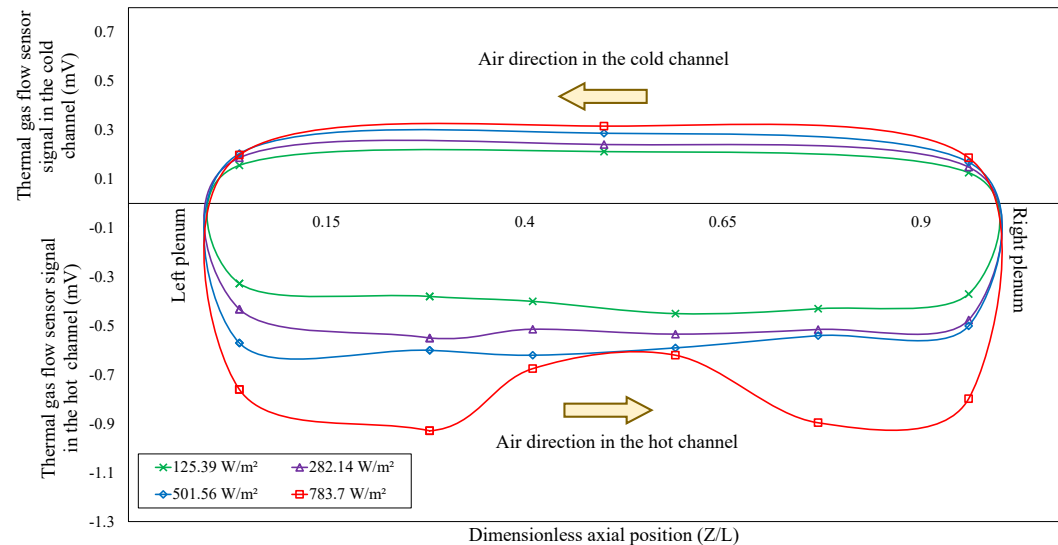
3. Effect of uniform heating and pressure on gas thermal hydraulics in the horizontal dual channel plenum P2PF

- Experimental conditions:

| Experiment | Air pressure (psi) | Heating Intensity (W/m ²) | Cooling water temperature (°C) |
|------------|--------------------|---------------------------------------|--------------------------------|
| 1 | 14.5 | 783.7 | 5 |
| 2 | 25 | | |
| 3 | 40 | | |
| 4 | 60 | | |
| 5 | 60 | 501.56 | |
| 6 | | 282.14 | |
| 7 | | 125.39 | |

- Gas flow direction
- Effect of heating intensity

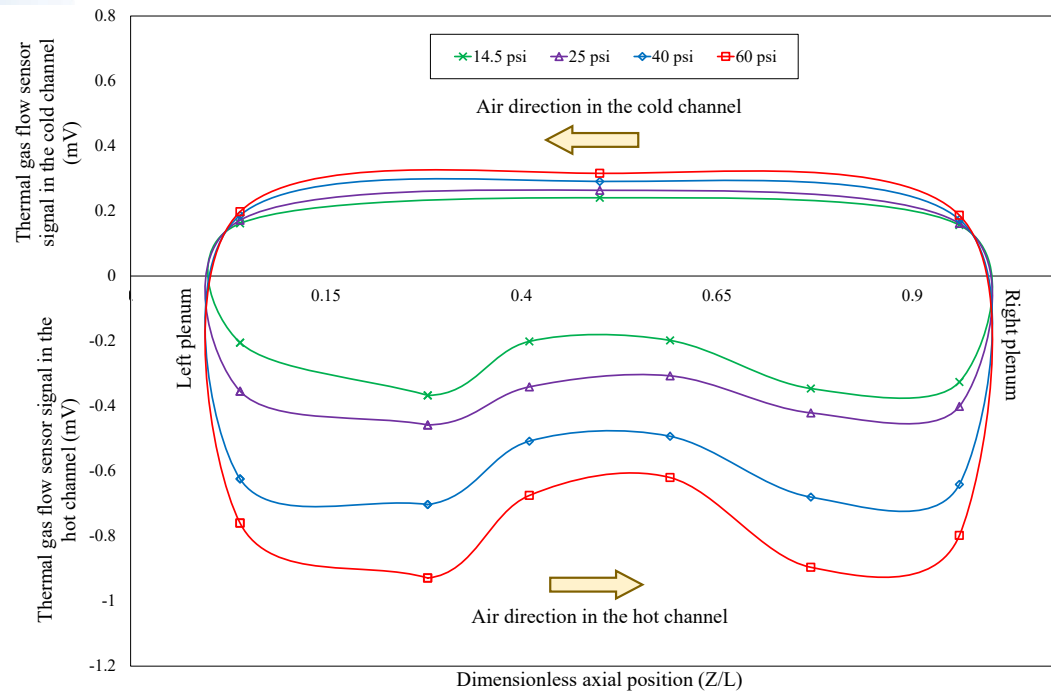
$$\Delta T_p = T_{air, right\ plenum} - T_{air, left\ plenum}$$



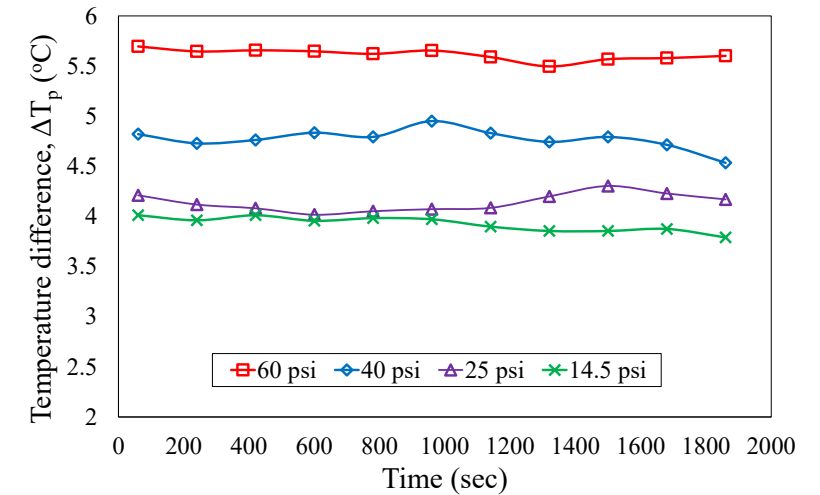
3. Effect of uniform heating and pressure on gas thermal hydraulics in the horizontal dual channel plenum P2PF

- Gas flow direction

Effect of pressure



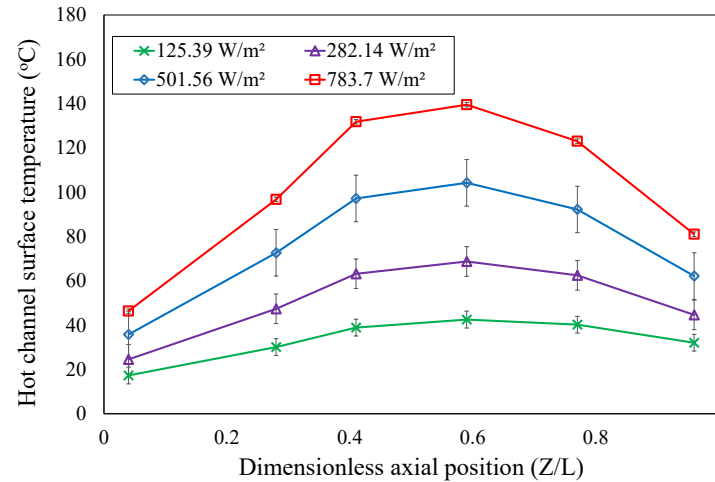
$$\Delta T_p = T_{air, right\ plenum} - T_{air, left\ plenum}$$



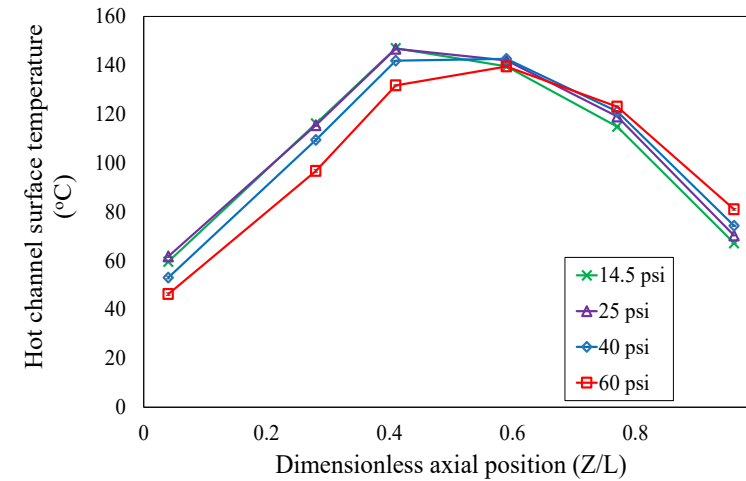
3. Effect of uniform heating and pressure on gas thermal hydraulics in the horizontal dual channel plenum P2PF

- Hot channel inner surface temperature

Effect of heating intensity

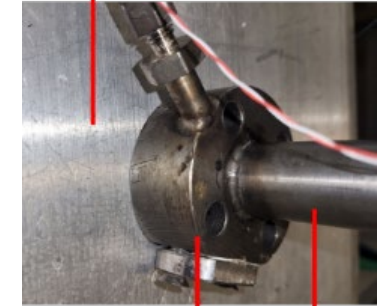


Effect of pressure



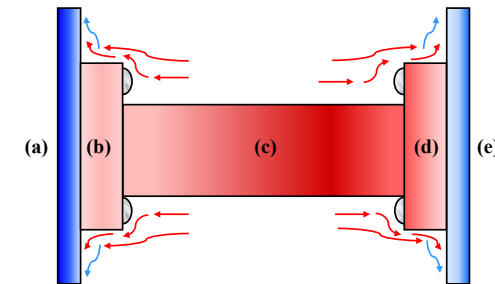
- There is a notable peak at the channel midsection as the heating intensity increases.
- The location of the peak surface temperature is shifted from the axial position ($Z/L=0.409$) to ($Z/L=0.59$) as the pressure increases.

Lower surface of the plenum



Flange connecting the plenum to the hot channel

Hot channel

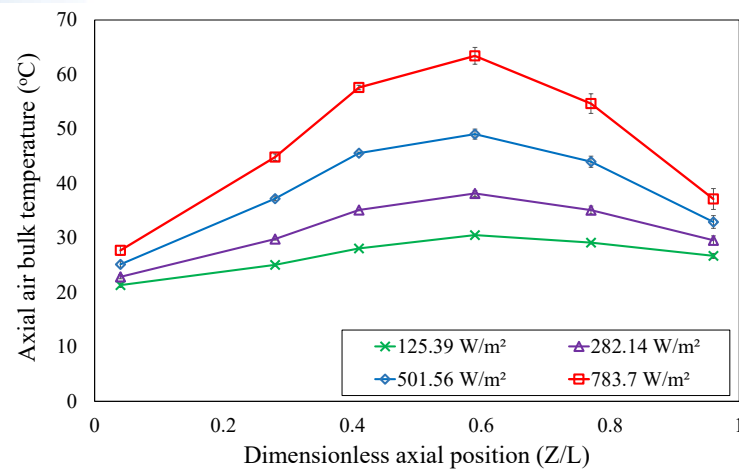


| | |
|---|---|
| a | Lower surface of the left plenum |
| b | Flange connecting the left plenum by the hot channel |
| c | Hot channel |
| d | Flange connecting the right plenum by the hot channel |
| e | Lower surface of the right plenum |

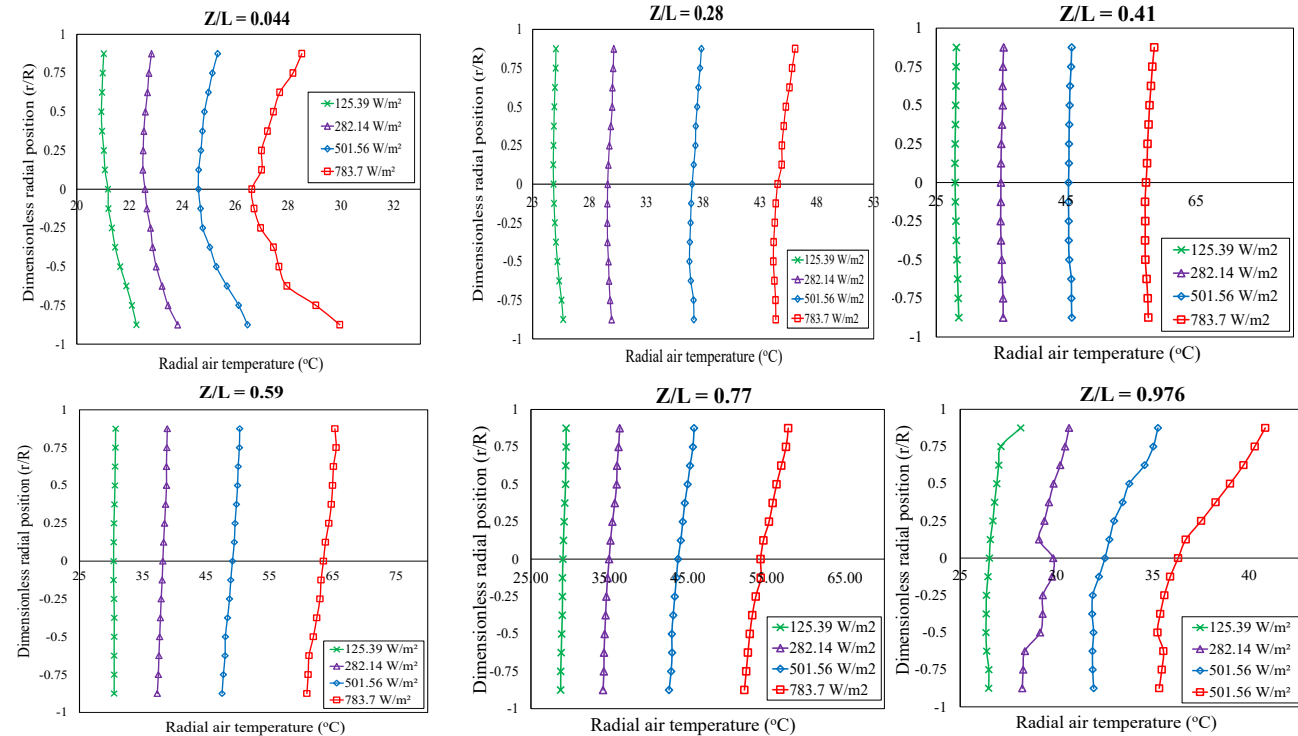
3. Effect of uniform heating and pressure on gas thermal hydraulics in the horizontal dual channel plenum P2PF

- Gas temperature distribution
 - Effect of heating intensity

➤ Axial temperature distribution



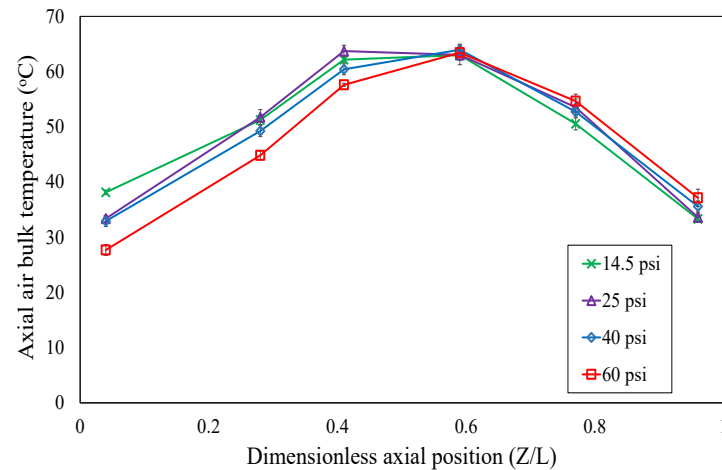
➤ Radial temperature distribution



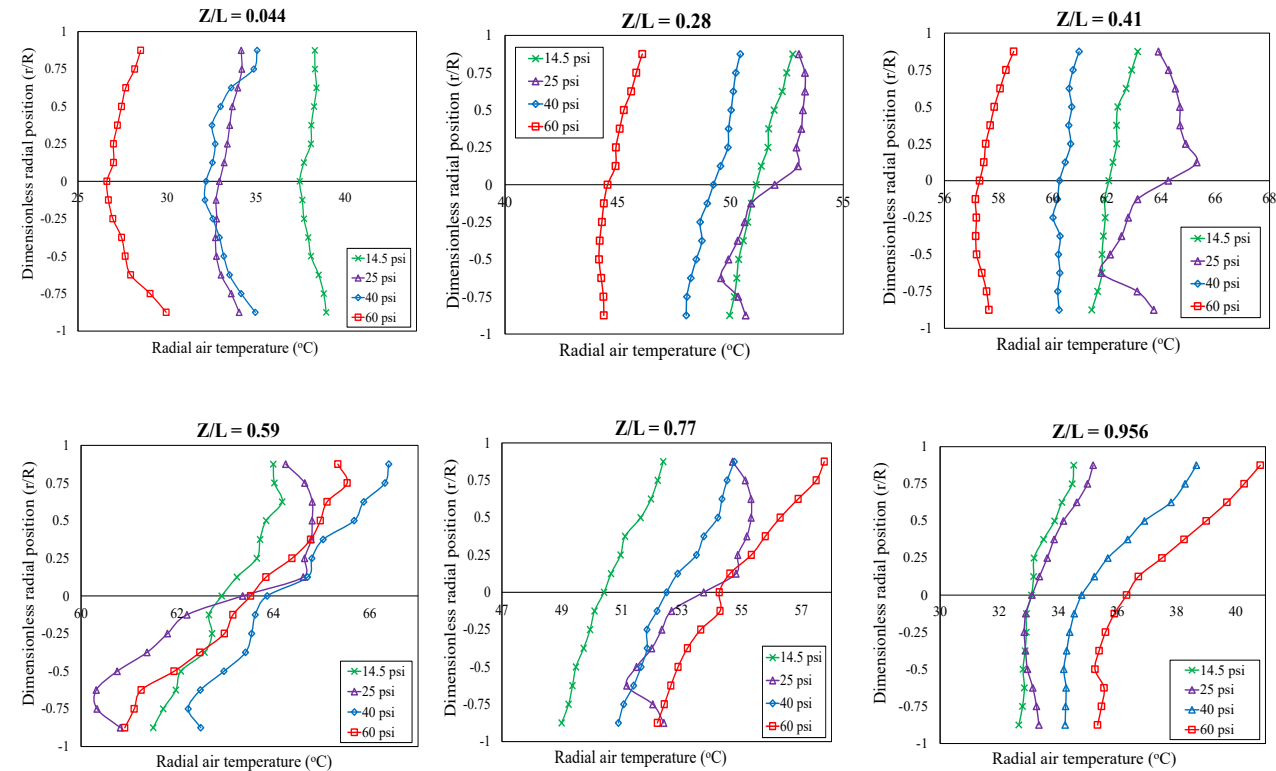
3. Effect of uniform heating and pressure on gas thermal hydraulics in the horizontal dual channel plenum P2PF

- Gas temperature distribution
 - ✓ Effect of pressure

➤ Axial temperature distribution

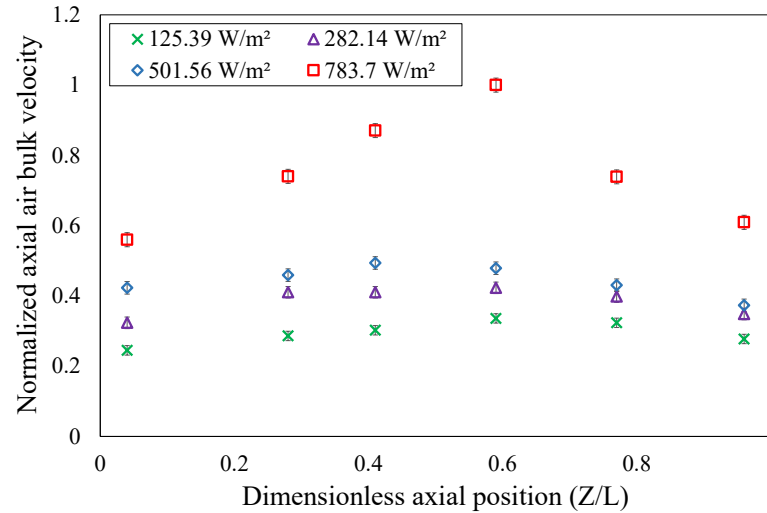


➤ Radial temperature distribution

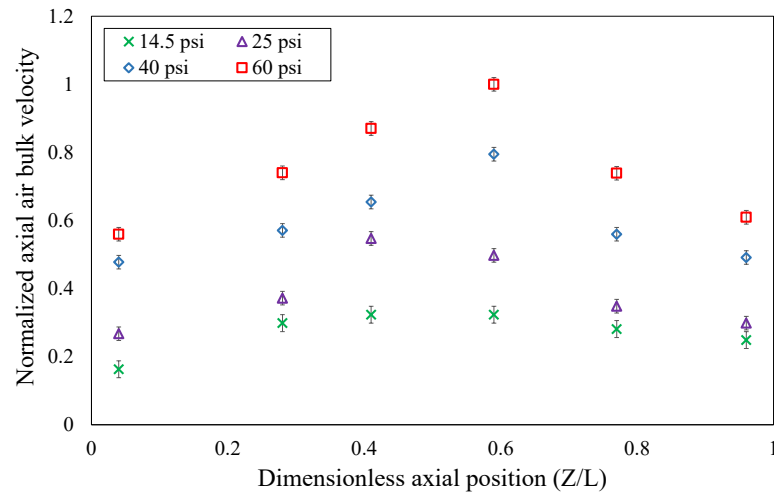


- Gas velocity distribution

- Effect of heating intensity

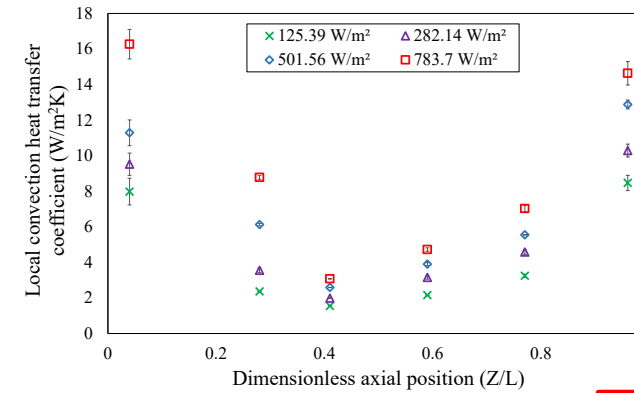


- Effect of pressure

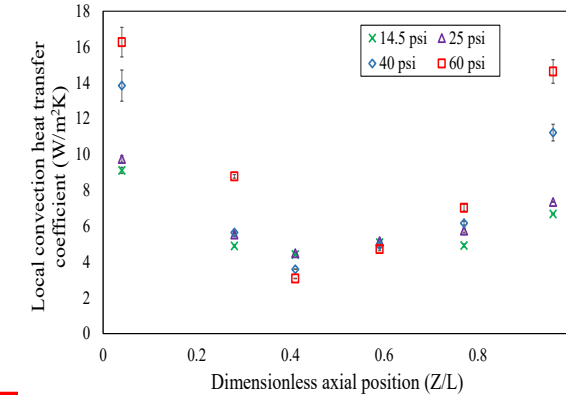


- Local convection heat transfer coefficient

- Effect of heating intensity

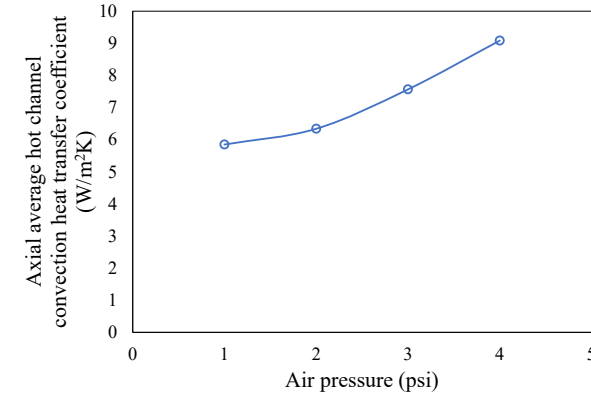
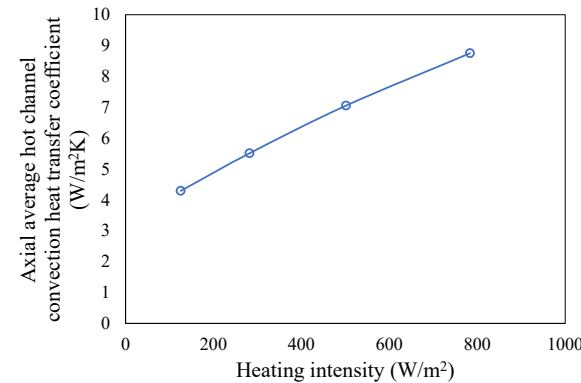


- Effect of pressure



$$h_m = \frac{1}{n} \sum_{N=1}^{n=6} \bar{h}$$

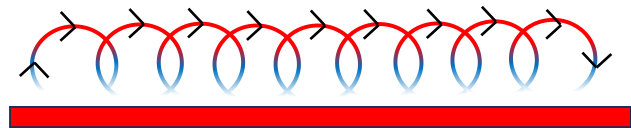
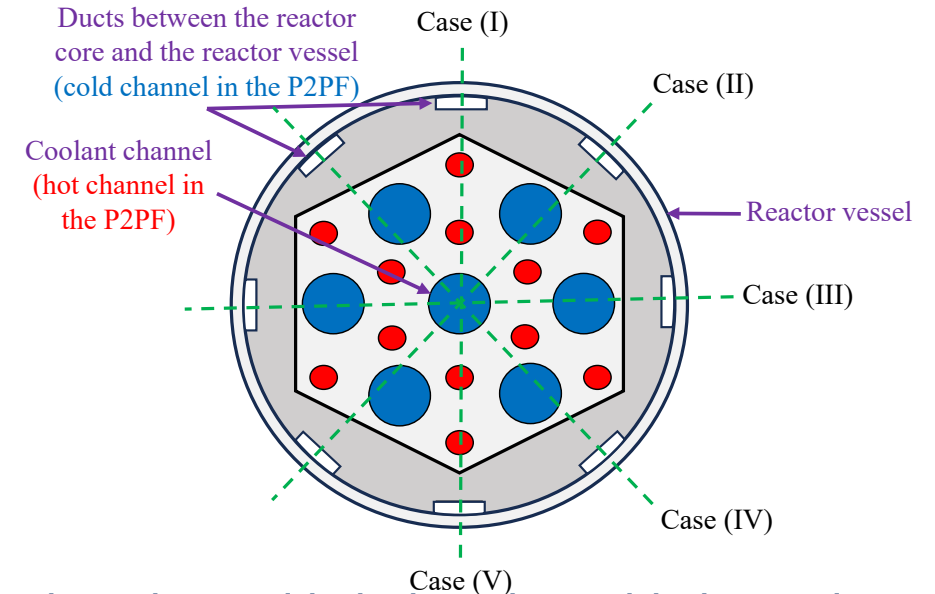
| | |
|-----------|--|
| n | Number of axial positions |
| h_m | Axial average hot channel convection heat transfer coefficient |
| \bar{h} | Local time-averaged convection heat transfer coefficient |



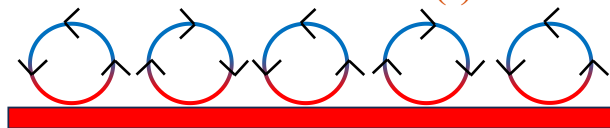
4. Effect of different horizontal orientations on gas thermal hydraulics in the horizontal dual channel plenum P2PF.

Experimental conditions:

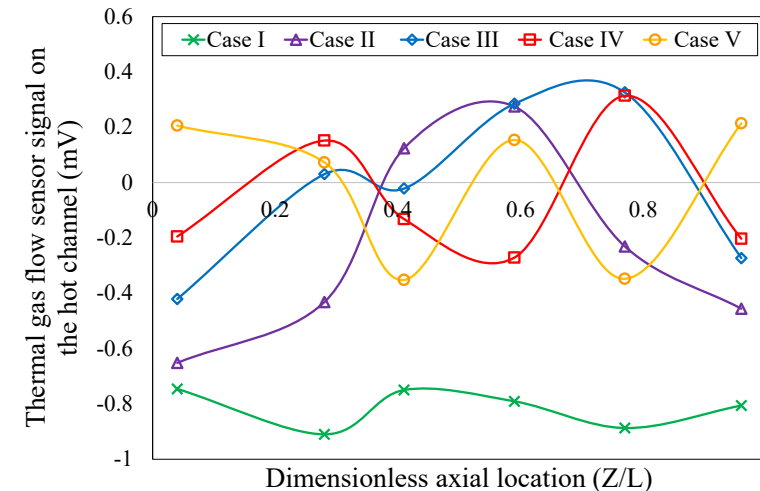
- Helium pressure (60 psi)
- Cooling water temperature (5 °C)
- Heating intensity (783.7 W/m²)
- Gas flow direction
- The flow is unidirectional for Case I only as the hot channel is below the cold channel, while the flow is unstable and there is no unidirectional flow for all other cases.



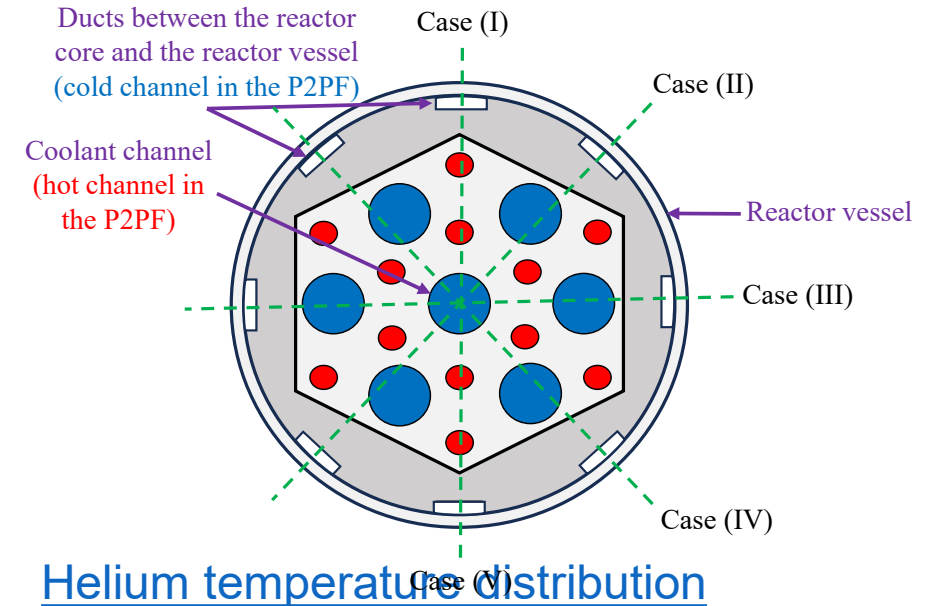
Schematic representation for the flow motion for Case (I)



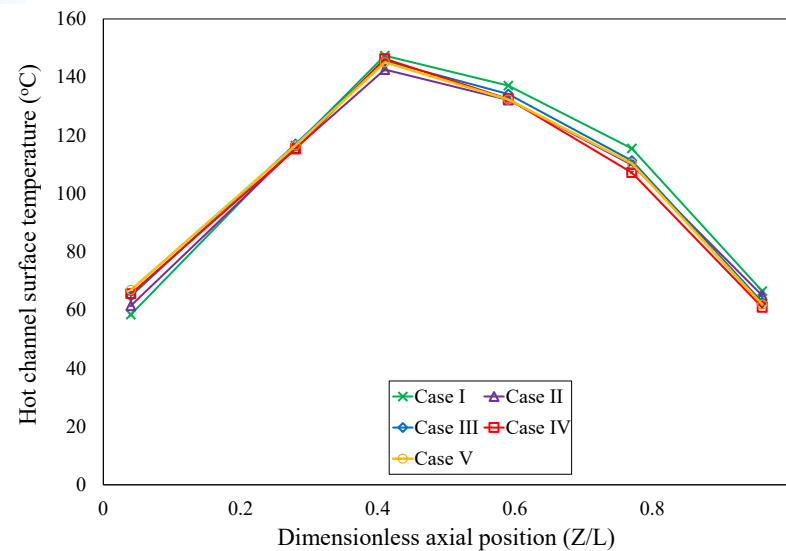
Schematic representation for the flow motion for Cases (II, III, IV, and V)



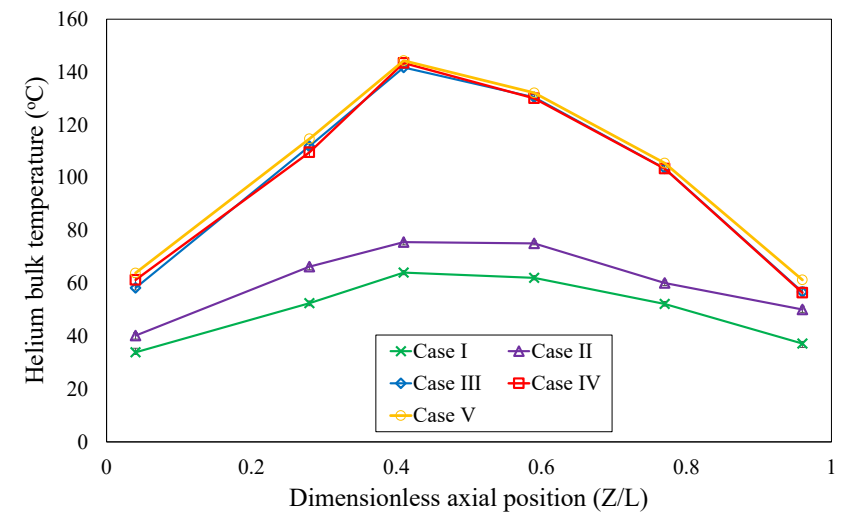
4. Effect of different horizontal orientations on gas thermal hydraulics in the horizontal dual channel plenum P2PF.



- Hot channel surface temperature distribution

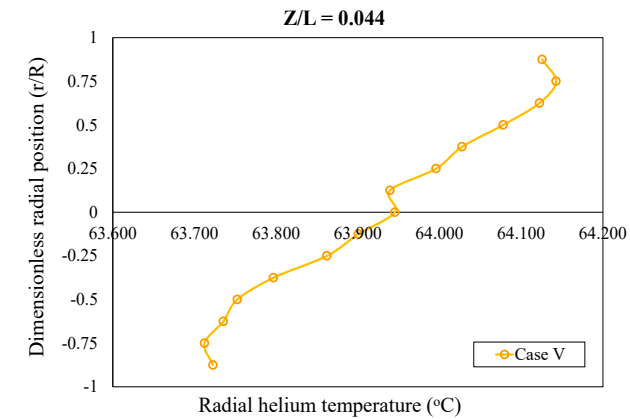
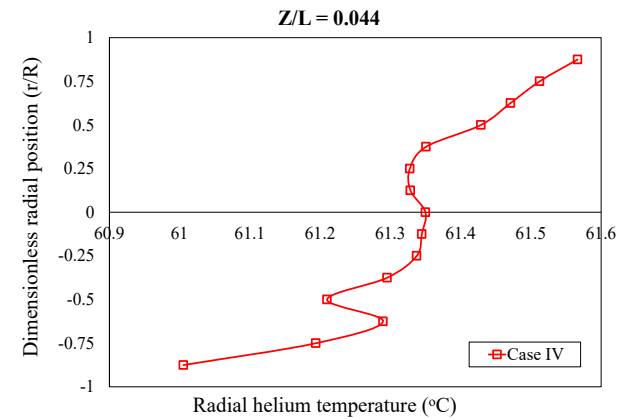
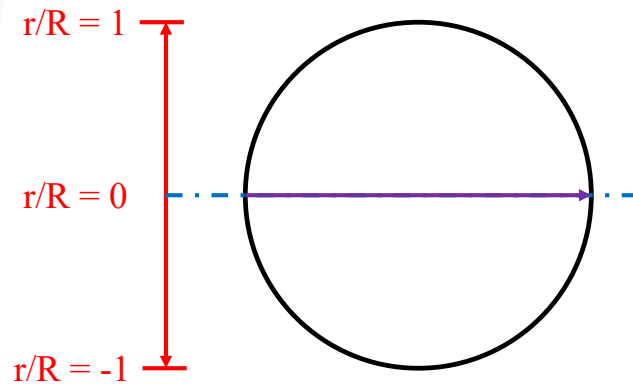
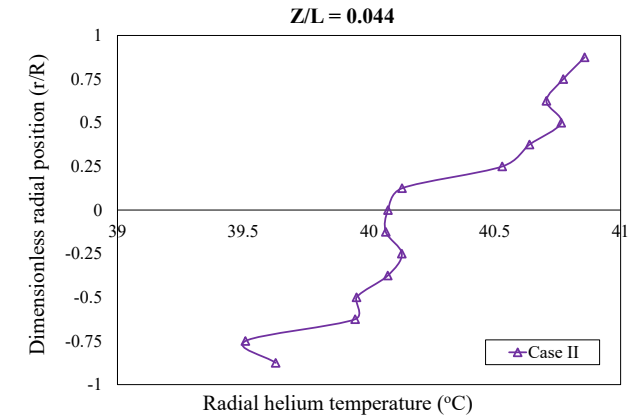
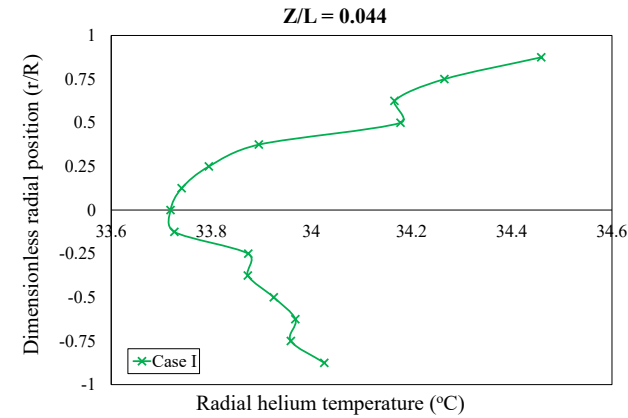
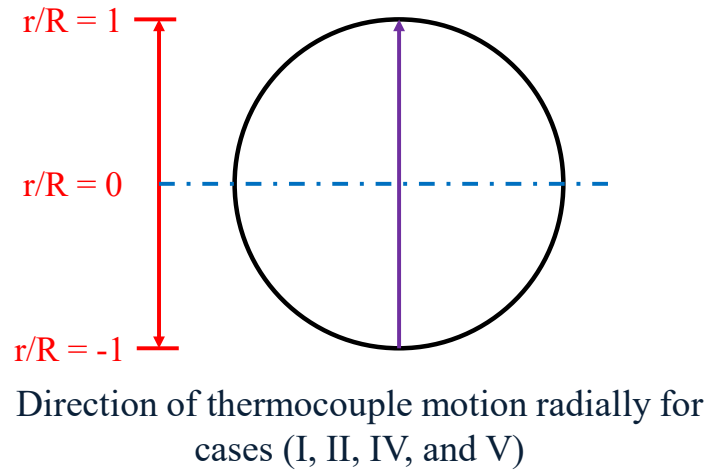


- Helium temperature distribution



4. Effect of different horizontal orientations on gas thermal hydraulics in the horizontal dual channel plenum P2PF.

- Radial helium temperature profile at $Z/L=0.044$



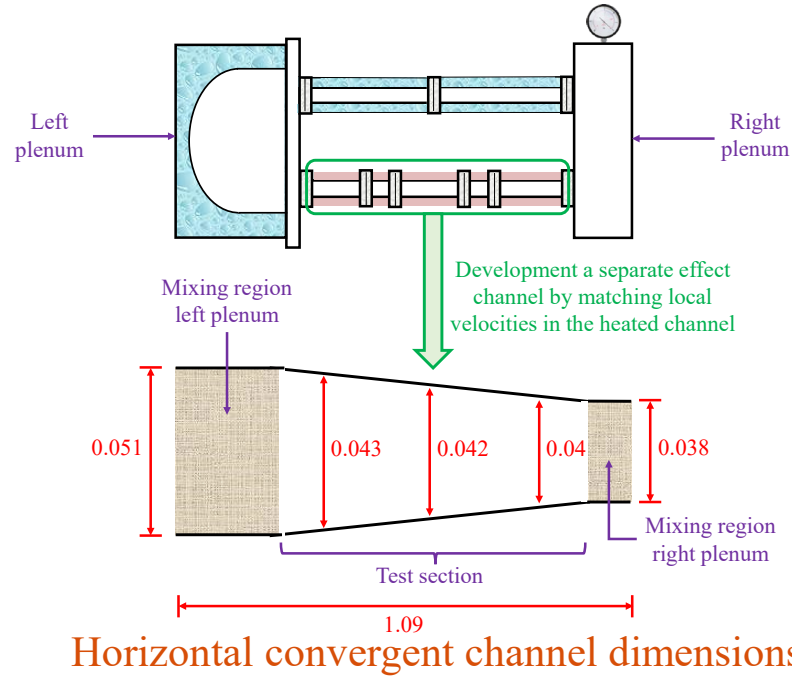
Direction of thermocouple motion radially for case (III)

Task 1.3. Investigate the gas dispersion in the horizontally oriented channels using the tapered tube to mimic local gas velocities inside the channels with gaseous tracer technique and methodology.

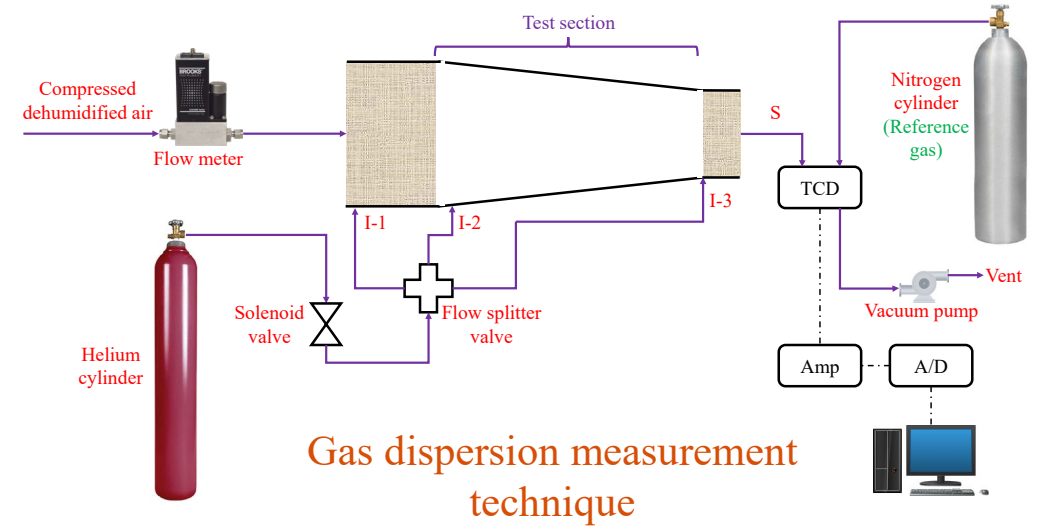
- Experimental investigation of gas dispersion inside the hot channel has been performed using the team's well-developed tracer technique, methodology and algorithm and implementing axial dispersion model on the horizontally oriented tapered tube that was designed to create the same local gas velocities measured along the lengths of the channels.



Horizontal orientation the gas dispersion convergent channel



- The convergent channel is divided into three regions:
 - ✓ Left mixing region (left plenum)
 - ✓ Right mixing region (right plenum)
 - ✓ Test section which mimics the hot channel without end effects
- To calculate the dispersion coefficient in the test section, we must determine:
 - a) The resident time in the left plenum
 - b) The output signal in the test section only



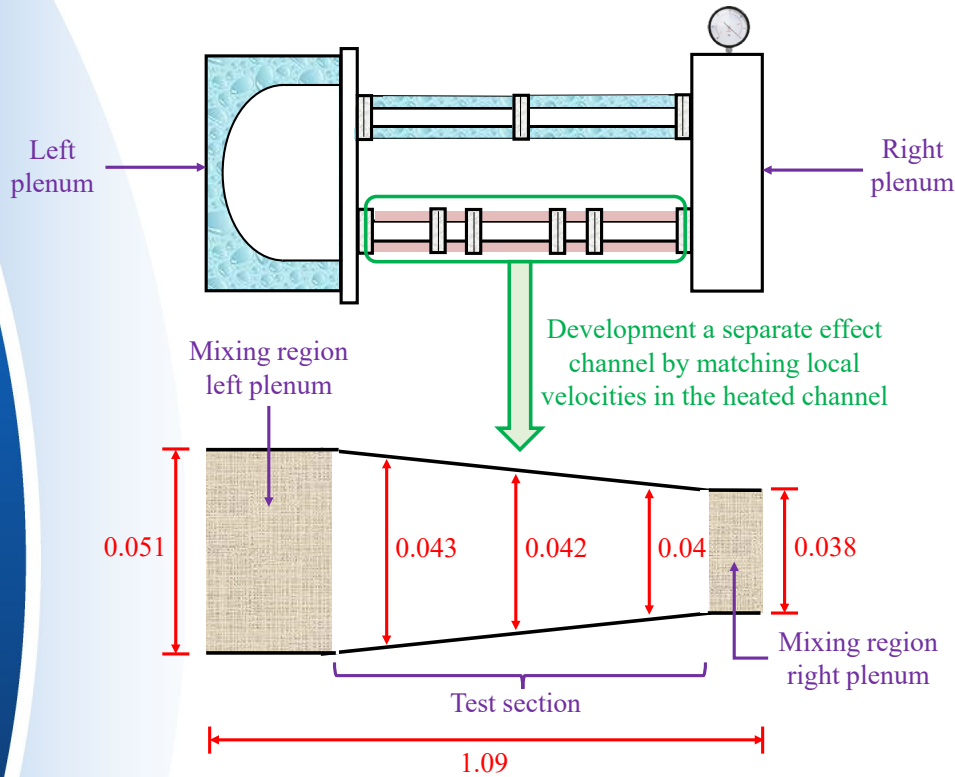
The designed three measurements for the gaseous tracer technique

| Measurement | Tracer injection | Tracer detection | Tracer signal | Dispersion zones |
|-------------|------------------|------------------|---------------|---|
| 1 | I-1 | S | C(1) | Sampling lines + measurement system + left plenum + test section + right plenum |
| 2 | I-2 | S | C(2) | Sampling lines + measurement system + test section + right plenum |
| 3 | I-3 | S | C(3) | Sampling lines + measurement system + right plenum |

- By using the deconvolution and one-dimensional axial dispersion model (1D-ADM), the axial gas dispersion coefficients can be estimated



Gas dispersion at different heating intensities



The convergent channel dimensions

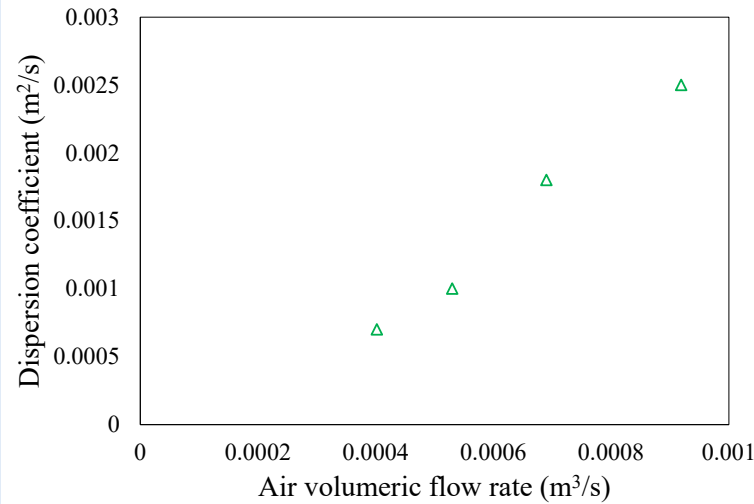
Air velocity in the convergent channel and the corresponding air velocity in the hot channel of the P2PF

| Heating intensity (W/m ²) | Inlet air volumetric flow rate to the convergent channel (m ³ /s) | Average air velocity in the convergent channel (m/s) | Average air velocity in the hot channel of the dual channel P2PF (m/s) |
|---------------------------------------|--|--|--|
| 125.39 | 0.000402 | 0.279 | 0.24 |
| 282.14 | 0.00053 | 0.368 | 0.314 |
| 501.56 | 0.00069 | 0.479 | 0.46 |
| 783.7 | 0.000919 | 0.638 | 0.628 |

- The convergent channel is divided into three regions:
 - ✓ Left mixing region (left plenum)
 - ✓ Right mixing region (right plenum)
 - ✓ Test section which mimics the hot channel without end effects



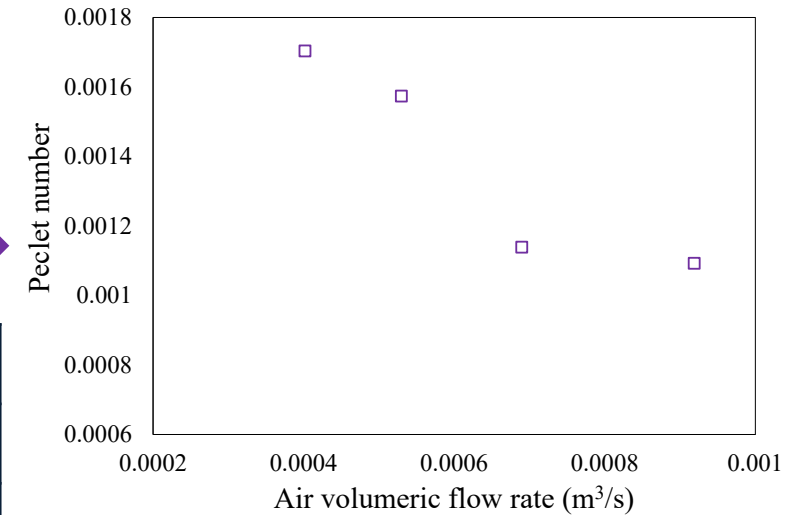
- Gas dispersion at different heating intensities



$$N_{pe} = \frac{Vd}{D}$$



| | |
|------------------------------|--|
| <i>V</i> | Average gas velocity in the convergent channel |
| <i>d</i> | Average convergent channel diameter |
| <i>D</i> | Axial gas dispersion coefficient |
| <i>N_{pe}</i> | Peclet number |



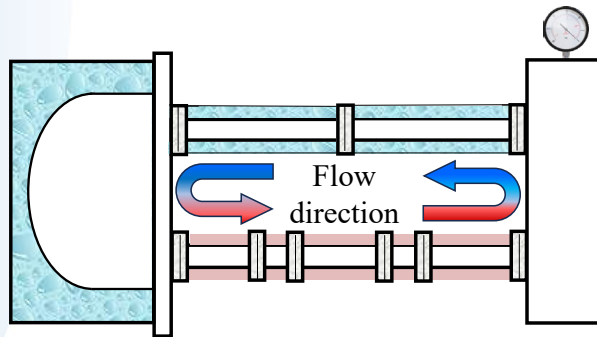
- ✓ Peclet number is a dimensionless group defined as the ratio of the advection transport rate to the diffusion transport rate.
- ✓ As the gas volumetric flow rate increases, Peclet number decreases. This shows that the diffusion rate dominates the mass transport by increase the gas volumetric flow rate



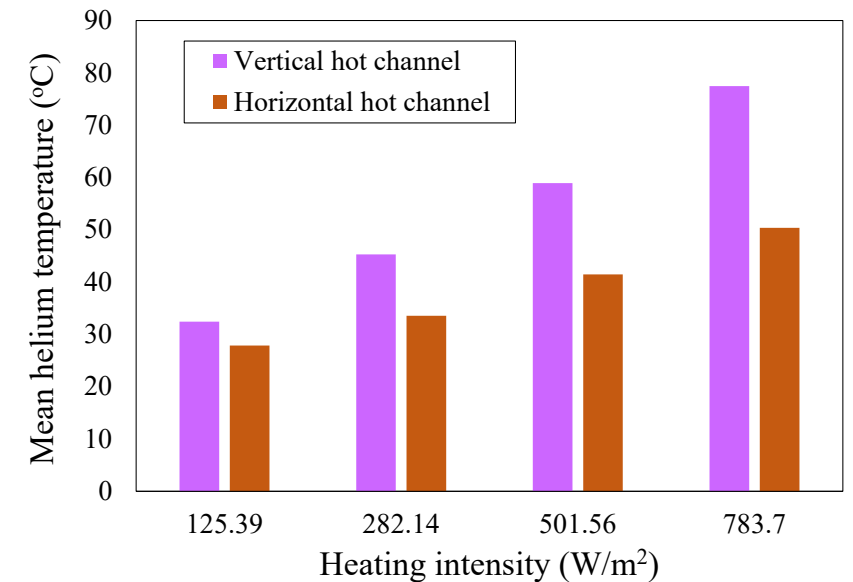
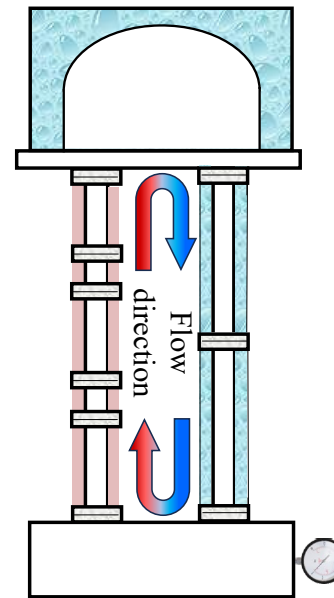
Task 1.4. Compare and discuss the results and findings between horizontally and vertically oriented dual-channel units.

- Comparing the effect of natural circulation between the horizontal and vertical configuration at different heating intensities (125.39 W/m², 282.14 W/m², 501.56 W/m², 783.7 W/m²)

Horizontal dual channel P2PF



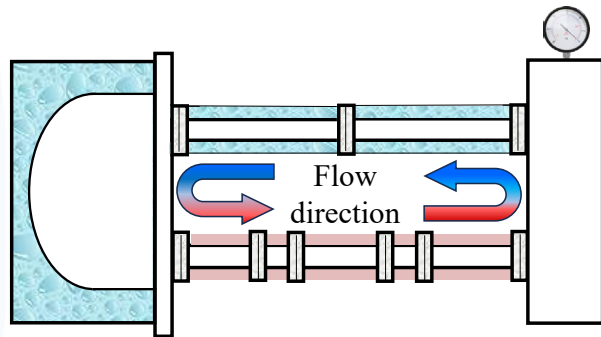
Vertical dual channel P2PF



Comparison between the natural circulation of helium in the horizontal and vertical P2PF at different heating intensities (125.39 W/m^2 , 282.14 W/m^2 , 501.56 W/m^2 , 783.7 W/m^2), gas pressure (60 psig), and cooling water temperature ($5 \text{ }^\circ\text{C}$)

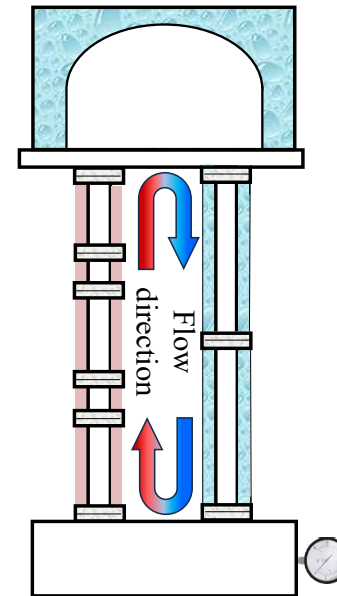
✓ Flow direction

➤ Horizontal dual channel P2PF



Helium flow is from the left plenum (referred to as the upper plenum in the vertical P2PF) to the right plenum (referred to as the lower plenum in the vertical P2PF) through the hot channel

➤ Vertical dual channel P2PF



Helium flow is from the lower plenum (referred to as the right plenum in the horizontal P2PF) to the upper plenum (referred to as the left plenum in the horizontal P2PF) through the hot channel

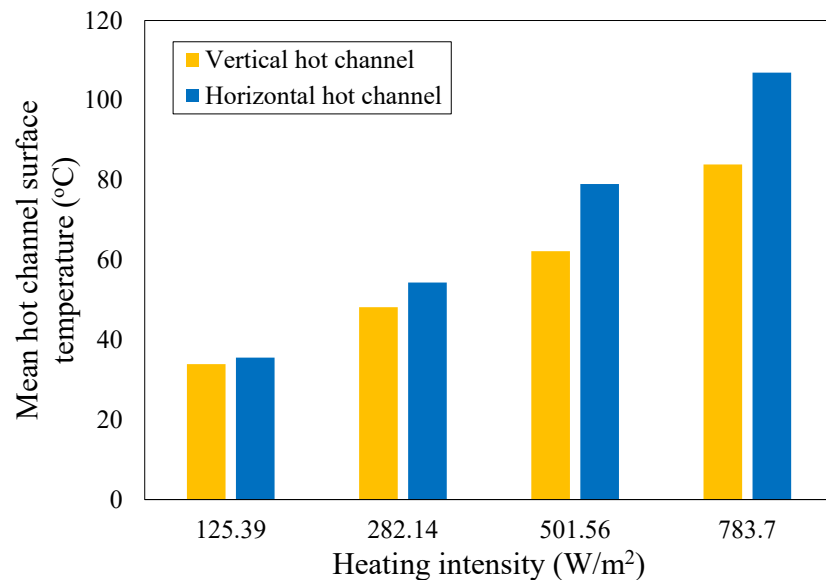


Comparison between the natural circulation of helium in the horizontal and vertical P2PF at different heating intensities (125.39 W/m², 282.14 W/m², 501.56 W/m², 783.7 W/m²), gas pressure (60 psig), and cooling water temperature (5 °C)

✓ Mean hot channel surface temperature

$$T_{s,m} = \frac{1}{n} \sum_{n=1}^{n=6} \bar{T}_s$$

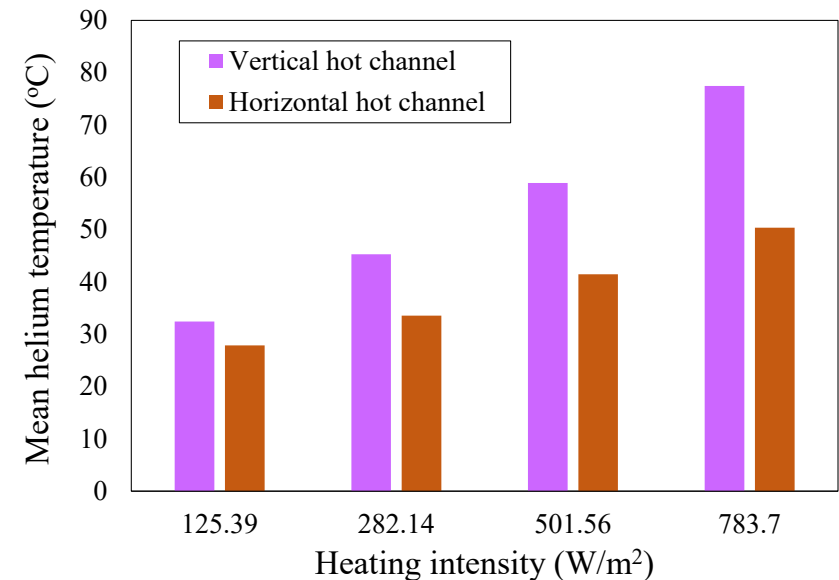
| | |
|-------------------------------|--|
| <i>n</i> | Number of axial positions |
| \bar{T}_s | Hot channel surface temperature at each axial location |
| $T_{s,m}$ | Mean hot channel surface temperature |



✓ Mean helium temperature

$$T_{b,m} = \frac{1}{n} \sum_{n=1}^{n=6} T_{b,i}$$

| | |
|-----------------------------|---|
| <i>n</i> | Number of axial positions |
| $T_{b,i}$ | Helium temperature at each axial location |
| $T_{b,m}$ | Mean helium temperature |

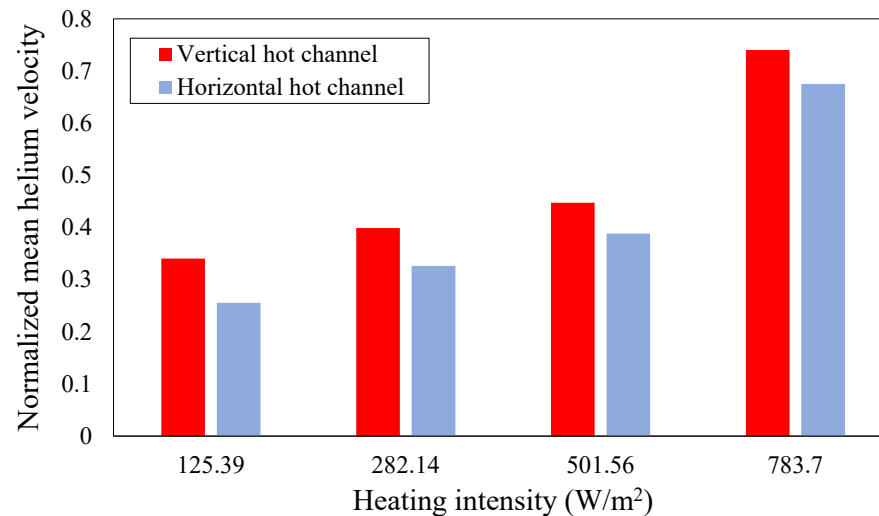


Comparison between the natural circulation of helium in the horizontal and vertical P2PF at different heating intensities (125.39 W/m², 282.14 W/m², 501.56 W/m², 783.7 W/m²), gas pressure (60 psig), and cooling water temperature (5 °C)

✓ Mean hot channel helium velocity

$$V_m = \frac{1}{n} \sum_{n=1}^{n=6} \bar{V}$$

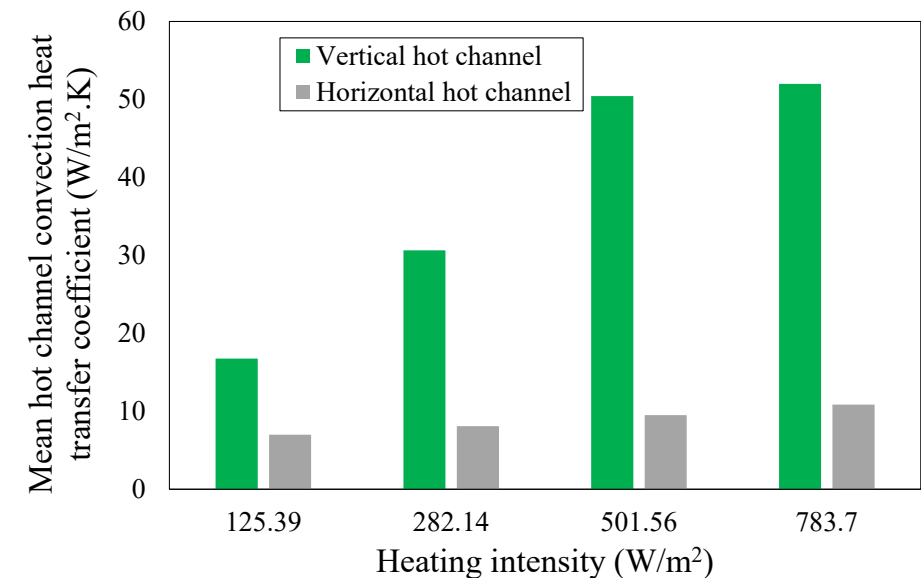
| | |
|-----------|--|
| n | Number of axial positions |
| \bar{V} | Helium velocity at each axial location |
| V_m | Mean helium velocity |



✓ Mean hot channel convection heat transfer coefficient

$$h_m = \frac{1}{n} \sum_{n=1}^{n=6} \bar{h}$$

| | |
|-----------|---|
| n | Number of axial positions |
| \bar{h} | Convection heat transfer coefficient at each axial location |
| h_m | Mean convection heat transfer coefficient |



Task 1.6. Execute uncertainty quantification and sensitivity analysis to the experimental measurements and the computed parameters.

- Uncertainty quantification for the gas temperature, velocity, and heat transfer coefficient has been carried out for the vertical and horizontal measurement for the dual channel plenum-to-plenum facility



Uncertainty quantification for the experiments carried out in the vertical dual channel plenum-to-plenum facility

- Uncertainty of gas temperature measurements
 - The uncertainty in temperature measurements arises from both the accuracy of the T-type thermocouple and the data acquisition system.
 - Through thermocouple calibration, it was determined that errors associated with the data acquisition system are negligible compared to the measurement error (i.e., thermocouple accuracy).
 - Therefore, the uncertainty in temperature measurements is primarily based on the thermocouples themselves, which have an accuracy of $\pm 1^\circ\text{C}$ or 0.75% of the measurement. This indicates that the maximum uncertainty in temperature measurements is $\pm 1.5^\circ\text{C}$



Uncertainty of gas velocity measurements

- The standard uncertainty values for the first three sources of velocity measurement uncertainties are 0.01, 0.005, and 0.0013, respectively.
- Temperature variation uncertainties result from two effects: (i) changes in the HWA sensor temperature and (ii) changes in air temperature. The standard uncertainty for both effects is determined as follows:

$$\text{Standard uncertainty due to HWA sensor temperature} = \frac{T_{b,i} - T_{\text{ambient}}}{U_{b,i}(T_w - T_o)} \left(\frac{1.396}{0.895} U_{b,i}^{-0.5} + 1 \right)$$

$$\text{Standard uncertainty due to air temperature} = \frac{T_{b,i} - T_{\text{ambient}}}{273}$$

Where T_{ambient} is the ambient room temperature, T_w is the wire temperature, and T_o is the calibration temperature.

- The overall temperature variation uncertainty is calculated by summing the results of the above equations. Afterward, the measured velocity uncertainty is determined as follows

$$\text{Uncertainty of measured } (U_{b,i}) = 2 \sqrt{(0.01)^2 + (0.005)^2 + (0.0013)^2 + \left(\text{Overall temperature uncertainty} \right)^2}$$

Therefore, the measured velocity uncertainty is found to range from 1.52 % to 1.76 % of the measured value.



• Uncertainty of heat flux measurements

- To quantify the uncertainty for the convection heat transfer coefficient, a differential approximation method is implemented. The uncertainty of the measured convection heat transfer coefficient ($W_{\bar{h}_i}$) depends on the uncertainties of three independent variables:
 - (1) surface temperature ($W_{\bar{T}_{s,i}}$),
 - (2) heat flux (W_{q_i}), and (3) air bulk temperature ($W_{T_{b,i}}$).

Therefore, the overall expression to assess the convection heat transfer coefficient uncertainty is formulated as follows:

$$W_{\bar{h}_i} = \pm \sqrt{\left(\frac{\partial h}{\partial q} \times W_{q_i}\right)^2 + \left(\frac{\partial h}{\partial T_s} \times W_{\bar{T}_{s,i}}\right)^2 + \left(\frac{\partial h}{\partial T_b} \times W_{T_{b,i}}\right)^2}$$

$$\frac{\partial h}{\partial q} = \frac{1}{T_{s,i} - T_{b,i}}$$

$$\frac{\partial h}{\partial T_s} = \frac{-q_i}{(\bar{T}_{s,i} - T_{b,i})^2}$$

$$\frac{\partial h}{\partial T_b} = \frac{q_i}{(\bar{T}_{s,i} - T_{b,i})^2}$$

$$W_{q_i} = \sigma_m \times q_i$$

$$W_{\bar{T}_{s,i}} = \sigma_m \times \bar{T}_{s,i}$$

$$W_{T_{b,i}} = \sigma_T \times T_{b,i}$$

It is found that the maximum uncertainty in the local heat transfer coefficient is equal to $\pm 0.23\%$.



Uncertainty quantification for the experiments carried out in the horizontal dual channel plenum-to-plenum facility at different heating intensities (125.39 W/m², 282.14 W/m², 501.56 W/m², and 783.7 W/m²)

- Uncertainty of gas temperature measurements
 - ✓ The uncertainty in temperature measurements arises from both the accuracy of the T-type thermocouple and the data acquisition system. Through thermocouple calibration, it was determined that errors associated with the data acquisition system are negligible compared to the measurement error (i.e., thermocouple accuracy). Therefore, the uncertainty in temperature measurements is primarily based on the thermocouples themselves, which have an accuracy of $\pm 1^\circ\text{C}$ of the measurement. **This indicates that the maximum percentage uncertainty in temperature measurements is 4.5%.**



Uncertainty quantification for the experiments carried out in the vertical dual channel plenum-to-plenum facility at different heating intensities (125.39 W/m², 282.14 W/m², 501.56 W/m², and 783.7 W/m²)

- Uncertainty of heat flux measurements
 - ✓ To quantify the uncertainty for the convection heat transfer coefficient, a differential approximation method is implemented. The uncertainty of the measured convection heat transfer coefficient ($W_{\bar{h}_i}$) depends on the uncertainties of three independent variables: (1) surface temperature ($W_{\bar{T}_{s,i}}$), (2) heat flux (W_{q_i}), and (3) air bulk temperature ($W_{T_{b,i}}$). Therefore, the overall expression to assess the convection heat transfer coefficient uncertainty is formulated as follows:

$$W_{\bar{h}_i} = \pm \sqrt{\left(\frac{\partial h}{\partial q} \times W_{q_i}\right)^2 + \left(\frac{\partial h}{\partial T_s} \times W_{\bar{T}_{s,i}}\right)^2 + \left(\frac{\partial h}{\partial T_b} \times W_{T_{b,i}}\right)^2}$$

$$\frac{\partial h}{\partial q} = \frac{1}{\bar{T}_{s,i} - T_{b,i}}$$

$$\frac{\partial h}{\partial T_s} = \frac{-q_i}{(\bar{T}_{s,i} - T_{b,i})^2}$$

$$\frac{\partial h}{\partial T_b} = \frac{q_i}{(\bar{T}_{s,i} - T_{b,i})^2}$$

$$W_{q_i} = \sigma_m \times q_i$$

$$W_{\bar{T}_{s,i}} = \sigma_m \times \bar{T}_{s,i}$$

$$W_{T_{b,i}} = \sigma_T \times T_{b,i}$$

It is found that the maximum uncertainty in the local heat transfer coefficient is equal to $\pm 3\%$.



Uncertainty quantification for the experiments carried out in the vertical dual channel plenum-to-plenum facility at different heating intensities (125.39 W/m², 282.14 W/m², 501.56 W/m², and 783.7 W/m²)

- Uncertainty of gas velocity measurements
 - ✓ The uncertainty in velocity measurements arises from both the accuracy of the thermal gas flow sensor and the data acquisition system. The data acquisition system error is negligible in comparison to the error of the thermal gas flow sensor. Therefore, the uncertainty in velocity measurements is primarily based on the thermal gas flow sensor itself, which have an accuracy of less than 2% of the measured value.



Step 2



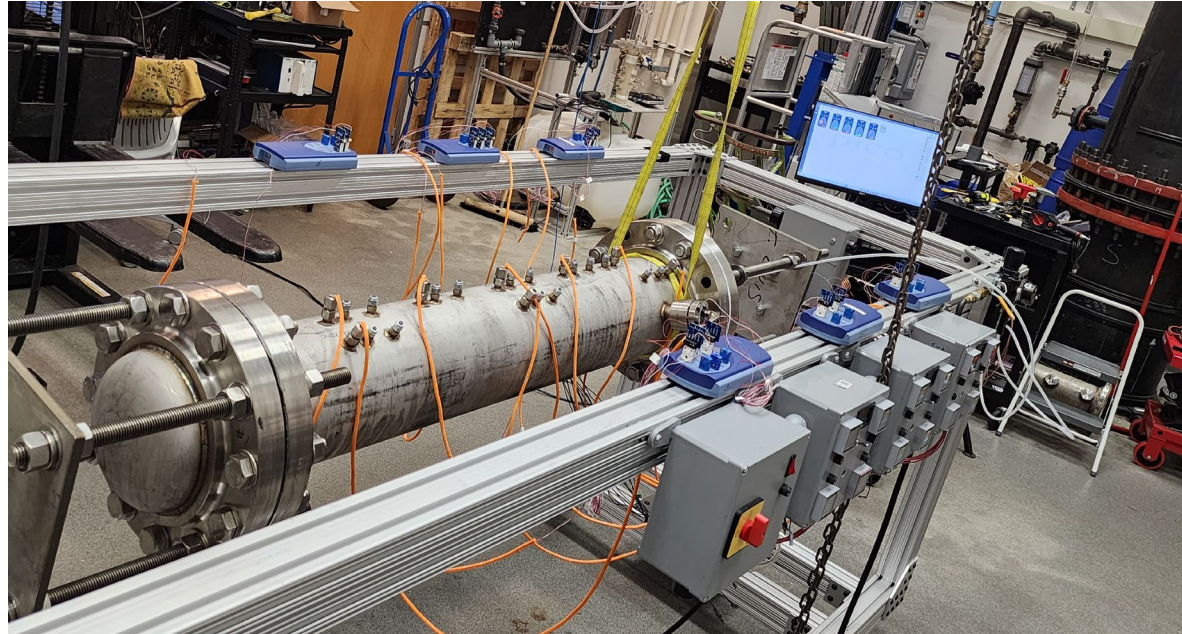
Task 2.1. Comprehensive literature review

- A comprehensive literature review of the high-temperature, gas-cooled prismatic reactor core and of CFD simulations of heat transfer in prismatic reactors under normal and PCC conditions has been performed.
- This review has aided in designing the experimental prismatic core and in overcoming the design challenges.
- Additionally, this review is also used for critical evaluation of the differences between vertically and horizontally orientated prismatic blocks.



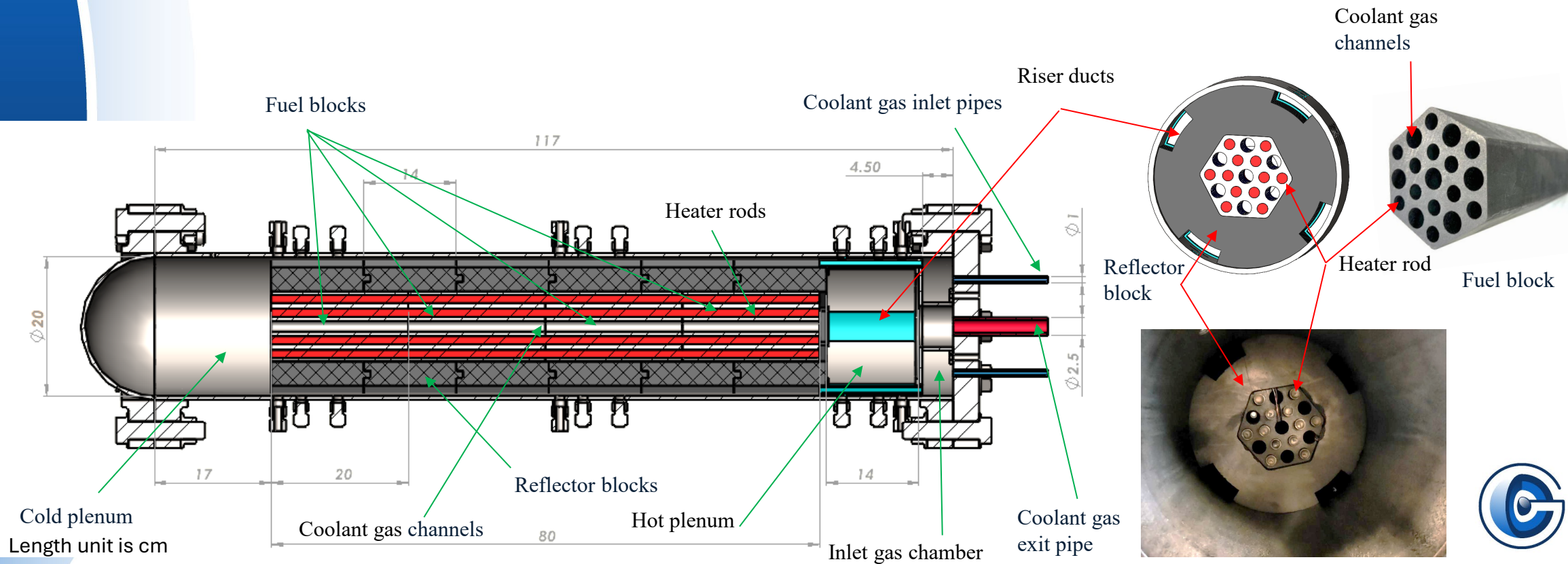
Task 2.2: Design, manufacture, test, and employ scaled-down separate and mixed-effects multiblock and multilayers of prismatic core experiments representing the standard Fort St. Vrain/MHTGR-350 prismatic core that can be operated up to 5 MPa and 1,500°C.

- Based on geometrical similarities and dimensionless ratios, a high-temperature, high-pressure experimental system mimicking the core of a micro HTGR reactor was designed and manufactured.



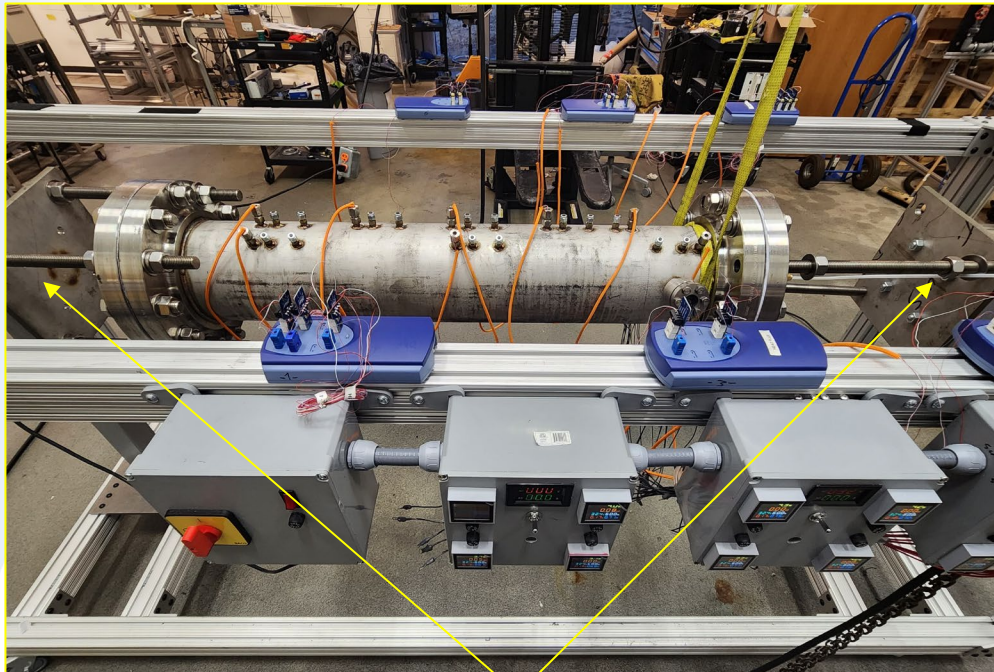
Major Design Characteristics

- The reactor core consists of hexagonal graphite fuel blocks, graphite reflector blocks, and cold and hot plena, all contained in a reactor pressure vessel (RPV) and can operate at temperatures up to 1500°C and pressures up to 5 MPa.
- The fuel blocks contain coolant channels and blind channels for heater rods.

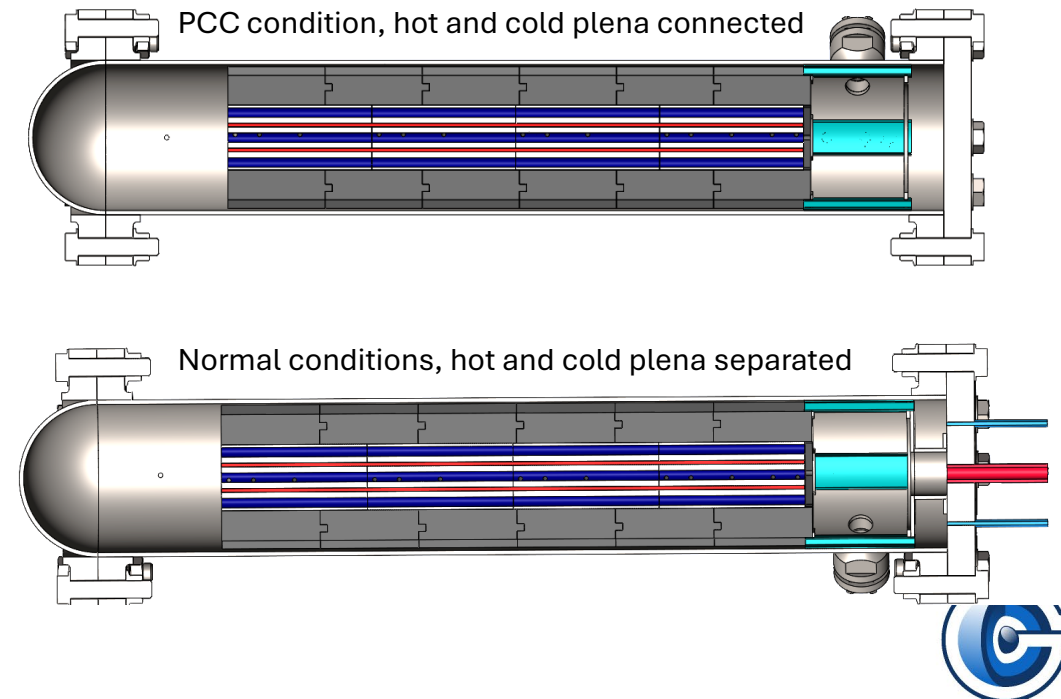


Major Design Characteristics

- The system can adapt to both vertical and horizontal orientations.
- The whole unit is mounted on a circle gear that can be rotated to change the position of the integrated measurement techniques: hot wire anemometer, heat transfer sensor, thermal flow sensors, and thermocouples.
- The system is designed to operate under normal operation (with coolant flow) and pressurized conduction cooldown (PCC) conditions.



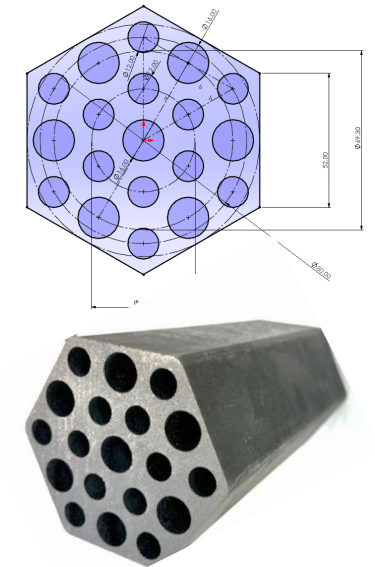
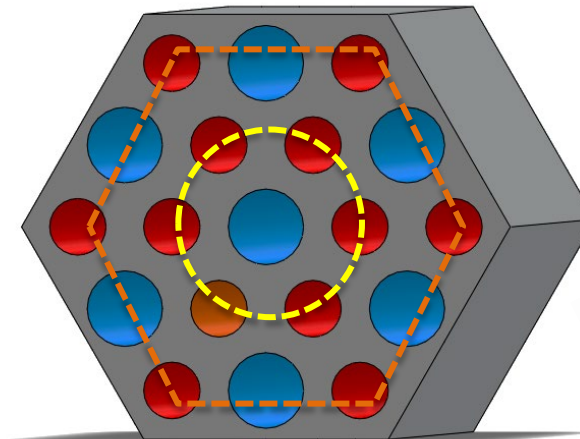
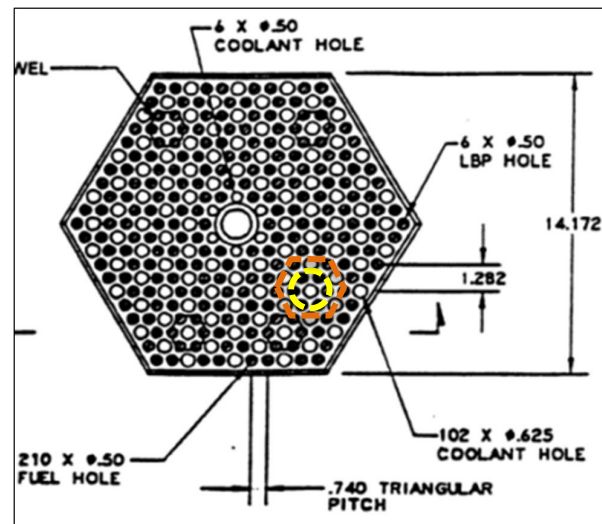
Rotation gear



Fuel and Reflector Elements Description

- The fuel blocks are scaled versions of the reference reactor fuel block and are stacked in 4 layers to form a single fuel column.
- Each fuel block contains 7 coolant channels and 12 blind heater rod channels.
- The size of the coolant channels and the fuel rod channels is kept the same as in the real-scale design of the MHTGR-350.

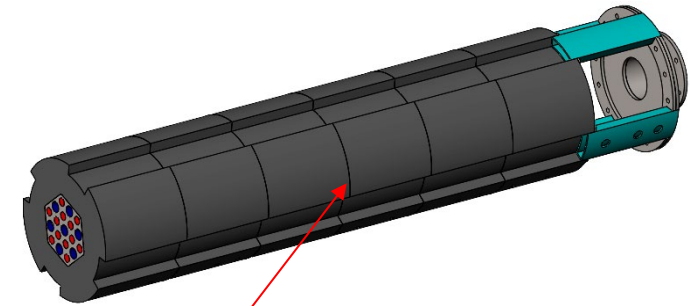
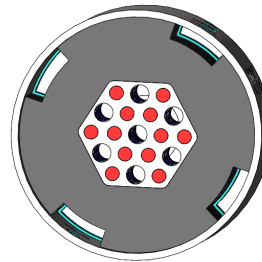
MHTGR-350 fuel block



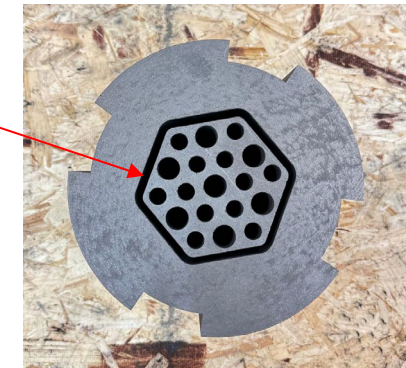
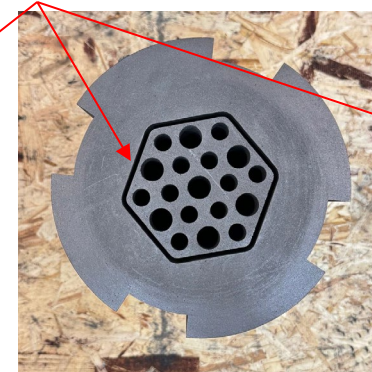
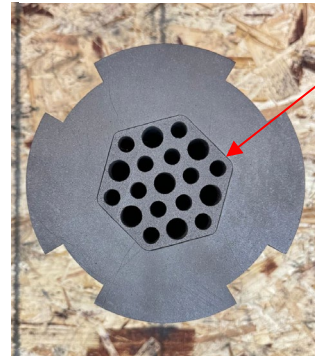
| | | |
|--|---------|--------|
| Coolant Hole Diameter | 1.6 cm | 1.6 cm |
| Fuel Hole Diameter | 1.2 cm | 1.2 cm |
| Fuel/Coolant Pitch (triangular) | 1.8 cm | 2 cm |
| Number of Fuel Holes/Number of Coolant Holes | 2/1 | ~ 2/1 |
| Block Pitch | 36 cm | 9 cm |
| Cross-section area of cooling channels | 18.28 % | 20% |
| Cross-section area of the fuel channels | 21.67% | 19 % |

Fuel and Reflector Elements Description

- The reflector blocks are stacked in 6 layers to form a cylindrical structure surrounding the fuel column.
- The riser channels in the reflector blocks connect the hot and cold plena.
- The fuel and reflector blocks' designs incorporate bypass gaps of different sizes, including no gap, 3 mm, and 5 mm.



Adjustable bypass gaps



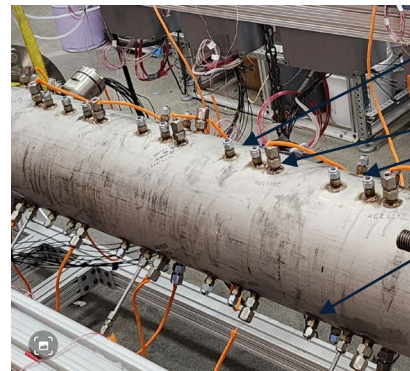
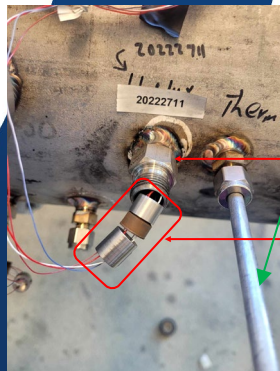
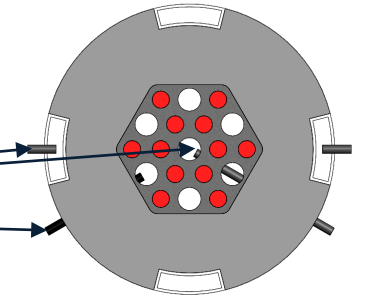
Task 2.3. Design, develop, test, and utilize a novel scaled-down block of integrated advanced measurement techniques.

Advanced measurement techniques have been integrated and embedded in the reactor as following

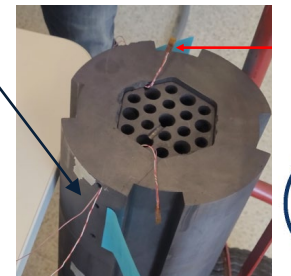
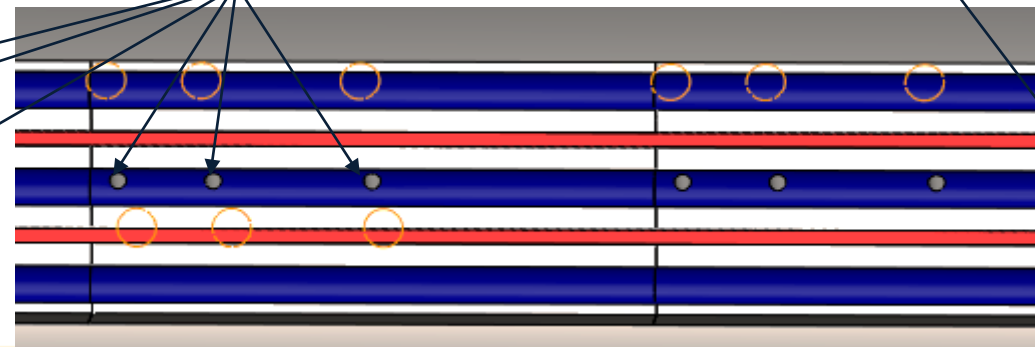
- 16 surface flush-mounted heat transfer sensors to measure convective heat transfer coefficients along the coolant and riser channels and bypass gaps, surface temperatures, and comparative rates of convective and radiative heat transfer.
- 16 thermocouples to measure temperature profiles of the coolant gas in the channels and gaps, and the location of peak temperature and its temporal variation profiles axial length channel and over diameter, and gap thickness.
- 14 HWA probes thermal flow sensors to measure local gas velocity profiles and flow direction across the diameter of the channels and thickness of the gaps, and timescales for the onset of natural convection.
- Pressure gauge to measure system pressure.
- Voltmeters and ammeters measure the heating power.



flush-mounted
heat transfer
sensors



Measurement ports



Major Challenges

- Machining the Graphite Blocks

Although our team designed and created 3-D models of the fuel and reflector blocks, finding a vendor to machine the blocks consistent with our design posed challenges and often required long lead times.



- Preventing Gas Leaks around the sensors and heater wires

Preventing gas leaks around the heat flux and heater wires posed serious challenges, especially at high pressures. Extensive research and testing of various proof-leak fitting designs were necessary to resolve this issue. These proof-leak fittings are crucial for the reactor design as they allow the dismantling of the fuel and reflector blocks for gap-size adjustments without compromising the sensor and heater wires, which could happen when the wires are glued at the measurement ports to prevent leaks. It is worth mentioning that the reactor is equipped with a comprehensive array of sensors, each with 0.5 mm wires.

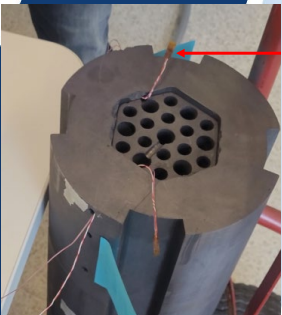


Heat flux foil sensor port

Leak-proof fittings

- Fixing the Heat Flux Sensors in Narrow Channels

Fixing the flush-mounted heat flux sensors on the graphite surface and routing the sensor wires through tiny holes in the fuel and reflector blocks required multiple attempts and trials to resolve.



Work in Progress and Future Work

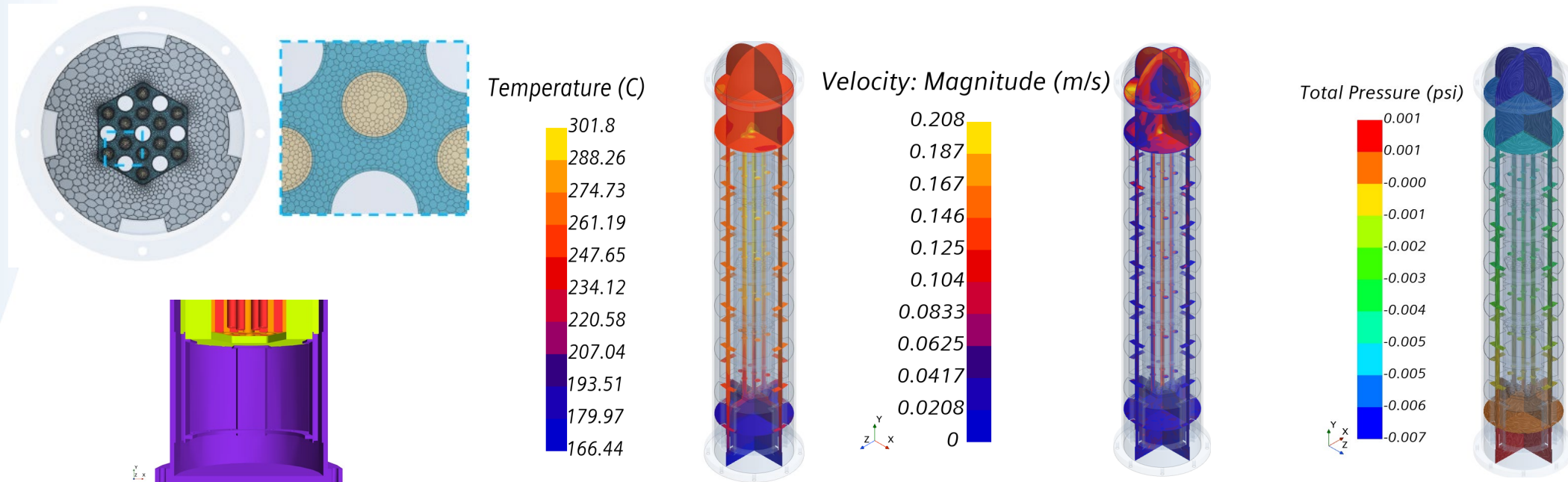
Task 2.4. Perform experimental investigations under normal operation and PCC conditions and analyzing the results

- Due to supply delays and manufacturing challenges, the experimental work of this task has been delayed.
- Currently, experiments to investigate the mentioned parameters are in progress for horizontal and vertical orientations.
- The investigations include normal operations occurring when helium flows continuously (high gas flow rates) and under natural convection (PCC) conditions when helium flow is interrupted in horizontally oriented channels.
- The experimental conditions include combinations of various power rates and system pressure.
- The measurement techniques will only be used within their critical limitations using the three developed measurement blocks.



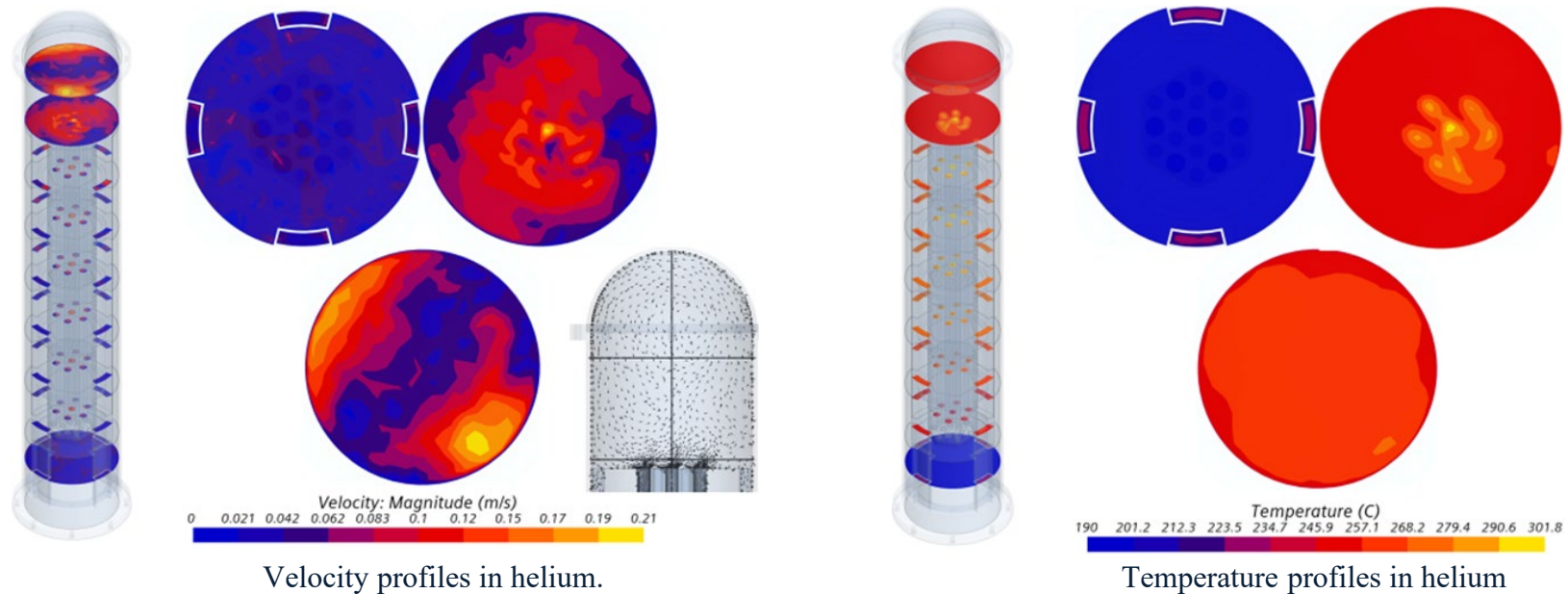
Meanwhile, we performed CFD simulation of thermal hydraulics for the designed setup at the designed experimental conditions.

- Using this design, PCC conditions in the vertical configuration were analyzed at a power density of 6.3 MW/m^3 (integrated heat load of $\sim 6 \text{ kW}$) operated at a pressure of 6.39 MPa using helium as the working fluid.
 - Highest temperature occurs in the core, due to convective cooling of the fuel rod ends, as well as indirect heat transfer from the fuel rods through the fuel blocks



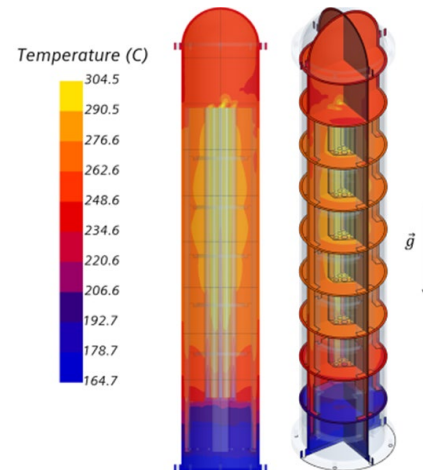
Selected CFD results

- In the core, it is suggested that a greater portion of the heat is transported to the cold plenum (top). Coupled with impingement on the plenum surface, recirculation patterns arise
- Coupled with impingement on the plenum surface, recirculation patterns arise, and vector plots of flow exiting the core confirm this observation

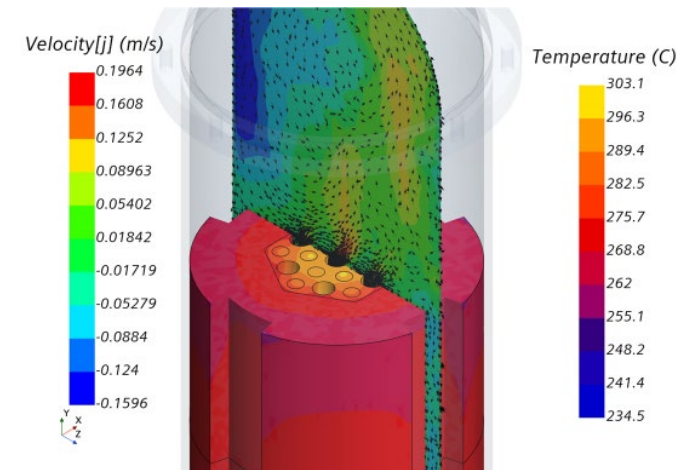


Selected CFD results

- The average temperature along the core axis rises uniformly and also exhibits uniform dissipation along the active length
- Favorable mixing patterns are observed in the upper plenum (top) due to convective gradients formed by heat transfer from the top ends of the fuel rods and indirect heat from the fuel blocks and reflector blocks
- A cumulative increase in temperature of the helium is suggested to induce sufficient buoyant flow and establish a reactor-scale circulation effect using connectivity of plena through the annular downcomers



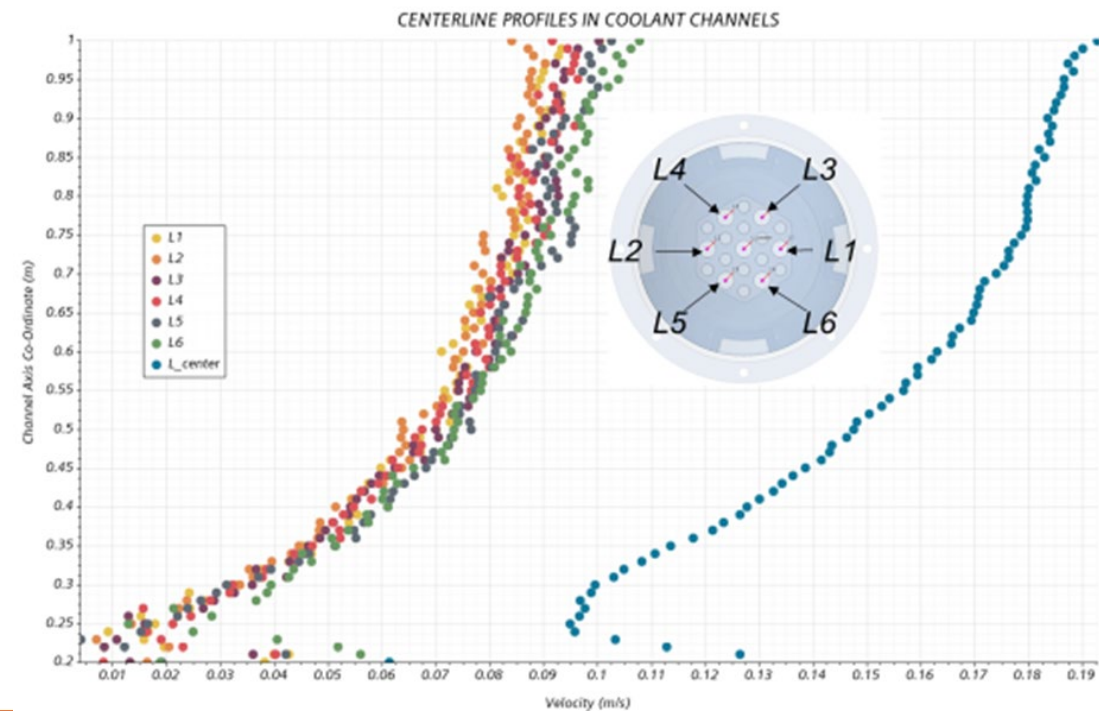
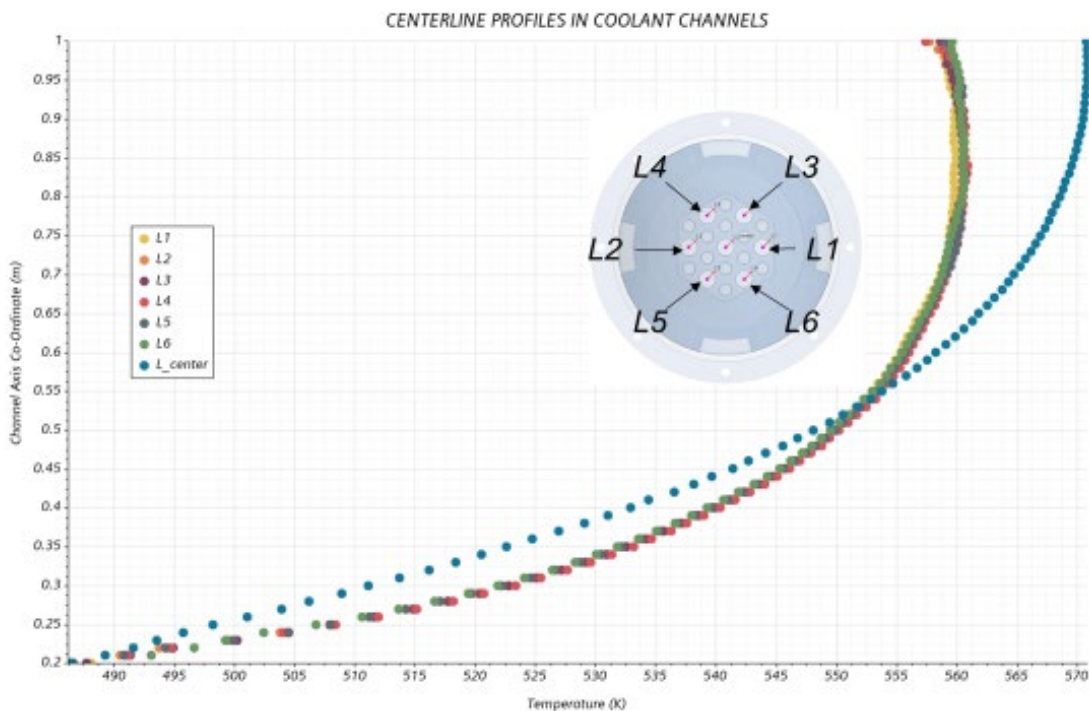
Temperature profiles in the reactor, represented on cross-section planes.



Temperature in fuel rods, fuel blocks, reflector blocks, and velocity in helium

Selected CFD results

- A clear distinction is made between profiles in the peripheral channels and the central channel.
- Higher temperatures and velocities were observed in the central channel. It is likely due to a higher mass flow of gas through the channel and a greater removal of heat from the conduction circuit.
- The peripheral channels show uniform velocity and temperature distributions as expected to increase along the active length, and do not exhibit any adverse flow or thermal patterns.

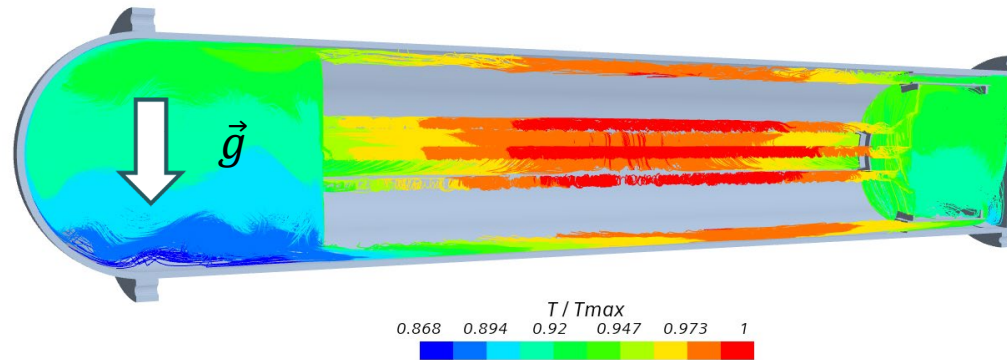


Selected CFD results

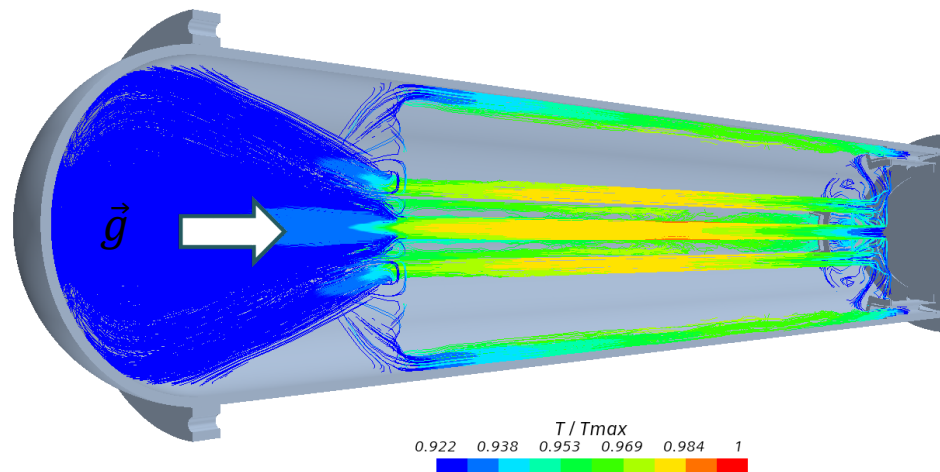
Benchmark Case: 500 W Heat Supply, PCC Condition

Helium Thermal Profiles

Horizontal



Vertical

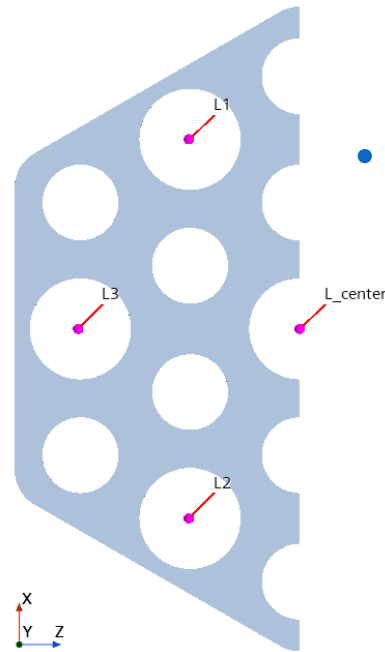


$$T_{max} = T_{max_H}$$
$$T_{max_H} > T_{max_V}$$



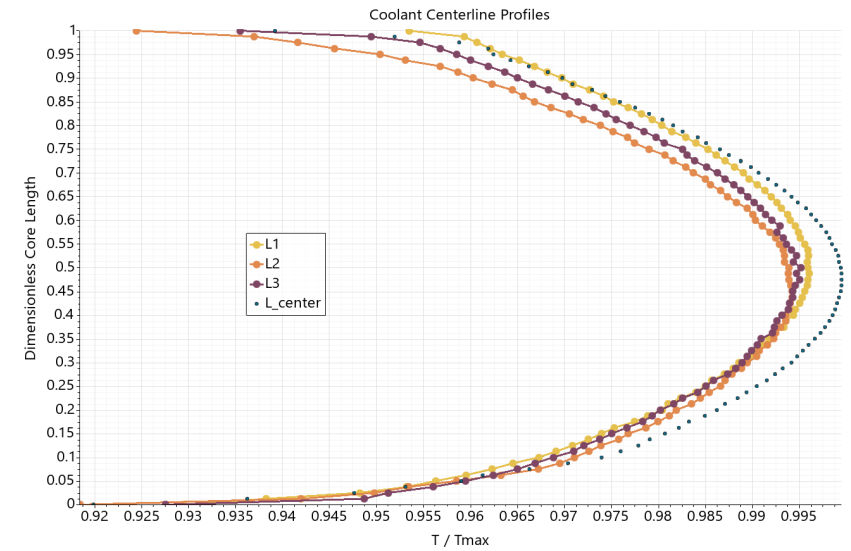
Selected CFD results

Coolant Centerline Temperature Profiles



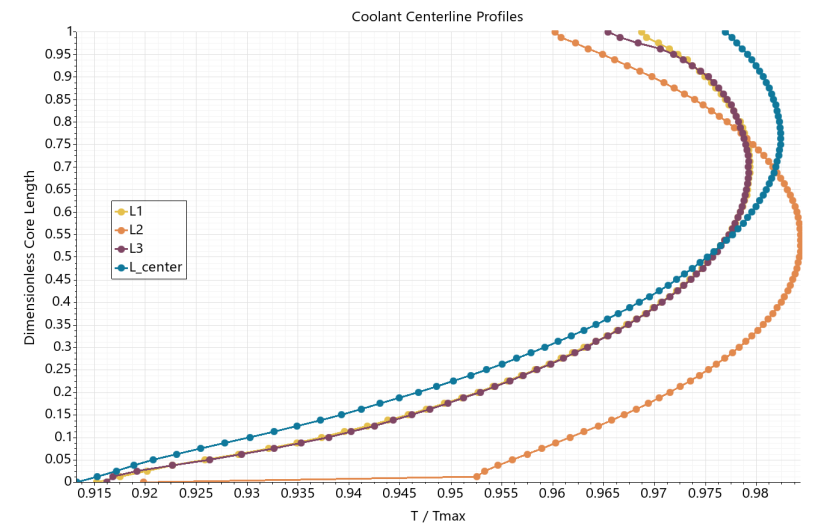
Horizontal

- Locations of peak cooling channel temperature are similar owing to axial conduction gradient



Vertical

- Locations of peak cooling channel temperature are different owing to lateral (gravity-normal) conduction gradient

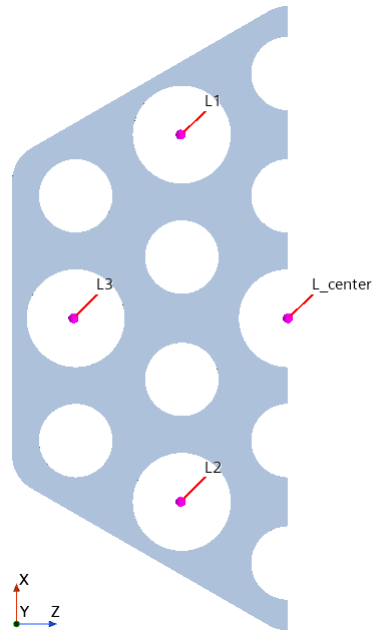


Selected CFD results

Coolant Centerline Velocity Profiles

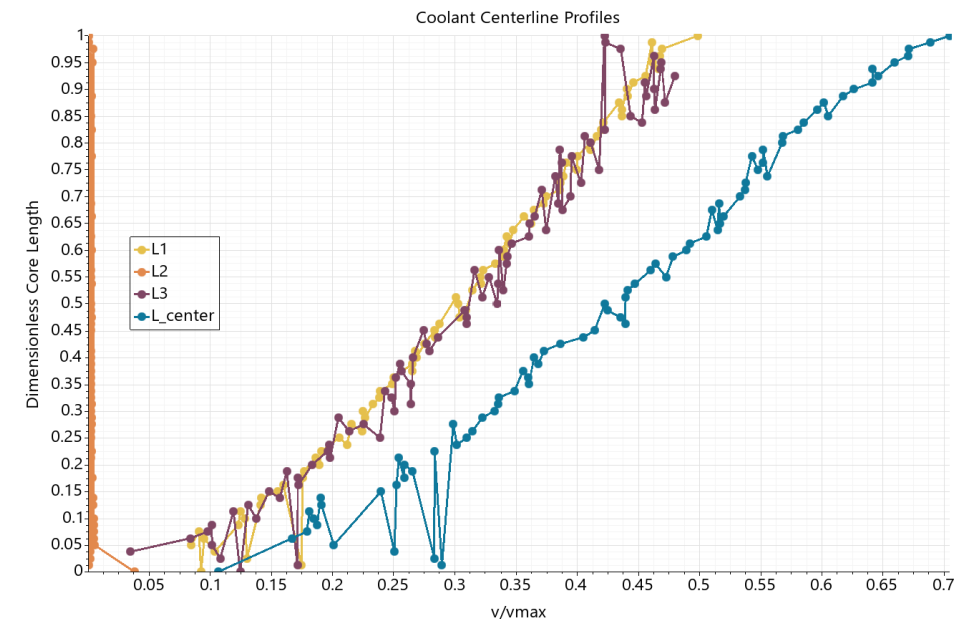
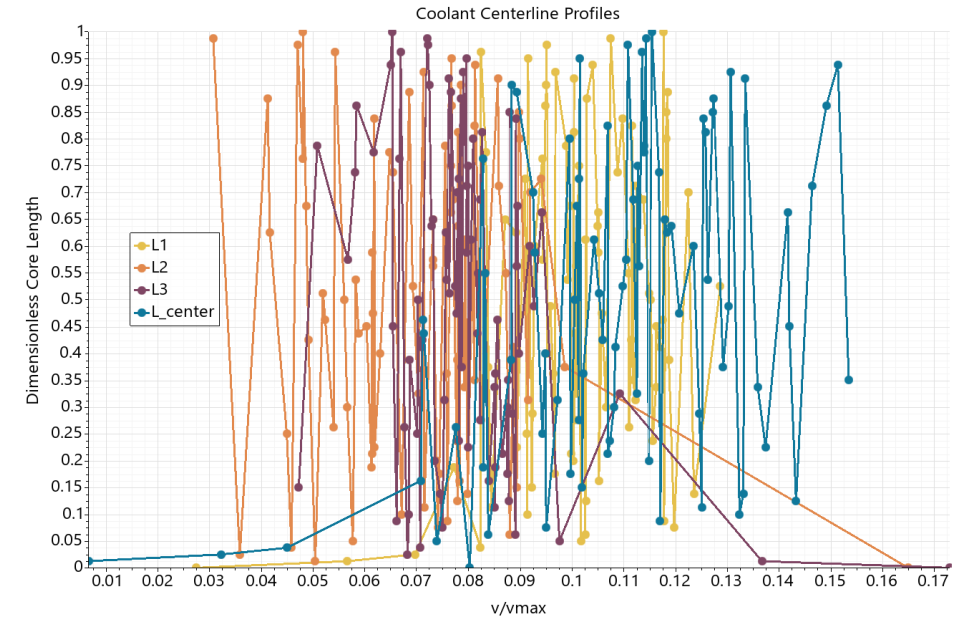
Horizontal

- Horizontal configuration produces lower velocities owing to a larger blocked area normal to the gravity axis



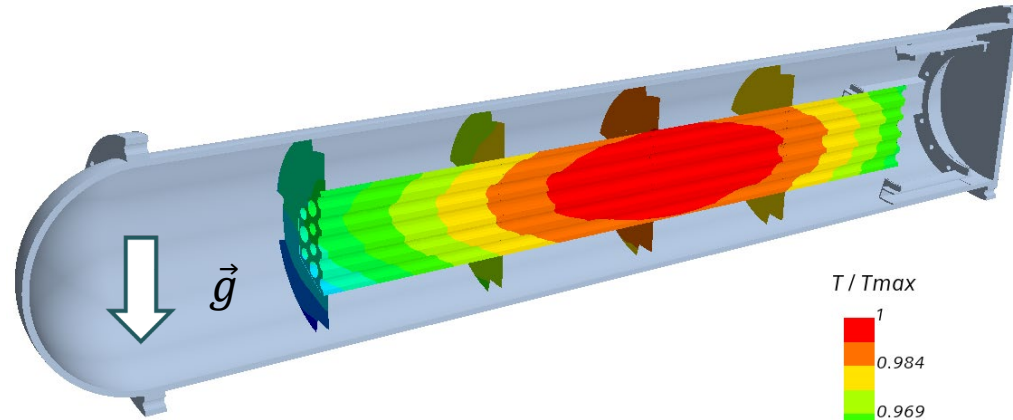
Vertical

- Vertical configuration produces higher velocities owing to a larger unblocked area normal to the gravity axis

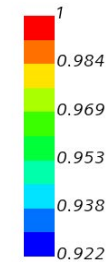


Solid Temperature Profiles

Horizontal



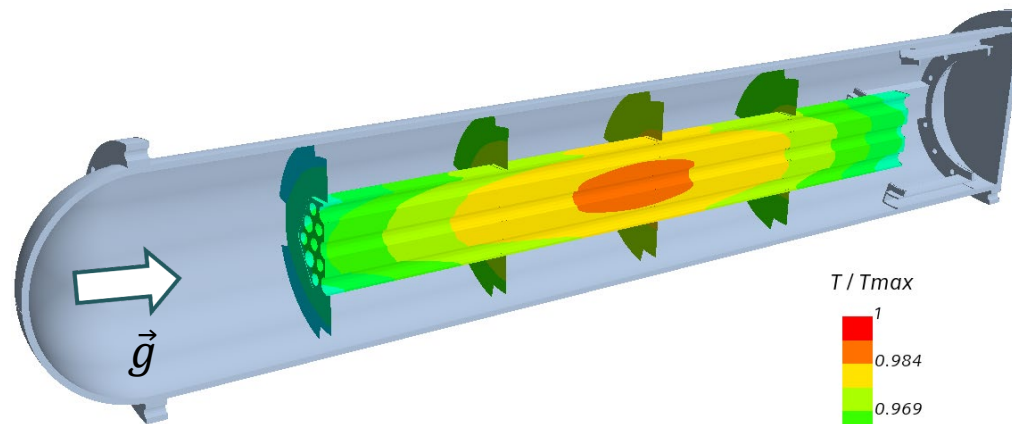
T / T_{max}



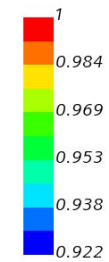
$T_{max_H} > T_{max_V}$

$T_{max} = T_{max_H}$

Vertical



T / T_{max}



Future Work

Task 2.5. Assess and quantify the contribution of the heat radiation and convection on heat transfer at low-velocity flow regime under PCC conditions and compare the results with those obtained under normal operation conditions.

Task 2.6. Investigate the gas dispersion in horizontally oriented channels and gaps using a tapered tube and slabs to mimic their local gas velocities with gaseous tracer technique and methodology.



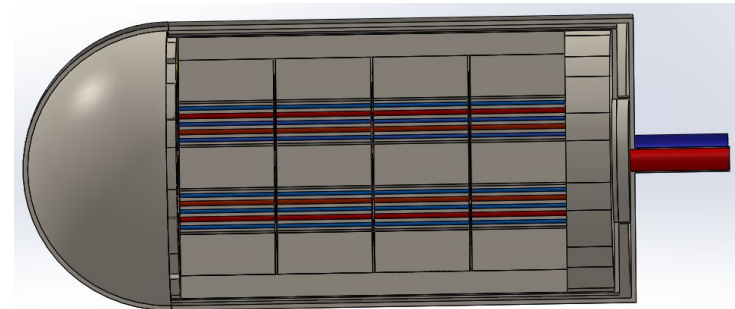
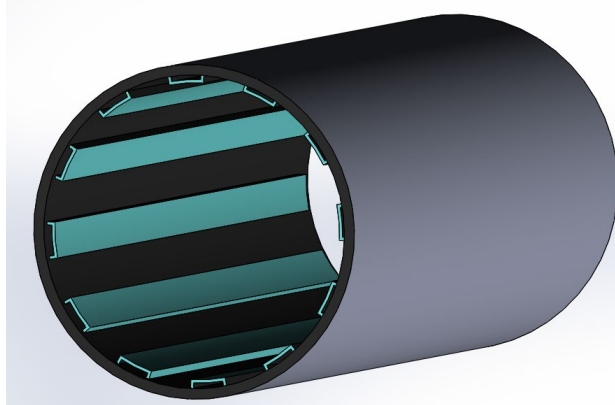
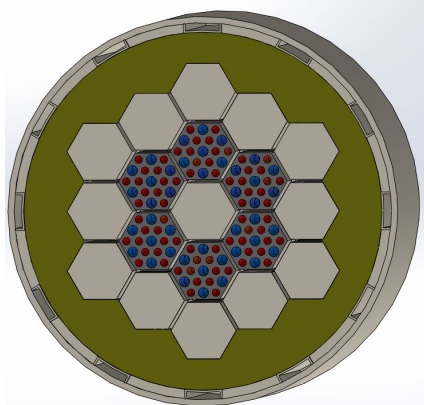
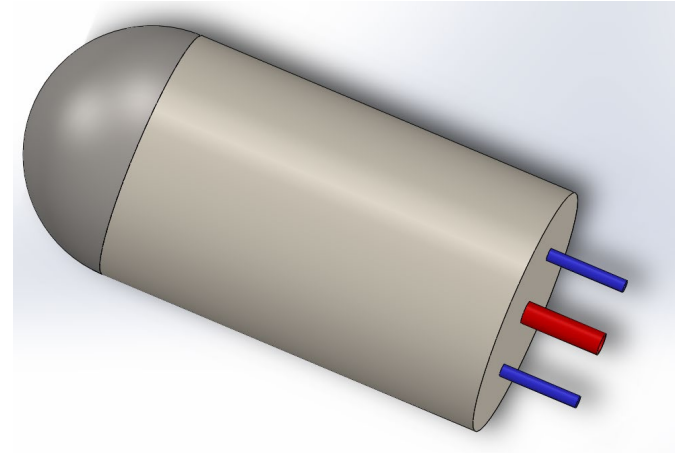
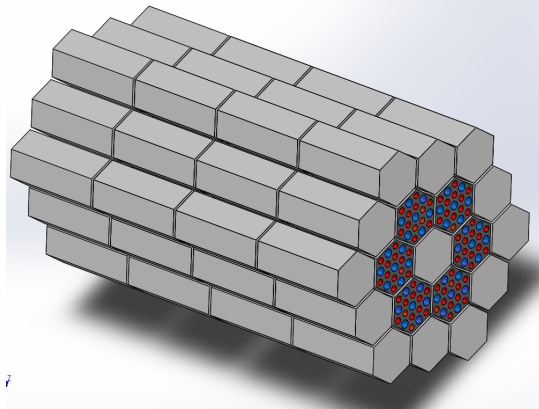
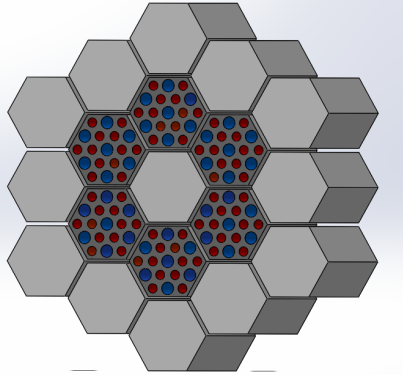
Future Work

Task 2.7. Further, validate and implement CFD and heat transfer calculations. The validated CFD models and closures from Step 1 will be further assessed and validated using the benchmarking data obtained in the horizontally oriented scaled-down micro HTGR unit up to the limitation of the measurement techniques mentioned above. The validated CFD and the heat transfer calculations will then be used to study, predict, and estimate the parameters mentioned above at temperatures up to 1,500°C and pressures up to 5 MPa

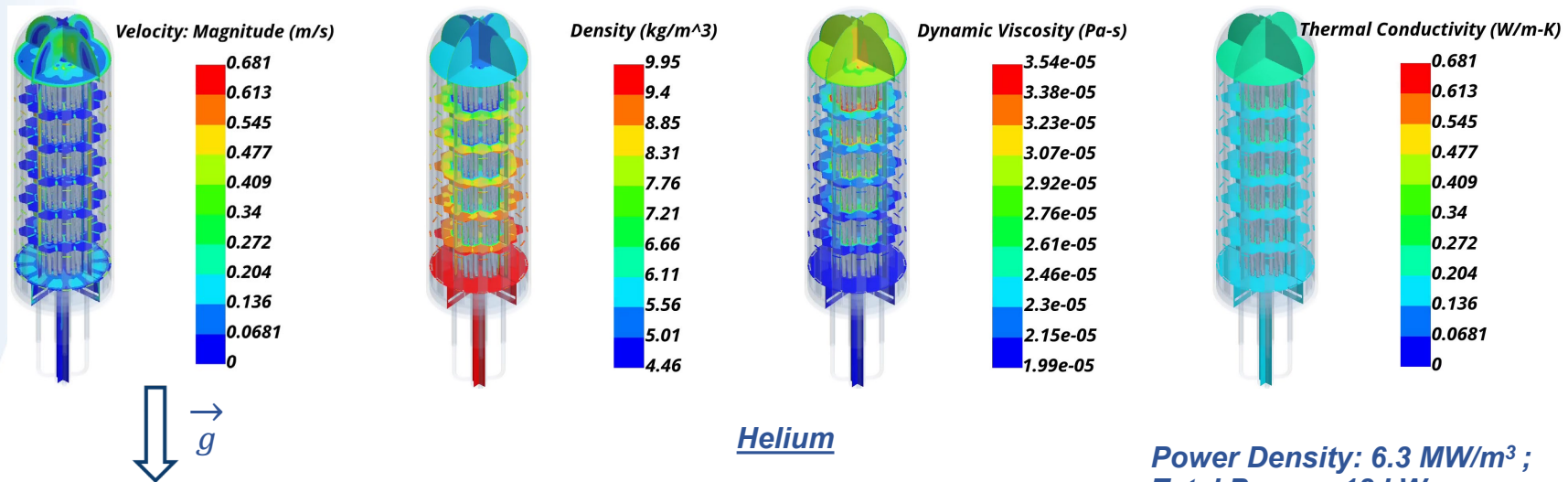
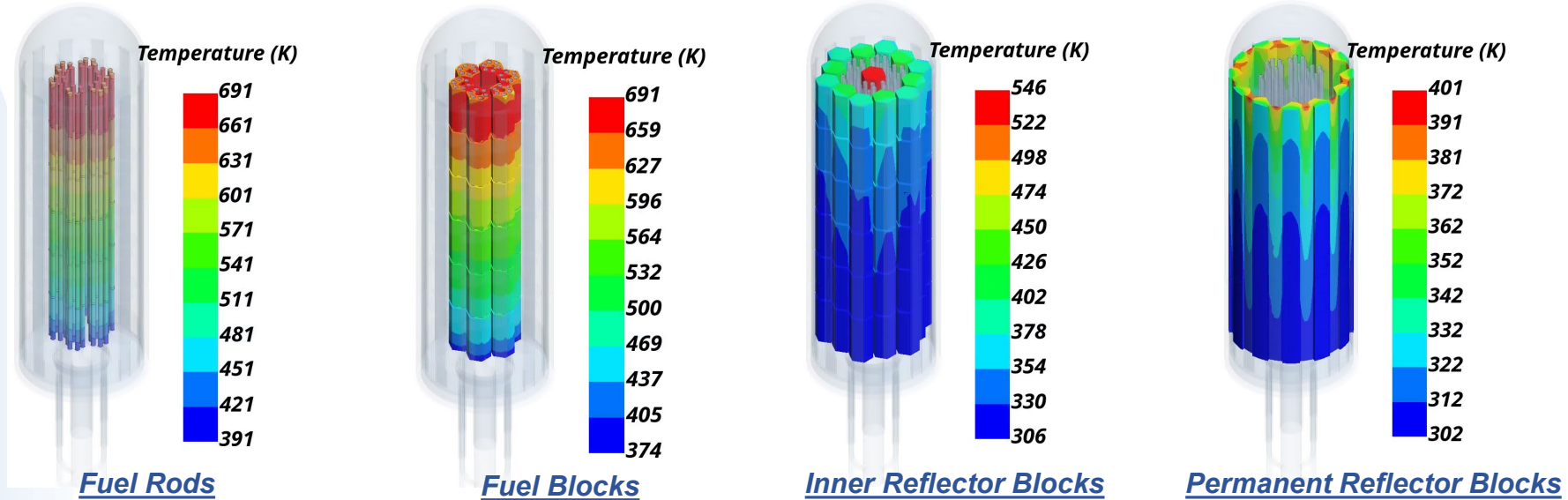


Future Work

- The validated CFD and the heat transfer calculations will then be used to study, predict, and estimate the parameters mentioned above at temperatures up to $1,500^{\circ}\text{C}$ and pressures up to 5 Mpa in a 10:1 scaled-down version of the reference reactor



Analysis – Vertical Orientation



Power Density: 6.3 MW/m³ ;
 Total Power= 18 kW ;
 System Pressure = 6.39 MPa ;



Analysis – Horizontal Orientation (1/3)

Fuel Rods



Fuel Blocks



Inner Reflector Blocks



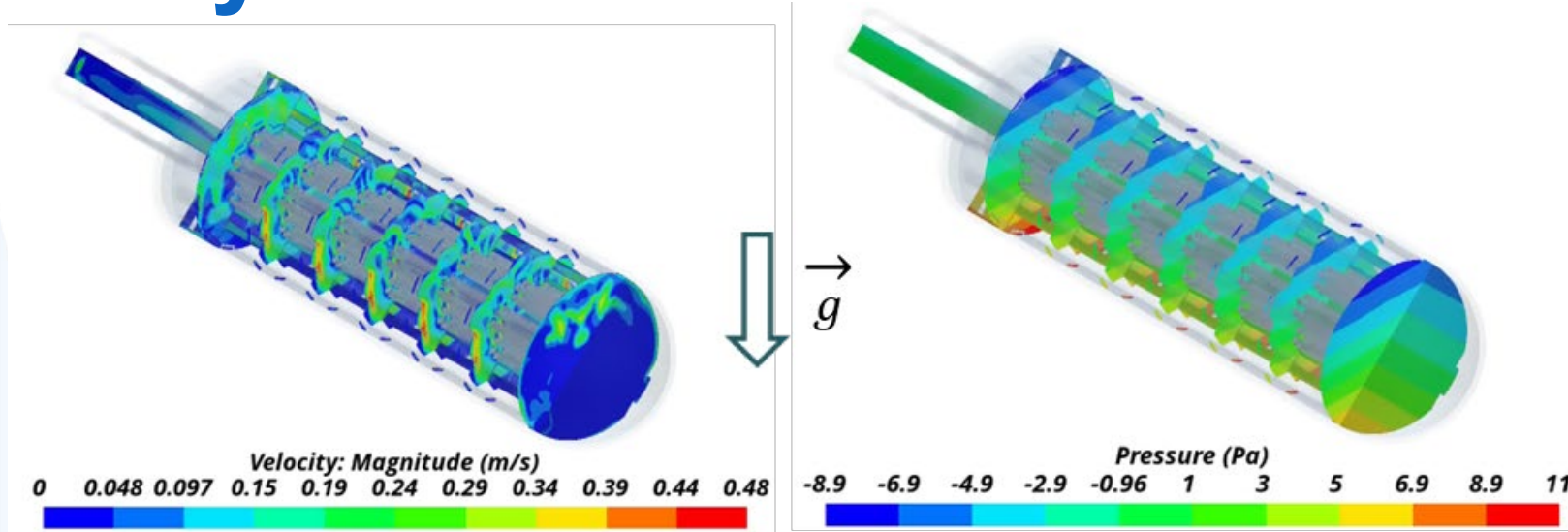
Permanent Reflector Blocks



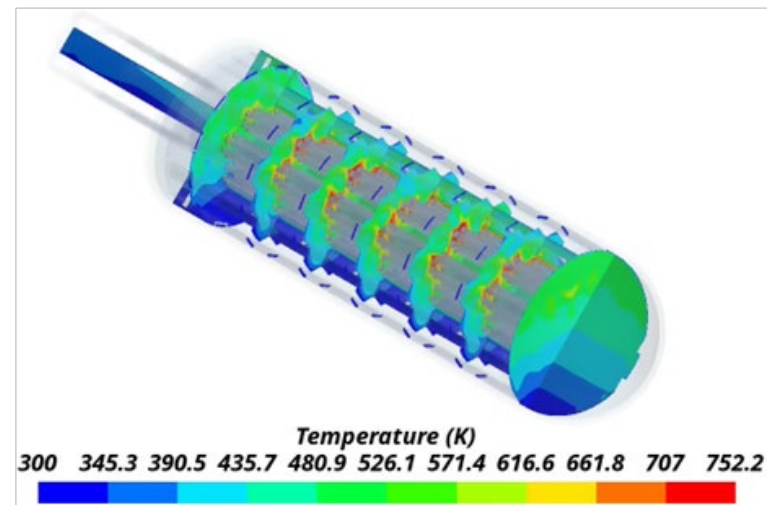
Power Density: 6.3 MW/m³ ;
Total Power= 18 kW ;
System Pressure = 6.39 MPa ;



Analysis – Horizontal Orientation (2/3)



Helium

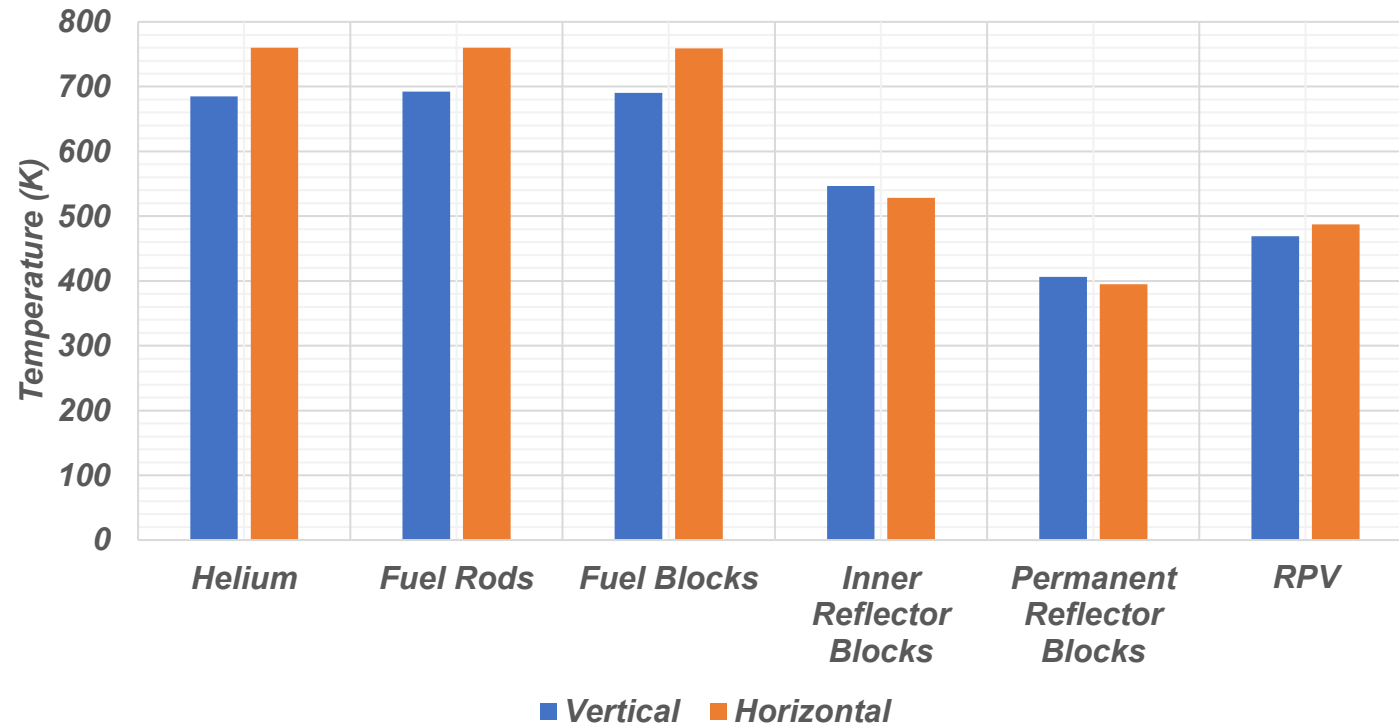


Power Density: 6.3 MW/m³ ;
Total Power= 18 kW ;
System Pressure = 6.39 MPa ;



Summary of Orientation

Maxima of Temperature, Comparison of Orientation



Future Work

Task 2.8. Perform uncertainty quantification and sensitivity analysis on the experimental results and computed parameters.

- The same uncertainty quantification methodology and sensitivity analysis outlined in Step 1, Task 1.6 will be adopted and applied to all experimental and computed data obtained in Step 2, Tasks 2.4, 2.5, and 2.6.



Milestones and deliverables

- Modify and test the horizontal dual-channel P2PF and investigate the gas dispersion. (Task 1.1, Task 1.3) - **Delivered**
- Investigate the effect of natural circulation intensity on convective heat transfer, and temperature and gas velocity profiles in the horizontal dual channel. (Task 1.2)-**Delivered**
- Compare between horizontally and vertically oriented dual-channel natural circulation. (Task 1.4, Task 1.5, Task 1.6) - **In Progress**
- Literature review and Design, develop, test, and utilize a horizontally oriented scaled-down micro-HTGR.(Task 2.1, Task 2.2) - **In Progress**
- Design, develop, test, and utilize a block integrated with advanced measurement techniques. (Task 2.3) - **In Progress**



Milestones and deliverables

- Design, develop, test, and utilize a block integrated with advanced measurement techniques. (Task 2.3) - **In Progress**
- Provide New knowledge and Perform Investigation under normal operation and PCC conditions. (Task 2.4, Task 2.6) - **In Progress**
- Assess and quantify the contribution of radiative and convective heat rates under PCC conditions. (Task 2.5) - **In Progress**
- Perform uncertainty quantification. (Task 2.8) - **In Progress**
- Develop new benchmarking data and CFD validation with heat transfer calculations. (Task 2.7) - **In Progress**





GAS-COOLED REACTOR

**ADVANCED REACTOR
TECHNOLOGIES PROGRAM**

Thank you

Muthanna Al-Dahhan

aldahhanm@mst.edu